UNIVERSITÀ DEGLI STUDI DI PADOVA

DIPARTIMENTO DI INGEGNERIA DELL'INFORMAZIONE

DIPARTIMENTO DI INGEGNERIA DELL'INFORMAZIONE

CORSO DI LAUREA IN BIOINGEGNERIA.

"ENZYMATIC DEGRADATION KINETICS OF STRAINING FLOW SPUN SILK FIBROIN FIBERS"

Relatore: Prof. Pavan Piero

Laureando: Carturan Nicholas

ANNO ACCADEMICO 2022 – 2023

Data di laurea 5 Settembre 2023

POLITÉCNICA

UNIVERSIDAD POLITÉCNICA DE MADRID

CTB centro de tecnología biomédica

Ai miei genitori,
a chi mi ha supportato durante questo percorso

INDEX

INTRODUCTION

The development of medicine and medical technologies enabled the global population to reach an ever-increasing average lifespan. As the population's age increases, so does the emergence of diseases requiring organ transplants, which are still considered the gold standard for the treatment of tumors and organ failures, two of the world's leading causes of death. The demand for organ transplants far exceeds their availability. In the United States the waiting list for receiving a transplant exceeds more than 105,000 people and it is estimated that about 17 people a day die waiting for a new organ. This data underlines the medical urgency of finding a viable alternative to transplants to ensure patients with an alternative treatment or therapy that allows them to reach their place on the waiting list.

In recent years the concept of Tissue Engineering has made its way into medicine and biomedical research, precisely to ensure a fallback from transplantation. Tissue engineering developed from the field of biomaterials and refers to the practice of combining media, cells and biologically active molecules into functional tissues. The goal of tissue engineering is to assemble functional constructs that restore, maintain, or enhance damaged tissues or entire organs by combining several principles and methods. With a view to tissues replacement, the biomaterial chosen to interact with the human organism are of fundamental importance, and properties such as their biocompatibility, bioresorbability and biodegradability are crucial in their selection. The concept of biocompatibility refers to the ability of a biomaterial to perform the desired function compared to a medical therapy, without eliciting undesirable local or systemic effects in the host or beneficiary of that therapy but generating the most appropriate beneficial cellular or tissue response in that specific situation and optimizing the clinically relevant performance of that therapy. Bioresorbability and biodegradability are characteristics related to the behavior of biomaterials once grafted into the body, a chemically extremely aggressive and dynamic environment. In tissue engineering, biodegradability and bioresorbability play a key role in guided tissue replacement because over time, these materials will be replaced directly by newly formed tissue without triggering hostile responses towards their degradation products. Indeed, resorbable materials are often created from biological materials whose main components consist of amino acids or carbohydrates, elements already present in living organisms, which can be degraded by enzymatic means. Not only the chemical properties are fundamentals in the design of biocompatible scaffold. Mechanical properties, structure and fabrication methods must be considered to create a scaffold that can replicate the characteristics of the tissue that it should replace.

In light of these considerations, this study wants to investigate the degradation kinetics of silk fibroin fibers derived from *Bombyx mori* silkworms and regenerated with an innovative technique called Straining Flow Spinning exposed to the enzyme proteinase K. Fibroin is in fact a biocompatible and bioresorbable material that also exhibits excellent mechanical properties. Firstly, a mechanical evaluation of the regenerated fibers through the spinning technique will be presented by testing single fibers both in air and in water. Parameters allowing to obtain good quality fibroin fibers will then be showed.

To determine the incidence of enzymatic degradation, mass loss analysis and microscopic observations will be made to evaluate changes both macroscopical and microscopical changes in the fibers. A model will be created to estimate the degradation incidence.

From these analysis, data of the degradation behavior of fibroin fibers exposed to an aggressive environment will be deduced to determine whether silk fibroin fibers are suitable in research concerning the creation of guides for polybrancate nerve or vascular regeneration.

SOMMARIO

Lo sviluppo della medicina e delle tecnologie mediche ha permesso alla popolazione mondiale di raggiungere una durata di vita media sempre maggiore. Con l'aumentare dell'età della popolazione, aumenta anche la comparsa di malattie che richiedono trapianti di organi, che sono ancora considerati lo standard di riferimento per il trattamento dei tumori e delle insufficienze d'organo, due delle principali cause di morte al mondo. La domanda di trapianti di organi supera di gran lunga la loro disponibilità. Negli Stati Uniti la lista d'attesa per ricevere un trapianto supera le 105.000 persone e si stima che circa 17 persone al giorno muoiano in attesa di un nuovo organo. Questi dati sottolineano l'urgenza medica di trovare una valida alternativa ai trapianti per garantire ai pazienti un trattamento o una terapia alternativa che permetta loro di raggiungere il proprio posto in lista d'attesa.

Negli ultimi anni il concetto di ingegneria tissutale si è fatto strada nella medicina e nella ricerca biomedica, proprio per garantire un ripiego al trapianto. L'ingegneria tissutale si è sviluppata dal campo dei biomateriali e si riferisce alla pratica di combinare mezzi, cellule e molecole biologicamente attive in tessuti funzionali. L'obiettivo dell'ingegneria tissutale è quello di assemblare costrutti funzionali che ripristinino, mantengano o migliorino tessuti danneggiati o interi organi, combinando diversi principi e metodi. Nell'ottica della sostituzione dei tessuti, i biomateriali scelti per entrare in contatto con l'organismo umano sono di fondamentale importanza e proprietà come la biocompatibilità, la bioriassorbibilità e la biodegradabilità sono cruciali nella loro selezione. Il concetto di biocompatibilità si riferisce alla capacità di un biomateriale di svolgere la funzione desiderata rispetto a una terapia medica, senza suscitare effetti locali o sistemici indesiderati nell'ospite o nel beneficiario di tale terapia, ma generando la risposta cellulare o tissutale benefica più appropriata in quella specifica situazione e ottimizzando le prestazioni clinicamente rilevanti di tale terapia. La bioriassorbibilità e la biodegradabilità sono caratteristiche legate al comportamento dei biomateriali una volta innestati nel corpo, un ambiente chimicamente molto aggressivo e dinamico. Nell'ingegneria tissutale, la biodegradabilità e la bioriassorbibilità giocano un ruolo chiave nella sostituzione guidata dei tessuti, perché nel tempo questi materiali saranno sostituiti direttamente da tessuti di nuova formazione senza innescare risposte ostili verso i loro prodotti di degradazione. Infatti, i materiali riassorbibili sono spesso creati a partire da materiali biologici i cui componenti principali sono costituiti da aminoacidi o carboidrati, elementi già presenti negli organismi viventi e che possono essere degradati per via enzimatica. Non solo le proprietà chimiche sono fondamentali nella progettazione di scaffold biocompatibili. Le proprietà meccaniche, la

struttura e i metodi di fabbricazione devono essere presi in considerazione per creare uno scaffold in grado di replicare le caratteristiche del tessuto che deve sostituire.

Alla luce di queste considerazioni, questo studio vuole indagare la cinetica di degradazione di fibre di fibroina di seta derivate da bachi da seta *Bombyx mori* e rigenerate con una tecnica innovativa chiamata "Straining Flow Spinning" esposte all'enzima proteinasi K. La fibroina è infatti un materiale biocompatibile e bioriassorbibile che presenta anche ottime proprietà meccaniche. In primo luogo, verrà presentata una valutazione meccanica delle fibre rigenerate attraverso la tecnica di filatura testando singole fibre sia in aria che in acqua. Verranno quindi mostrati i parametri che consentono di ottenere fibre di fibroina di buona qualità.

Per determinare l'incidenza della degradazione enzimatica, verranno effettuate analisi di perdita di massa e osservazioni microscopiche per valutare cambiamenti sia macroscopici che microscopici nelle fibre. Attraverso i dati ottenuti verrà creato un modello su cui basarsi per stimare l'incidenza della degradazione.

Da queste analisi, verranno dedotti dati sul comportamento di degradazione delle fibre di fibroina esposte ad un ambiente aggressivo per determinare se le fibre di fibroina di seta sono adatte nella ricerca riguardante la creazione di guide polibrancate per la rigenerazione della vascolatura periferica

1 – INTRODUCTION TO SILK FIBROIN

1.1 – Silk production process

In the field of tissue engineering many different polymers, both natural and synthetic, have been investigated to be used as biomaterials. To replicate the dynamic environment that characterizes every tissue that develops in an organism, many components of the extracellular matrix (ECM) such as collagen, fibronectin, laminin, elastin and glycosaminoglycans have been widely used as a natural basis to produce scaffolds to support tissue regeneration. Other natural polymers which are not present in the human body have also been used such as chitosan, alginate and cellulose. Although these materials possess excellent biocompatibility and biodegradability characteristics, they face some disadvantages such as high production cost, poor mechanical properties and large batch to batch variation. On the other hand, synthetic polymers such as polylactic acid (PLA), polyurethane (PU), polycaprolactone and lactic acid-glycolic acid copolymers (PLGA) are widely used for their excellent mechanical properties. However, many degradation products of these polymers comprise acidic compounds that can be harmful to the body and elicit undesired immune responses.

Recent studies have explored and documented the possibilities of silkworm silk fibroin as an excellent biomaterial.

Figure 1.1 – Bombyx mori silkworm and cocoon made of its own silk.

Silkworm has been used in the silk textile industry for a long time due to its outstanding physical properties, such as lightweight, flexibility, mechanical strength and absorbed energy. Moreover, silk has been approved by the Food and Drug Administration (FDA) for its use in resorbable sutures.

Silks are proteins which are produced within glands after biosynthesis in epithelial cells. Silks originating from silkworms and spiders are commonly used for biological applications. However, in the case of spider silk, once it is spun and contacts with air it hardens, which restricts mass production of spider silk as it should be stored in a controlled environment. Compared to spiders' silk, the yield of fibers obtained from one silkworm cocoon is around 10-fold that of one spider gland[1]. Thanks to the abundance and an easier extraction process respect to spider silk, silkworm silk can be spun in greater quantities with techniques that ensure to realize high quality fibers in a way that can also be upscaled to an industrial process.

The most common silk originates from *Bombyx mori* (*B. mori*), a mulberry feeding silkworm that produces higher quality fibers respect to other species of silkworms[2]. After being hatched from eggs, silkworms live through five instars before undergoing metamorphosis into a moth. Throughout the instar stages, the silk is produced in benign and aqueous conditions in silk glands. At the end of the fifth instar, B. mori silkworms spin a large amount of silk into a continuous thread to construct the silk cocoons. Figure 1.2 resumes silk natural spin process.

Proteins dope accumulates in the silk glands at very high concentrations (30% w/v fibroin in water-based solution), despite the tendency to self-assembly. It is thought that a neutral pH and controlled ions concentration (Na^+, K^+, Ca^{2+} and Cl^-) are essential to keep the fibroin as a soluble moiety[3]. Proteins might remain soluble due to their organization as liquid crystals, as micelles or as a combination of both phases. The acidification of the protein solution along the spinning duct triggers the self-assembly of the proteins into a new structure that can solidify after being subjected to mechanical shear stress.

Silkworms extrude silk naturally at speed oscillating between 4 and 15 $mm \cdot s^{-1}$ by moving their heads in "figure of eight" motion. Prior leaving the silk glands, the dope exists as a water-soluble liquid crystalline state that ensures a low viscosity for easy spinning into external environment. Being a liquid, silk viscosity is independent on environmental temperature. Nevertheless, temperature is known to be a parameter affecting the spinning rate of silkworms and a range between 22-25 °C provides the optimal condition. Moreover, studies devoted to the processing mechanism of silkworm silks have revealed not only a complex system from both anatomical and physiological perspectives, but also the capacity to modify the fiber during the spinning process depending on the requirements. The main event in natural spinning is the transition from a protein solution to a high-performance solid fiber. This process occurs in fraction of second and proceeds under extremely biosustainable, and thus environmentally friendly, conditions.

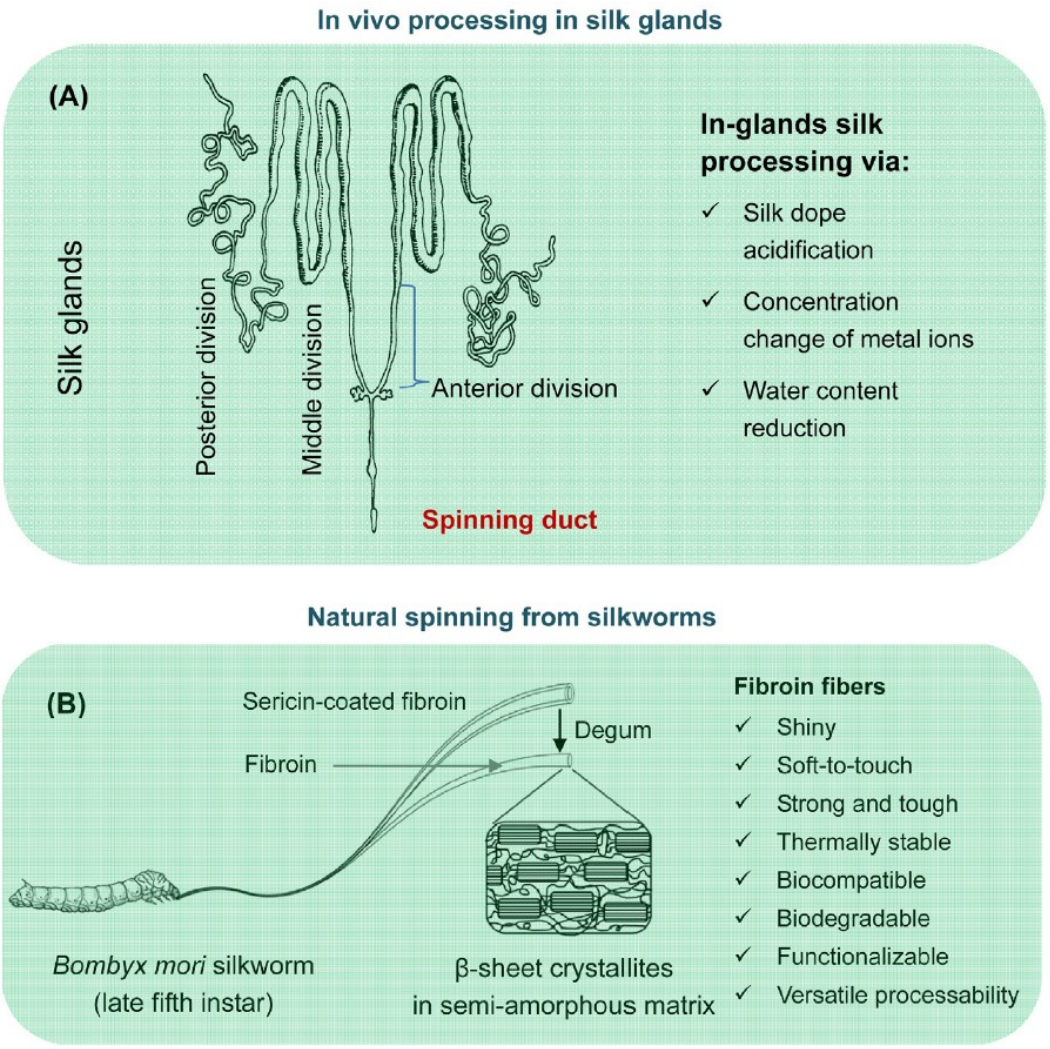

Figure 1.2 – (A) Processing of silk in Bombyx Mori silk glands and throughout the duct; process main steps are reported. (B) Natural spinning of the sericin coated fibroin by the silkworm. Degumming is necessary to isolate fibroin. Fibroin fibers unique characteristics are reported.

Once the cocoons are collected, silk must be treated to remove sericin in a degumming process and then dissolved in reach in ions solutions, similarly to the natural environment provided by the silkworms. This process, together with a dialysis and reverse dialysis protocol, must be carried out to produce a spinnable solution that is called Regenerated Silk Fibroin (RSF).
Fibers can be obtained by RSF solutions with spinning techniques, (that will be illustrated in the next chapters of this work), as well as many other constructs such as films, mats, sponges, hydrogels, 3D structured design and micro-patterning structures.

1.2 – Chemical and physical properties of SF

B. mori cocoons consists of 75-83.3 % of silk fibroin (SF) and 16.7-25 % of sericin as reported in the study performed by Liu et al.[4]. SF is a semi-crystalline structured protein, functioning mainly for its load-bearing capacity. On the other hand, sericin is an amorphous protein that mainly works as a gumming agent between the different chains of SF. It is known that sericin provokes an inflammatory reaction when enters in contact with the human body[5], so it must be removed before recreating the fibers. Moreover, it has been found by Vepari et al.[6] that sericin free fibroin fibers show better mechanical properties than sericin encapsulated ones. A 50% increase in tensile strength, with an elastic modulus (E) up to 15-17 GPa, and strain at break reaching 19% has been observed. Therefore, sericin proteins are often removed from SF to ensure biocompatibility and increase the mechanical behaviour of the fibers. Sericin is eliminated from the silkworm cocoons by a degumming process which protocol will be explained in detail in the next chapter of this study.

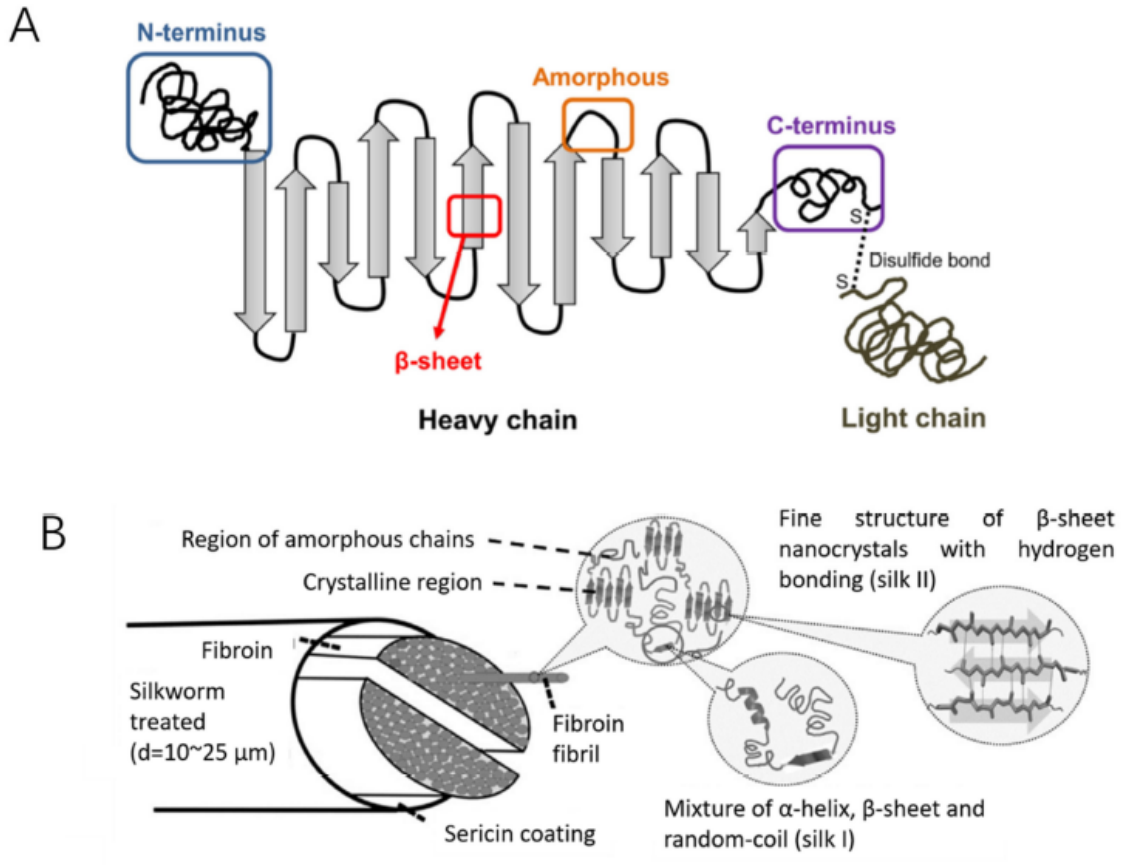

Figure 1.3 – Schematic diagram of the silk structure. (**A**) Heavy chain and light chain linked through a disulphide bond. (**B**) Silkworm thread, fibril overall structure and silk fibroin polypeptide chains.

SF consists of two main chains, a heavy (H-) chain that weighs about 390 kDa and a light (L-) chain that is only 26 kDa. The two chains are linked together via a single disulphide bond to form the H-L complex represented in Figure 1.3. The polypeptide P25 is observed to be linked to the complex via hydrophobic interactions to form an elementary micellar unit necessary to transport silk in such units before being spun in silkworms. However, this protein is not relevant to this study. The amino acid primary structure of the H-chain is composed by Glycine (~43-46%), Alanine (~25-30%), Serine (~12%), Tyrosine (~5%), Valine (~2%) as well as other amino acids representing a minor percentage. The fundamental amino acids are represented in Figure 1.4 where is also shown the amino acid Cysteine, responsible of the disulphide bond.
Organizationally, SF H-chain is a highly regular biopolymer that consists of 12 hydrophobic extended domains, where the Gly-X (G-X) dipeptide motif repeats itself for 60%-75% of the whole protein, and 11 smaller hydrophilic domains in which a repetitive sequence can't be identified. This hierarchical structure is showed in Figure 1.5.

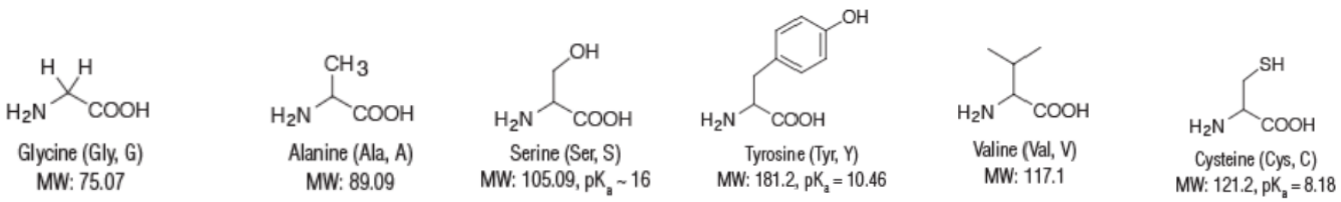

Figure 1.4 – List and representation of the fundamental amino acids composing the H-chain of silk fibroin. They are reported with their molecular weight (MW) and dissociation constant (pK_a).

Thanks to the low steric hindrance of Gly, which is the amino acid with the smallest residue (just one atom of Hydrogen) and the hydrophobic residues of the dipeptide motif, the proteins can assemble themselves in stable antiparallel β-sheet crystallites as demonstrated by Marsh et al.[7]. Nevertheless, the correct crystalline organization remains an open question with three possible arrangements of strands.
The alternation of large (Ala, Ser) and small (Gly) residues is fundamental for the correct piling up of the sheets, so that the van der Waals interactions can act cooperatively to stabilize the crystallites. Due to the high packing degree, the H-chain serves as the main structural component responsible for the superior mechanical properties, while L-chain plays little mechanical role as its size is much smaller than H-chain and besides, its sequence is not associated with the formation of the crystalline region in SF. In fact, silk I and silk II are the dominant crystalline structures of SF. Silk I is a metastable crystalline structure that includes bounded water molecules, while silk II is the most stable state thanks to strong hydrogen

bonding between adjacent peptide blocks, resulting in increased mechanical properties including rigidity and tensile strength.

The secondary structure of the SF can be crystalline, when it includes β-turns (silk I) and insoluble structures formed by folded β-sheets (silk II), or amorphous when it consists in α-helices, turns and random coils regions. There are compounds that can convert silk I to silk II which are used to produce regenerated silk fibroin solutions. The protocol followed in this study to obtain a spinnable solution will be explained in detail later.

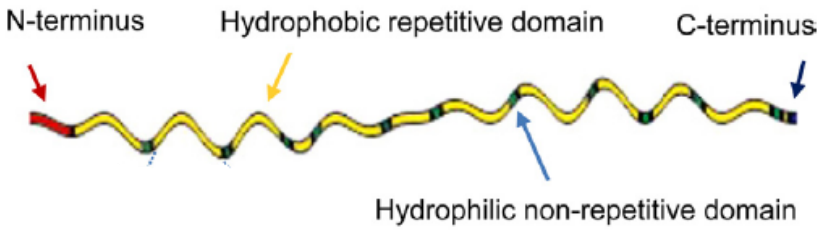

Figure 1.5 – Each fibroin heavy chain consists of hydrophobic repetitive domains interrupted by hydrophilic non-repetitive domains.

Biocompatibility is a key factor for the implementation of SF based constructs, which enables cells to adhere to their surfaces and migrate into the internal portion, undergoing proliferation and differentiation within the construct. SF is known to be a biologically inert and therefore biocompatible natural polymer. Since 1989, SF has been shown to have blood compatibility in *in-vivo* experiments, and in 1993 SF was approved by FDA for use in a suture material.

Minoura et al.[8] conducted pioneering research and successfully grew fibroblast cells on SF coated films, proving that SF could be used as a support to the growth of human cells. Moreover, SF has more recently been used as an alternative to collagen in cell culture guided bone regeneration, demonstrating that SF membranes could replace collagen membranes. But silk fibroin has also been investigated as a potential biomaterial with excellent results also in regenerative medicine applied to regeneration of peripheral nerve, cartilage tissue, ligament and tendon, skin and wound and tympanic membrane thanks to this material outstanding mechanical properties and exceptional biocompatibility and tendency to promote cellular growth.

Highlighting its biocompatibility, in vitro studies showed that there is no significant macrophage response to SF films or fibers. Additionally, the *in vivo* inflammatory reaction to SF fibers is similar to that of collagen. These characteristics raise SF as a great biomaterial with optimal adaptability to different applications. Moreover, it is possible to functionalize the fibers or the fibroin solutions to enhance the bioactivity of the material.

Biodegradability and bioresorbability are important features too for successful scaffold materials, as it should be gradually replaced with patients' autologous cells and ECM over the course of the recovery. Therefore, it is essential that products of biodegradation are non-toxic and don't interfere with other tissue, organs and functions when being metabolize in the body. SF is an enzymatically degradable polymer and has been shown not to cause an immunogenic response. The degradation process starts when enzymes are adsorbed onto the surface of the SF scaffold via surface bonding-domains. The enzymes then digest SF via hydrolysis of ester bonds. SF can be proteolytic degraded through enzymes such as α-chymotrypsin, protease XIV, proteinase K, collagenase IA and more[1]. The enzymatic degradation process is schematically represented in Figure 1.6. As the degradation products of SF are amino acids and peptides, they are easily absorbed *in-vivo*. Studies performed on SF porous scaffold proved that they are not only biodegradable, but also bioresorbable.

The degradation of native silk fibers is much slower compared to that of RSF silk scaffolds. This is because native silk fibers have a higher content of β-sheet secondary structure than RSF structures have. The degradation rate of SF is therefore highly dependent on the amount of β-sheet secondary structures present. This is a key factor to determine the rate of degradation of the fibers.

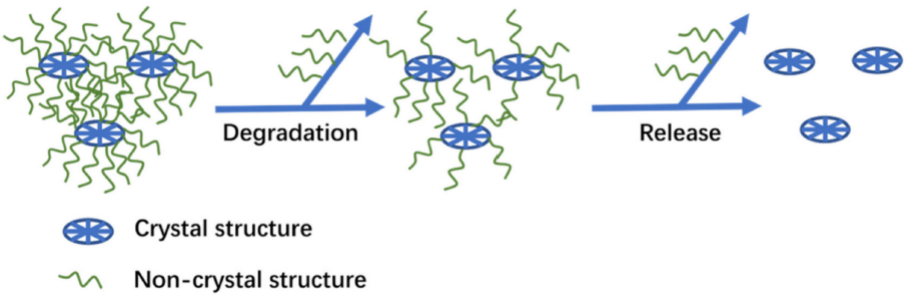

Figure 1.6 – Schematic illustrating the silk fibroin degradation process mechanism.

1.3 – Mechanical properties of SF

To explain the mechanical properties of the SF fibers an introduction to the most important quantities must be done. Continuum mechanics defines the deformation of a body as a transition from a reference configuration to a current configuration. A deformation can occur, for example, because of external loads, intrinsic activity (e.g. muscle contraction), body forces (such as gravity or electromagnetic forces), or changes in temperature. Depending on the amount of strain, or local deformation, the analysis of deformation is subdivided into two deformation theories:

- Finite strain theory, also called large strain/deformation theory, deals with deformations in which both rotations and strains are arbitrarily large. In this case, the undeformed and deformed configurations of the continuum are significantly different, and a clear distinction must be made between them. This is commonly the case with elastomers, plastically deforming materials and other fluids and biological soft tissue.

- Infinitesimal strain theory, also called small strain/deformation theory, small displacement theory, where strains and rotations are both small. In this case, the body undeformed and deformed configurations can be assumed identical. This theory is used in the analysis of deformations of materials exhibiting an elastic behaviour, such as materials found in mechanical and civil engineering applications, stiff materials etc.

Regarding this study, the application of the finite strain theory would be too complicated. Thus, an infinitesimal approach is undertaken with some important considerations and correction.
The change of configuration of a body is expressed in the following equation:

$$x(X,t) = X + u(X,t) \tag{1.1}$$

Where *t* is the time, indicating that generally the deformation is time dependant, **X** is the material points reference position of the body, $\boldsymbol{u}$ is the displacement function and **x** is the new position of the points after a force creates a deformation (or a rigid motion) to the body.
To analyse the body behaviour is possible to study the variability of the displacement field. In other words, we need to understand how the displacement function varies:

$$u(X + dX) = u(X) + \nabla u(X) \cdot dX$$

(1.2)

$$\nabla u_{ij} = \frac{\partial u_i}{\partial X_j}$$

Since the first term of right side of the equation is independent on d**X**, it describes the rigid motion while the second represents the combination of rigid rotation (**w**) and effective strain (**ε**). From now on the rigid motion term will be ignored since it is not relevant. Rewriting the equation, we obtain:

$$u(X + dX) = u(X) + w(X) \cdot dX + \varepsilon(X) \cdot dX \tag{1.3}$$

Where **w** and **ε** are, respectively, antisymmetric and symmetric tensors described as it follows:

$$\varepsilon(X) = \frac{1}{2}[\nabla u(X) + \nabla u(X)^T] \qquad w(X) = \frac{1}{2}[\nabla u(X) - \nabla u(X)^T] \tag{1.4}$$

The form of the strain tensor referred to a set of general directions $\{x_1, x_2, x_3\}$ is the following:

$$\varepsilon = \begin{bmatrix} \varepsilon_i & \frac{1}{2}\gamma_{ij} & \frac{1}{2}\gamma_{ik} \\ \frac{1}{2}\gamma_{ji} & \varepsilon_j & \frac{1}{2}\gamma_{jk} \\ \frac{1}{2}\gamma_{ki} & \frac{1}{2}\gamma_{kj} & \varepsilon_k \end{bmatrix} \tag{1.5}$$

$$\varepsilon_i = \frac{\partial u_i}{\partial x_i} \qquad \gamma_{ij} = \frac{\partial u_i}{\partial x_j} + \frac{\partial u_j}{\partial x_i}$$

Where u_i represents a general component of the displacement function and x_i stands for one general direction. The direct components are written in the diagonal, while the other quantities are the so-called shear strain components.

Because of the symmetry of **ε**, it is always possible to identify a triplet of eigenvectors such as the strain tensor is diagonal, where the diagonal terms are the so-called principal strains $\{\varepsilon_1\ \varepsilon_2\ \varepsilon_3\}$. Since this study is limited to the mechanical analysis of fibers in traction tests, it is sufficient to reduce the problem to 1D, considering only the strain component in the direction of the fiber axis.

Thus, in the range of small deformation we can the nominal strain ε of a material line element or fiber, as the change in length ΔL per unit of the original length L_0 of the line element or fiber, defined as in the following equation:

$$\varepsilon = \frac{L-L_0}{L_0} = \frac{\Delta L}{L_0} = \frac{L}{L_0} - 1 \tag{1.6}$$

For the definition of ε, normal strain is positive if the material fibers are stretched and negative if they are compressed.

This simplification can be used in deformation range under 3% of the initial length, but SF fibers can reach much higher deformation at break, so a correction must be made. Let's assume a fiber of initial length l_0 to which a force is applied to bring it to the length l. We can think to subdivide the deformation in n steps, each one small enough to apply the small deformation theory. Thus, we can express the deformation in one step as:

$$\varepsilon_i = \frac{l_{i+1}-l_i}{l_i} \tag{1.7}$$

So, to bring the fiber to the desired length with an arbitrary number of steps we have:

$$\varepsilon = \lim_{n\to\infty} \sum_{i=0}^{n+1} \frac{l_{i+1}-l_i}{l_i} \tag{1.8}$$

Considering infinitesimal increments, we can write the equation to the *true strain e* as it follows:

$$e = \int_{l_0}^{l_f} \frac{(l+dl)-l}{l} = \int_{l_0}^{l_f} \frac{dl}{l} = \ln\left(\frac{l_f}{l_0}\right) \tag{1.9}$$

Combining equation (1.6) to the last obtained, we have that the true strain is correlated to the engineering strain from the simple relationship:

$$e = \ln(\varepsilon + 1) \tag{1.10}$$

From now on, talking about the mechanical characterization of the fibers *e* will be assumed as the main definition of strain.

The other quantity that we need to characterize the fibers in a tensile test is the measurement of the stress that arises in the fibers when a deformation is imposed. From the continuum mechanics we can introduce the stress vector *t* defined by:

$$t = \frac{dF}{dA} \tag{1.11}$$

Then, **t** represents the density of an infinitesimal force dF applied over an infinitesimal section dA. So, its unit is equivalent to a pressure one. Applying stress theory and Cauchy fundamental hypothesis, we know that t is dependent on the material points reference position **X** and on the normal direction *n* relative to a section of the body. At this point we can divide t in two components, one acting in the same direction of ***n*** called normal stress (σ) and one acting tangentially to the surface, called shear stress (τ). Thus, we can define the stress tensor referred to a general set of direction $\{x_1, x_2, x_3\}$:

$$\sigma(X) = \begin{bmatrix} \sigma_i & \tau_{ij} & \tau_{ik} \\ \tau_{ji} & \sigma_j & \tau_{jk} \\ \tau_{ki} & \tau_{kj} & \sigma_k \end{bmatrix} \tag{1.12}$$

In the same way as the deformation tensor, **σ** is symmetric and thus it can be reduced to a triplet of principal stress $\{\sigma_1\ \sigma_2\ \sigma_3\}$. For the assumption of uniaxiality of the tensile test, we can reduce the whole tensor to the only scalar value σ.
Finally, we have the formulation of the uniaxial stress for small strain from equation (1.13):

$$\sigma = \frac{F}{A} \tag{1.13}$$

In this definition the surface A is considered as the initial one in every instant. This assumption is not true when large strain is reached.
Finally, one of the most important mechanical parameters in defining materials properties can be introduced as it follows.

$$E = \frac{\sigma}{\varepsilon} \tag{1.14}$$

E is called Young's modulus or elastic modulus and represents the slope of its stress–strain curve in the elastic deformation region.

Fibroin volume constancy should be investigated to characterize its mechanical behaviour.

Regarding the fibroin fibers, in the work of Guinea et al.[9] is proved the volume constancy of silk in the following experimental way.

Strained volume V was computed as the product of the actual fiber length, L, times the actual cross section, A, calculated form the diameter measured on the strained fiber with scanning electron microscopy.

$$V = AL \qquad V_0 = A_0 L_0 \tag{1.15}$$

To deduce the initial volume, both the initial fiber length L_0 and the initial cross-sectional area A_0 were considered. The initial area A_0 was obtained from the averaged diameter, φ_0 measured to both ends of the fiber tested. The volume ratio was calculated as:

$$\frac{V}{V_0} = \frac{A/A_0}{L/L_0} = \left(\frac{\varphi}{\varphi_0}\right)^2 (1+\varepsilon) \tag{1.16}$$

with φ being the fiber diameter at the engineering strain ε. Figure 1.7 shows the plot of V/V_0 as a function of the engineering strain e. Although some scatter appears, all the experimental points lie around the horizontal line that indicates the volume constancy condition $V=V_0$. Different points are used for points of the same silking process, indicating that the fiber production doesn't affect the volume constancy assumption. The mean value and standard error of all the measurements is 0.933 ± 0.013, so the stretching of silk fibers can be considered to proceed at almost constant volume. Anyway, volume variation of about 15% can't be completely ignored especially if they are found at strain around 10%.

Proved that, we can write the relationship of constancy as:

$$A_0 L_0 = AL \tag{1.17}$$

In this case, true and engineering stress are related by the following expression.

$$s = \sigma \frac{L}{L_0} = \sigma(1+\varepsilon) \tag{1.18}$$

At this point all the quantities implied in the tensile test are known and their use is well motivated.

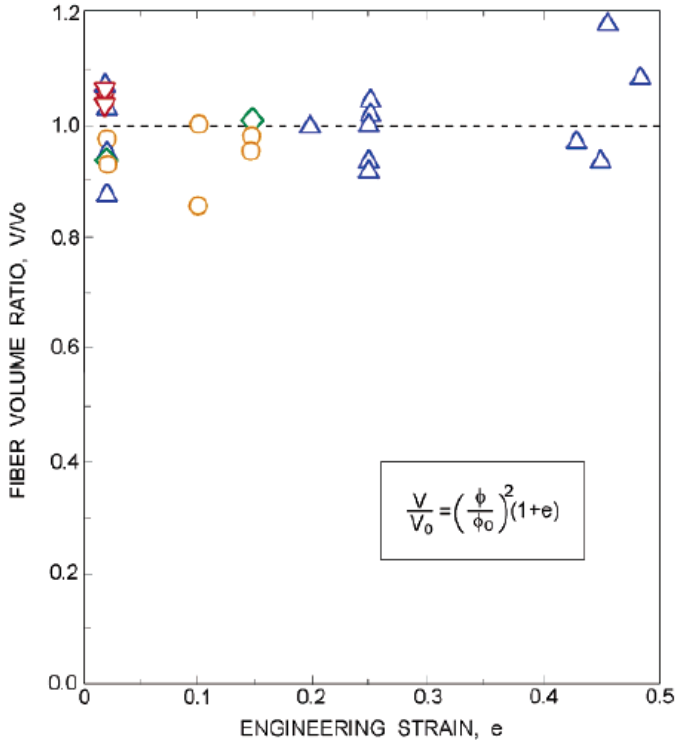

Figure 1.7 – Ratio between the volume of strained fibers and the initial volume as a function of engineering strain[9].

SF fibers has demonstrated outstanding mechanical properties. These include a large break strain (4-26%), ultimate strength (300-740 MPa) and toughness (70-78 MJm^{-3}). Toughness is the ability of a material to absorb energy and plastically deform without fracturing. It represents the strength with which the material opposes to the rupture. One definition of material toughness is the amount of energy per unit volume that a material can absorb before rupturing, and is defined as it follows:

$$\frac{energy}{volume} = \int_0^{\varepsilon_f} \sigma \, d\varepsilon \tag{1.19}$$

Where ε is the strain, ε_f is the strain upon failure and σ is the stress. In other words, the toughness represents the area under the stress strain curve, in this case the true strain – true stress one.
In addition, the reported toughness is higher than many synthetic fibers such as Kevlar (50 MJm^{-3}), carbon fiber (25 MJm^{-3}) and some collagens such as tendon collagen (7.5 MJm^{-3}).

Mechanical properties are listed in Table 1.1 along with those of other natural and synthetic fibers.

These impressive mechanical properties are closely related to SF hierarchical structures. The strength and stiffness are dictated mainly by β-sheet crystallites stabilized by a large amount of hydrogen bonds and van der Waals interactions, while the extensibility and toughness are governed mainly by the semi-amorphous matrix. Respectively, the matrix and the crystallites of silk govern its mechanical behaviour at small and large deformations during tensile loading. Upon tensile loading, the material undergoes homogeneous stretching until it reaches the onset of yielding, when the material starts to deform plastically, and the deformation can't be completely recovered. This is when the semi-amorphous components start to unravel, after which the load is transferred to the β-sheet crystallites, that subsequently handle the load up to the point of fracture. In the Figure 1.8 the average behaviour of a silk fibroin. Since it is a bio-produced material it has an intrinsic variability that depends on many factors.

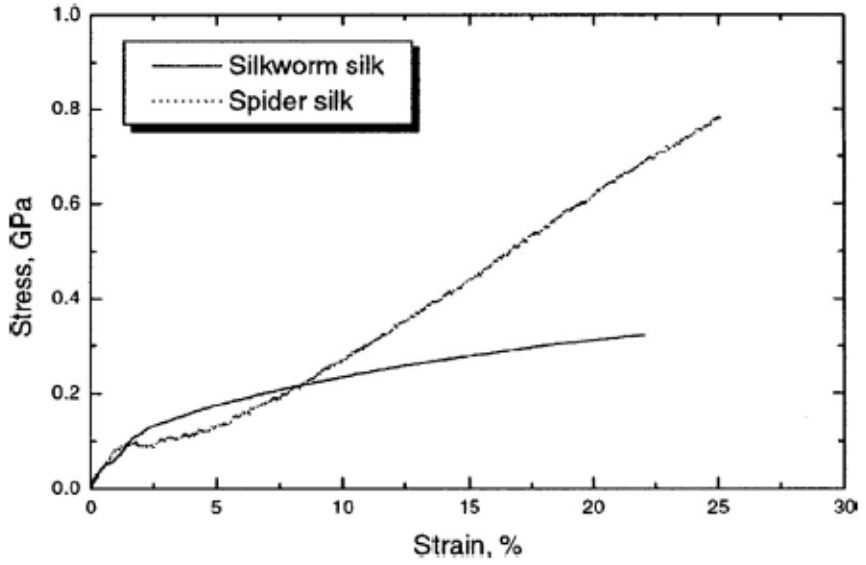

Figure 1.8 – Typical stress-strain curve for the single filament of silkworm silk (*Bombyx mori*) along with that of spider silk tested in air[2].

Materials	Young's Modulus (GPa)	Ultimate strength (MPa)	Breaking at strain (%)	Toughness (MJm^{-3})
Silkworm silk fibroin (Bombyx mori)	10 -17	300-700	4-26	70-78
β-sheet crystallites (Bombyx mori)	16-18	-	-	-
Spider silk (Araneus)	10	1100	27	160
Collagen	0.0018-0.046	0.9-7.4	24-68	-
Wool	0.5	200	50	60
Nylon	1.8-5	430-950	18	80
Kevlar	130	3600	2.7	50
Polypropylene	4.6	490	23	-

Table 1.1 – Mechanical data of silkworm silk compared to other fibrous materials as reported by Koh et al.[2]

Another thing to bear in mind is that SF scaffolds in biomaterial engineering are normally made from Regenerated Silk Fibroin (RSF) solutions and the produced scaffold are usually brittle and weak. The poor mechanical properties of regenerated silk as compared to native silk fibers are often attributed to the protein degumming and dissolution processes, during which some level of chain hydrolysis inevitably occurs. This creates fibers that lacks hierarchical and secondary structures compared to unprocessed raw SF fibers. The mechanical properties of the regenerated silk have been enhanced considerably through various processing strategies depending on the final application. Various factors, including fibroin concentration, processing temperature, methanol/salt treatment, water annealing treatment, pore size/distribution, blending the solution with other molecules to create composites, crosslinking, 3D bioprinting and spinning methodologies are known to affect the mechanical properties of fibroin regenerated silk and can thus be adopted as strategies for mechanical enhancement. Among these, variations in the spinning processes are the easiest to realize and they do not require pre-treatment of the solutions.

1.4 – Objectives of this work

Knowing all the remarkable mechanical, biocompatibility and biodegradability properties illustrated in the previous paragraphs, is clearly understandable why silk fibroin is increasingly studied and applied to the field of biomaterials and tissue engineering in the recent years. This study aims to investigate the possibility of creating tubular guides for the regeneration of medium-small blood vessels based on regenerated fibroin fibers produced with an innovative technique called Straining Flow Spinning (SFS) that allows to obtain fibers of controlled diameter and with improved mechanical characteristics compared to classic spinning techniques.

Given the great toughness at breaking of the material, which at the same time shows great characteristics of stress and strain at breaking, and the proven adaptability as a substrate for the growth of different cell lines, it can be imagined that SF leaves freedom to the cells to migrate and start the healing process without triggering excessive inflammation in the graft region and, at the same time, that it can ensure mechanical stability to the tubular framework until complete substitution with native structure. In addition, SF is an economic material and highly available in nature, characteristics that could lead fibroin fibers to be applied in the clinical field in a brief time.

The existing tubular guides are usually developed along a single axis, excessively simplifying the native system and therefore limiting their applicability to sections that are not located at branches. The possible achievement of a branched guide would be a great step forward to better simulate the intrinsic complexity of the vascular structure. To investigate this possibility, degradation kinetics of SF fibers subjected to enzymatic degradation by the enzyme proteinase K, known to rapidly degrade distinct types of silk, will be studied with methodologies which will be explained later. The results of macroscopic degradation and the effect it has on the mechanical behavior of SFS spun SF fibers will be presented. Based on the results acquired, the best enzymatic concentration to obtain a sufficient level of degradation to hypothetical join two tubular guides without affecting mechanical stability will be discussed.

2 – Production of SFS regenerated silk fibroin fibers

2.1 – Fibroin degumming and dissolution

Proper dissolution of SF is an essential step before processing it into different structures for various applications in tissue engineering. The procedure applied in this work to create the RSF solutions will now be explained.

The first step to take is to weight the desired mass of the cocoons and dissolve them into a solution. In this study each solution was obtained from 5 grams of raw silk. The cocoons are then cut and divided into small pieces to expose more surface. Once the raw silk is ready, a solution of 2 litres of distilled water (with a conductivity of 10 μS) is prepared to reach the boiling temperature. This solution will be named degumming solution from now on since its aim is to eliminate the sericin from cocoons silk.

2 grams of Sodium Carbonate (Na_2CO_3) per litre of degumming solution are added. This decreases the molecular weight of the regenerated solution to 55 kDa as described by Perez-Rigueiro et al.[10] to obtained easier to spin and less coagulating solutions in the spinning technique. It also lowers the boiling temperature and speeds up the process.

A stirring protocol of one minute performed with cleaned spoon is taken every five minutes of boiling to spread the woven and ensure high quality degumming. During this study different time intervals (20, 15, 10 minutes) have been explored to characterize the degradation kinetics of fibers derived from solutions at each degumming time. As soon as the degumming process ends, the fibroin skein is rinsed and squeezed twice in normal water to decrease its temperature, then other two times in deionized water to eliminate every residue of sericin that might have been remained on the surface. After being rinsed, the woven is unfold and spread over a cleaned surface and left to dry at room temperature overnight. To ensure that the skein is completely dry, it is put in the oven at 60°C for at least 20 minutes.

The second step in preparing a silk fibroin solution is to dissolve the degummed silk fibers. This dissolution step is inhibited by the strength of the hydrogen bonds and the hydrophobic nature of the β-sheet crystallites of silk fibroin. Proper dissolution of SF is essential to process it into various applications. Therefore, a rigorous dissolution protocol is necessary for the complete and correct dissolution of the obtained woven.

SF is insoluble in water-based solvents because of its highly packed structure which has a high content of β-sheets structures. To dissolve it in aqueous solutions, it must undergo a water-based dissolution process avoiding toxic solvents and solutions as regenerated SF is used for biological applications. Typically, concentrated salt solutions with various concentration of salt ions (Ca^{2+}, Sr^{2+}, Li^{2+}, Zn^{2+}) in combination with anions (Cl^-, Br^-,) are employed to dissolve

SF fibers. In this work the protocol designed by Rockwood et al.[11] will be applied and accurately explained.

Fibroin will be dissolved in a Lithium Bromide (LiBr) 9.3M solution in 20% w/V. The calculations for the quantities are based on the dried fibroin available. As 20% of the solution will be silk, 80% will be LiBr.

The following equation is used to obtain the final volume of the solution based on fibroin mass:

$$Solution\ Final\ Volume\ [ml] = \frac{Fibroin\ mass}{w/V\ ratio} \quad (2.1)$$

Once the final volume is known, it is possible to calculate LiBr mass to reach a solution of 9.3 M.

$$m_{LiBr}\ [g] = MW_{LiBr} * Molar\ concentration_{LiBr} * Solution\ final\ volume \quad (2.2)$$

Where m_{LiBr} stands for the LiBr mass, molar concentration is set at 9.3 mol/L, LiBr molecular weight is constant ad values 86.845 g/mol and the solution final volume is given in mL. Knowing LiBr mass and its density, which is 3.46 g/cm^3, it's possible to calculate the LiBr volume, and subsequently the distilled water volume to dissolve it in.

$$Final\ Volume\ H_2O\ [mL] = Solution\ final\ volume - \frac{m_{LiBr}}{\rho_{LiBr}} \quad (2.3)$$

An example of the volume results for 3.7 g of fibroin in 9.3 M LiBr solution is reported in table 2.1.

Final volume [mL]	LiBr mass [g]	LiBr volume [mL]	H_2O volume [mL]
18.5	14.94	4.32	14.18

Table 2.1 – Example of calculation of the solution component to dissolve 3.7 g of degummed fibroin.

The reaction is highly exothermic, so the compound must be added gradually to the distilled water. Once the solution is ready, the fibroin mass is put in a 50 ml glass and the solution is gently poured over the skein, trying to wet all the fibers. LiBr should be added to the silk rather than adding silk to the LiBr so that the silk will eventually be covered and dissolved by the

LiBr. It is also helpful to use the smallest glass container that will still hold the silk and LiBr solution.

LiBr rapidly starts to degrade the silk II β-sheet crystallites into α-helix silk I state, which is soluble, forming a gel-like substance. The process requires incubation at 60°C for 4h hours to totally complete the transformation of the fibroin mass. Once the silk fibroin is completely dissolved, it will appear amber in colour and will be transparent. Greater particles may be visible but will be removed later. This solution will be highly viscous but should not contain any intact fibers, as determined by visual assessment.

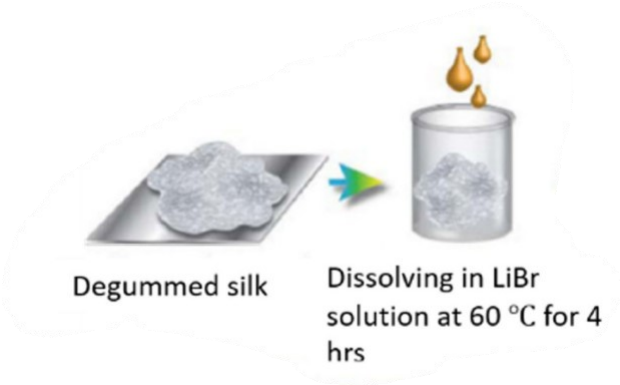

Figure 2.1 – Simple representation to transform degummed silk into a fibroin-LiBr solution.

2.2 – Dialysis and reverse dialysis

After the four hours of dissolution, it is necessary to realize a dialysis protocol to eliminate the over excessive ions. Dialysis works by concentration gradient diffusion, until an equilibrium is reached. In dialysis, unwanted molecules inside a sample-chamber diffuse through a semi-permeable membrane into a second chamber of liquid or dialysate. Because large molecules cannot pass through the pores of the membrane, they will remain in the sample chamber. By contrast, the small molecules will freely diffuse across the membrane and obtain equilibrium across the entire solution volume, effectively reducing the concentration of salts within the sample.

The fibroin-LiBr solution is directly poured into a 3.5 kDa cut-off membrane locked by two clips in the edges as can be seen in Figure 2.2. The dialysis process is the most time demanding step in the creation of RSF solutions and it lasts up to 72 hours with several water changes.

Firstly, the solution is submerged in room temperature deionized water with a magnetic agitator for one hour and stored in a refrigerated room at 4°C. In this step the ions gradient is the strongest and water quickly absorbs great amount of salts. To check if the process is correctly working, measurements of the water electrical conductivity are taken. Pure water is collected at 10 μS conductivity while after one hour dialysis it is found to be in the range of mS. After the first water change, the salts exchange slows down and another 4 dialysis cycles are carried out (alternatively of 6h and 18h) until the conductivity of the water returns in the range of hundreds of μS.

Once the dialysis protocol is finished, a small amount of solution is collected to check the actual concentration of fibroin. 100 μL of solution are picked up by a pipette and distributed in a previously weighed plastic dish. As soon as the solution is poured, another weight measurement is taken, then the dishes are left in a 60°C degree oven for a few minutes to completely dry the solution. In this way only a thin fibroin film will remain. Last weighing will be performed after the drying process. An example of the calculations is reported in Table 2.2.

Plate number	Plate mass [g]	Plates + Fibroin solution [g]	Plates + Dry fibroin [g]	Fibroin Concentration [%]
1	1.7269	1.8240	1.7309	4.12
2	1.8736	1.9796	1.8781	4.24
3	2.0691	2.1691	2.0735	4.40

Table 2.2 – Example of calculation of the fibroin concentration after the dialysis process. The concentration depends on the dialysis time but generally it is found to be around 4%.

To determine the fibroin concentration the equation (2.4) is used where m_{dry} represents the plate and fibroin film mass, $m_{solution}$ represents plate and fibroin solution mass and finally m_{plate} represents the mass of the plate only.

$$Concentration\ [\%] = \frac{m_{dry} - m_{plate}}{m_{solution} - m_{plate}} \tag{2.4}$$

Three repetitions of the measurements are always done to ensure an accurate estimation of the fibroin concentration. Normally after 3 days of dialysis a solution with an average concentration between 4% and 6% with a maximum SD of 0.5 is obtained. This value is important to know to decide the reverse dialysis time to concentrate the solution up to the target concentration.

Figure 2.2 – Cut off membranes after dialysis and reverse dialysis.

The dialyzed fibroin solution has now to be centrifuged to discard all the possible residues like silk filaments or macromolecules that were not dissolved completely. The fluid is poured into a falcon (such as the ones observable in Figure 2.3). To ensure a symmetrical disposition the

solution can be split into two falcon or another one, filled with water, can be used. In this way the weight is balanced and stability at high speed is maintained.

The solution is centrifuged at 5000rpm for 20 minutes at 4°C. The desired speed is reached through a 3-minute ramp acceleration setting and this process (as the deceleration one) should be supervised to avoid any complication.

To reach the desired temperature a centrifugation cycle must be undertaken until the machine cools down. If the cooling cycle is not done, there might be a gelification risk during the centrifugation.

After the centrifugation protocol, stuck at the bottom residues are observable in the falcon. The cleaned solution is transferred to a new falcon or directly into another dialysis membrane to undertake the reverse dialysis.

The reverse dialysis step is fundamental since it has been demonstrated by many studies that fibroin solution at poor concentrations will hardly be spinnable, in particular with the SFS technique. The process works in the same way as described before, but in the opposite direction, with a molecules flow towards the dope inside the membrane.

The reverse dialysis medium consists of a solution of Calcium Chloride 1M ($CaCl_2$), polyethyleneglicole 8000 (PEG 8000) 10% w/v and tris(hydroxymethyl)aminomethane (TRIS) 50mM in 500 ml of distilled water. PEG 8000 is a thickener agent with a medium molecular weight of 8000 Da, while TRIS is extensively used in buffer solutions. $CaCl_2$ is the most important component of the reverse dialysis medium since, as reported by Madurga et al.[12], it is found that fibroin solutions without it gel at concentrations of ~10% (w/v). In fact, when the reverse dialysis proceeds against the 1M $CaCl_2$ aqueous solution it is considered that the final concentration of $CaCl_2$ in the dope is 1M, assuming that equilibrium is established between the medium and the dope at the end of the process.

Equation 2.2 is used to determine the $CaCl_2$ and TRIS masses where molecular weights and molar concentrations varies for each component and a 500 mL solution volume is considered. It's easier to calculate PEG mass as it is one tenth of the water volume. The masses of each component to be dissolved are reported in Table 2.3.

Mass of PEG 8000 [g]	**Mass of $CaCl_2$ [g]**	**Mass of TRIS [g]**
50	73.51	3.03

Table 2.3 – Masses of the components to produce the reverse dialysis solution.

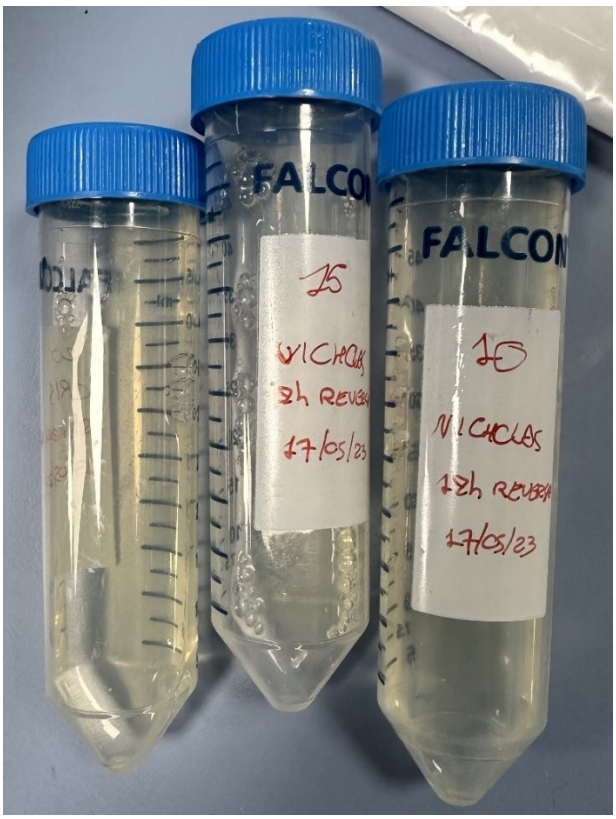

Figure 2.3 – Falcons containing silk fibroin solution at different degumming times, ready to be spun. From left to right the degumming time are 20, 15 and 10 minutes. Is possible to appreciate the typical yellowish colour of this solutions.

Once the reverse dialysis medium is complete, the dope is submerged in it with a magnetic agitator in the same fashion described before to ensure a good diffusion process. Temperature control at 4°C acquires more importance in this step to avoid spontaneous gelification at higher concentrations. Depending on the final fibroin concentration that one wants to achieve, the reverse dialysis can last different times. As already mentioned, solution from 14% up to 20% of fibroin concentrations were used in this study, so the different dwell times are reported in the following table. To determine the concentrations the same procedure described in the dialysis step is adopted and the results from the example in Table 2.2 is reported in Table 2.5.

Fibroin final concentration	**Reverse dialysis time**
14-15%	14 hours
15-16%	14-16 hours
16-18%	16-18 hours
20-22%	>18 hours

Table 2.4 – Fibroin solutions concentration depending on permanence time in reverse dialysis solution.

Plate number	Plate mass [g]	Plates + Fibroin solution [g]	Plates + Dry fibroin [g]	Fibroin Concentration [%]
1	1.8314	1.9124	1.8433	14.69
2	1.8733	1.9757	1.8892	15.53
3	1.8330	1.9366	1.8489	15.35

Table 2.5 – Example of mass data for the fibroin final concentration determination after reverse dialysis.

Once the desired concentration is obtained, the dope is ready to be spun and can be stored again in a falcon at 4°C. A schematic summary of the whole procedure is represented in Figure 2.4.

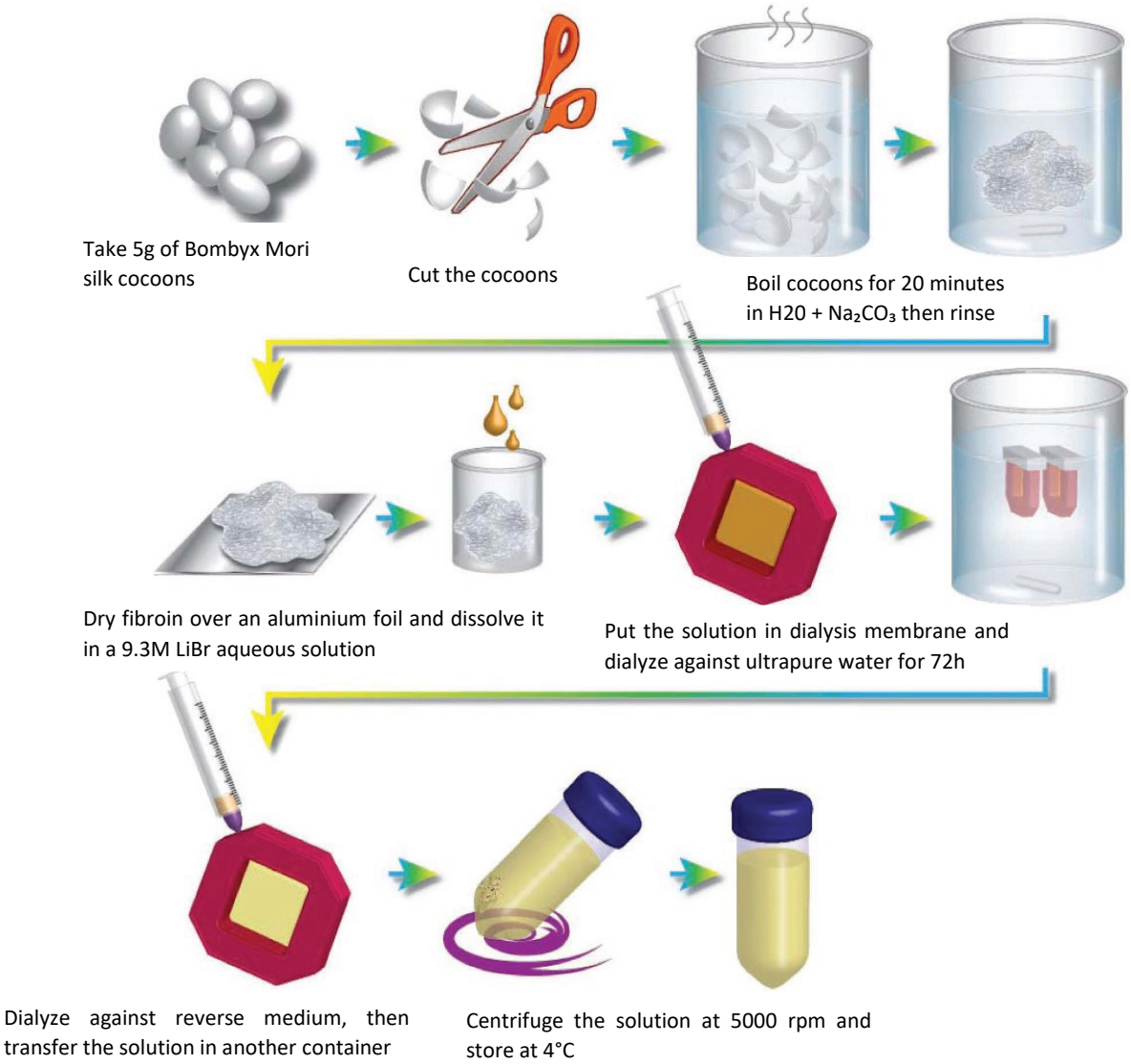

Figure 2.4 – A schematical representation of the LiBr dissolution process to obtain RSF solution. The degummed silk (20 minutes) is dissolved in 9.3 M LiBr solution at 60 °C for 4 h. The obtained solutions are dialyzed against ultrapure water to remove salt until a conductivity of < 10μS is reached. RSF solutions are centrifuged and stored at 4 °C.

2.3 – Fibers regeneration through Straining Flow Spinning

Biological silk production systems, which evolved independently in both silkworms and spiders, seem to converge, displaying several common spinning elements. Based on these similar characteristics, human manipulated fiber spinning systems should incorporate these common underlying principles, specifically (1) distinct zones of processing, (2) a combination of chemical and mechanical stimuli, and (3) an integrated process for spinning and drawing. The current simplified approach to silk spinning has led to the evolution of several different fiber spinning systems: (A) electrospinning, (B) wet-spinning, (C) dry-spinning, and (D) microfluidic spinning, reported in the study by Hoffman et al.[13] and synthesized in Figure 2.5. A brief overview of each method will be taken to introduce the state of the art of fibroin spinning.

As reported by Zhu et al.[14] electrospinning is an attractive method of producing fibers with diameters ranging from micrometres down to tens of nanometres. The electrospun silk fibers posses high specific surface area, high porosity and good biocompatibility. The electrospinning process is somewhat analogous to the spinning process of silkworm: after undergoing a shear flow in the tube and capillary, the jet of the solution is also elongated in air, although the elongation effect of electrospinning process is much stronger than that of the spinning process of silkworm. Nevertheless, electrospinning usually involves solvents (e.g. polyethylene oxide (PEO)), which can adversely affect biocompatibility.

When a sufficiently high voltage (kV range) is applied to a liquid droplet, the body of the liquid becomes charged, and electrostatic repulsion counteracts the surface tension and the droplet is stretched. At a critical point, a stream of liquid is ejected from the surface. As the stream flows, the liquid evaporates and only the polymer is left. The electrospun silk fibers, with high specific surface area, high porosity and great biocompatibility, have extensive applications in the field of biomaterials, such as wound dressing, scaffolds for tissue engineering and drug delivery. Also silk non-woven and mats can be efficiently produced, but the tensile properties of the individual fiber tend to be poor. Moreover, electrospinning is a technique that strongly alters the solution properties, especially for the strong electric field to which it is exposed. For these reasons it seems not useful to this study's aim to create resistant SF fibers.

Wet spinning is an easier process that tries to replicate the natural spinning by silkworms using specific solvents. It basically consists in the extrusion of the polymeric solution, in this case a classic LiBr-SF solution, through a spinneret into a coagulation mixture. Due to the mutual diffusion, the solvent molecules are removed, resulting in the assembly of the silk protein and in the formation of the fiber. These fibers can undergo different post processing step to tune their morphological and mechanical characteristics, especially their handleability. Fibers

obtained with this method are larger in diameter and continuous, but the use of chemical solvent comes with the risk of protein degradation and possible cytotoxicity when implanted in biological organisms.

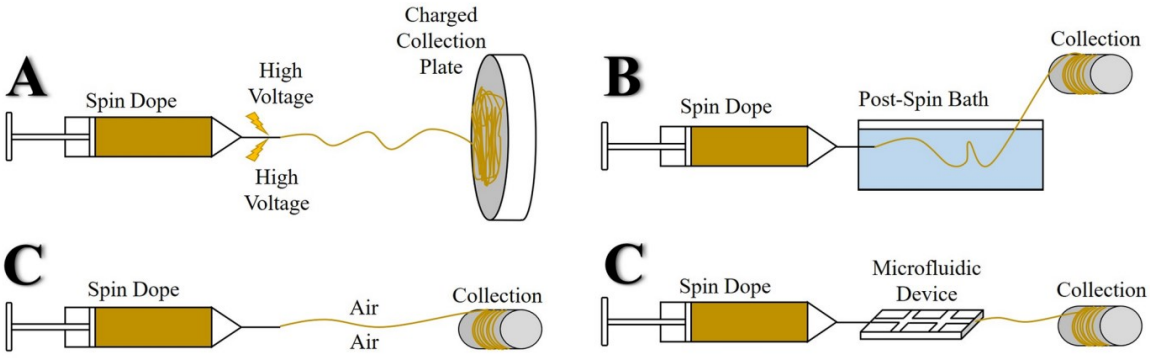

	Spinning Techniques	Diameters (um)	Disadvantages	Advantages
A	Electrospinning	0.03 - 1.8	Fiber Mats, Non-continuous Fibers, Dependent on Spin Dope	Small diameters, mechanical shear elongation, reliable scaffold material
B	Wet-spinning	10 - 60	Solvent Protein Degradation, Extensive post processing, Chemical Solvent Baths	Simple, High Productivity, Slower Spinning Higher Protein Alignment
C	Dry-spinning	15 - 20	Volatile Solvent System, Chemical Post-Treatment Processing, Lower Tensile Strength	Quick Fiber Formation, Uniform Continuous Fibers
D	Microfluidic Spinning	10 - 45	Continuous Uniform Fiber Production, Low Productivity	Small Geometry, Mimic Silk Flow Conditions, Small Amounts of Silk Spin Dope

Figure 2.5 – Multiple presented techniques to spin silk fibers synthetically**.** Popular silk spinning techniques including collected diameter value ranges with advantages and disadvantages of each technique.

Dry spinning is a variation of wet spinning in which the solvent evaporates to a gaseous environment instead of being removed through the interaction between the dope and the coagulating bath. This technique doesn't imply the use of chemical solvents for coagulation, replicating the dry spinning process of silkworms. Unfortunately, the SF fibers obtained with this method are extremely fragile and not mechanical resistant, although other studies as the one realized by Jin et al.[16] have found fibers with good tensile properties. Generally, they also require more treatment after the spinning process in a more complex setup compared to wet spinning.

Microfluidic devices have recently been implemented in the spinning process to exert more control on spinning parameters such as shear stress. Standing to the Liu et al.[15] study, silk fibers dry-spun from RSF aqueous solution using chips could be tougher than degummed natural silk. Anyway, to the aim of this study, much material is needed and the implementation of a microfluidic chip would have required too much time and low amount of fibers obtained.

In addition to these conventional spinning techniques, the increased knowledge on the principles of the natural spinning process has led to the development of a few biomimetic approaches that try to exploit these principles, for instance, the dependence of the natural assembly process on the pH of the solution. As reported by Madurga et al.[17], comparison of the natural spinning system in both silkworms and spiders with the artificial techniques reveals the convenience of the following: (1) increasing the interaction time between the dope and the coagulating bath in order to allow for the required conformational changes of the proteins to occur, (2) using a procedure that ensures controls geometrically (and stress induced) protein reorganization undergone by the dope proteins during spinning. Moreover, as mentioned before, regarding physiochemical condition, most artificial fibers have been produced by using toxic solvents and/or coagulants, or by placing them under aggressive environmental conditions.

Focusing on these characteristics, a new biomimetic approach called Straining Flow Spinning (SFS) have been developed in the last few years. This new spinning process is inspired in flow focusing technology and seeks to mimic certain characteristics of natural spinning like the ion exchange during the spinning process between the dope and the surrounding media.

The schematic experimental setup of the SFS technique is shown in Figure 2.6 from the work of Madurga et al.[17] where all its components can be appreciated.

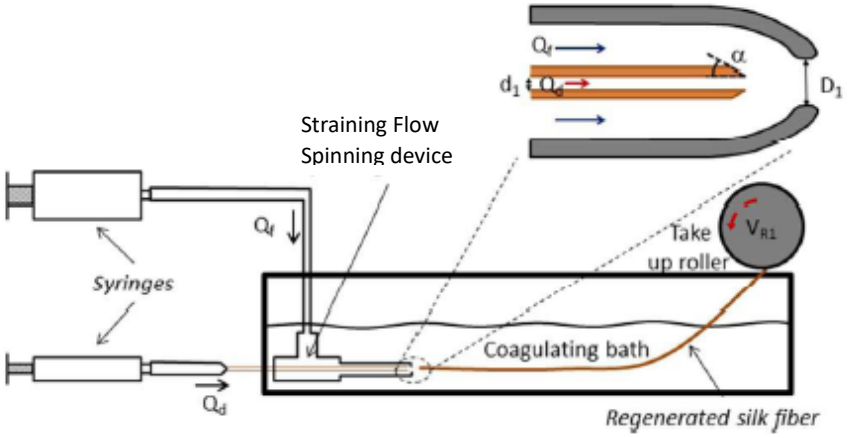

Figure 2.6 – Schematic representation of the straining flow spinning device and the main processing parameters: diameter of the orifice of the nozzle, D1, inner diameter of the capillary, d1, tapering angle at the end of the capillary, α, speed of the take up roller, VR1, and flow rate of the focusing fluid, Qf, and of the dope, Qd.

The core of techniques consists of a coaxial capillary nozzle system so that the nozzle presents a convergent profile in the outlet region. The capillaries are produced through a pulling machine (Figure 2.7) that heats up to a desired temperature the separation region of the glass tube inserted. Examples are reported in Figure 2.8. Then the outlet is created firstly by using

sandpaper 600 grit to remove most of the material and then sandpaper 1000 grit to refine the outlet zone. The nozzles are controlled for crakes or residual particles with a microscope.

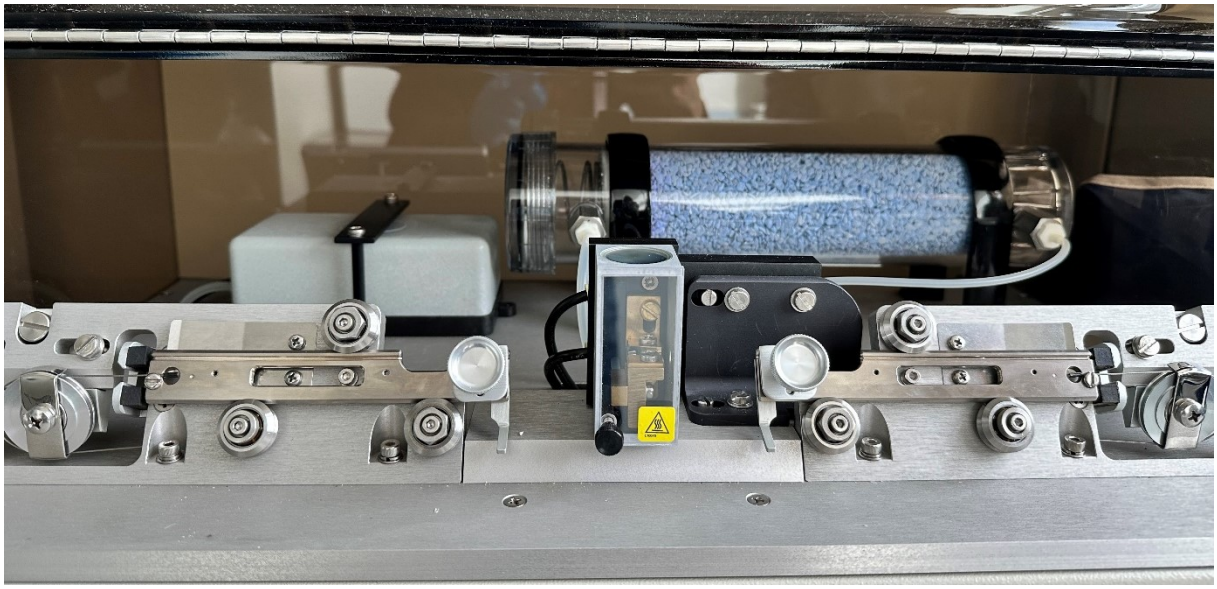

Figure 2.7 – Nozzle creating device. Nozzles are blocked by the aluminium plates and a heated ring applies heating cycles until separation in halves.

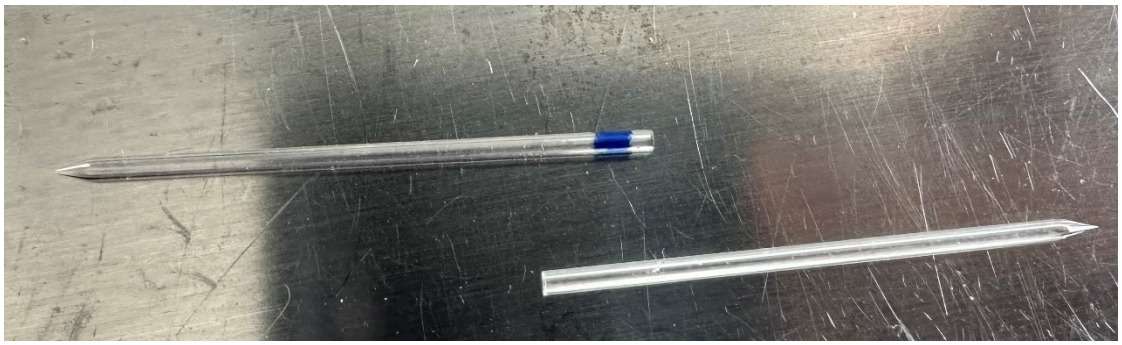

Figure 2.8 – Example of nozzles pre sandpaper treatment. The length of the nozzle is approximately 3 cm, while its outer diameter is 2 mm. Is possible to appreciate the conoidal separation site.

The dope and the focusing fluid flow along the capillary and in the region confined by capillary outer wall and the nozzle inner wall, respectively. Upon reaching the end of the capillary, a jet dope is formed and surrounded by the focusing fluid. Finally, both the dope and the focusing fluid enter a coagulating bath, which may have the same or a different composition to the focusing fluid one. The dope and focusing fluid flow rates are controlled by syringe pumps. The coagulated fiber is retrieved from the coagulating bath with tweezers and wound around a plastic sheet put around the take up roller to collect it. A post spinning drawing step may be added to the process, but it wasn't the case of this study. The experimental set-up is showed in Figure 2.9 which is a picture taken from above of the SFS device.

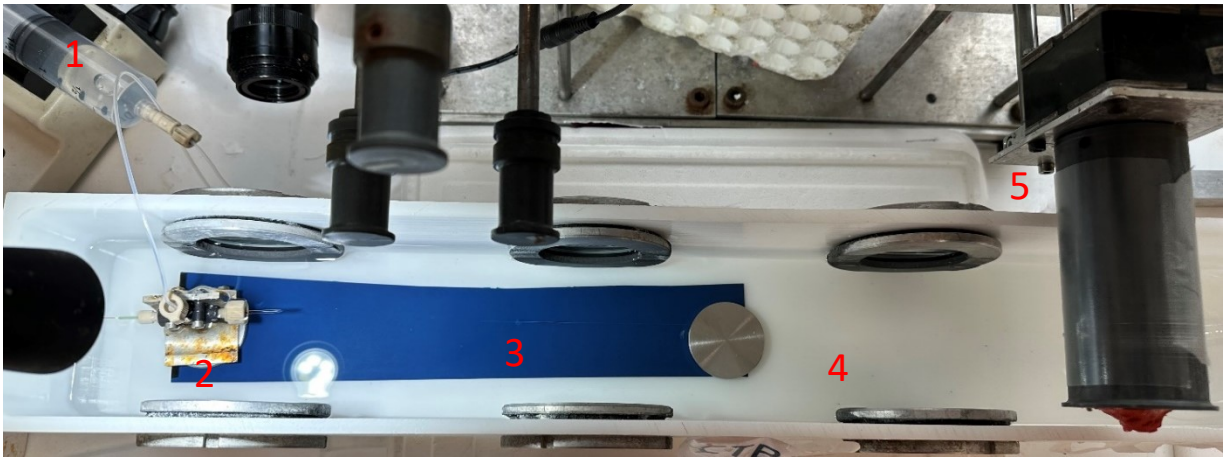

Figure 2.9 – Straining Flow Spinning experimental setup. (1) Syringe pump originating focusing fluid flow rate. (2) Nozzle-capillary assembly where both focusing fluid and fibroin dope flow confocally. (3) Light reflex on the SF fiber. It's difficult to see the fiber for their micrometric diameter, a steady light is used to help. (4) Coagulating bath composed by 80% ethanol and 20% acetic acid in distilled water, as well as the focusing fluid. (5) Take up roller with a plastic sheet to collect the fibers spun.

The comparison of SFS with other spinning techniques reveals one of its main singularities: its versatility in terms of control parameters number of the spinning process.

In this regard, as indicated in Table 2.6, the processing parameters in SFS can be divided into three groups: geometrical, hydrodynamic, and chemical. Generally, the geometrical parameters refer to the spatial assembly of the capillary–nozzle system and to the basic geometric features of their elements. The geometrical parameters comprise the inner and outer diameters of the capillary, the tapering angle at the end of the capillary, the distance between the end of the capillary and the nozzle outlet, the profile of the convergent region close to the nozzle outlet, and the nozzle outlet diameter. The hydrodynamic parameters correspond to the flow rates and speeds of the different components of the system and comprise flow rate of the dope, flow rate of the focusing fluid, velocity of the take-up roller, and in processes with a post-spinning drawing step, velocity of post-spinning drawing roller. In the following table only the parameters investigated in this study are reported.

The combined effect of the geometrical and hydrodynamical parameters controls the flow of both the dope and the focusing fluid, and more importantly their interaction. Finally, the chemical parameters comprise the compositions of the dope, the focusing fluid and the coagulating bath. The interaction between the two jets is represented in Figure 2.10, while the most important geometrical and hydrodynamic parameters are showed in Figure 2.11 along with their abbreviation.

Geometrical	Hydrodynamic	Chemical
• Capillary inner and outer diameter • Nozzle outer diameter • Capillary-nozzle outlet distance • Tapering angle • Convergent profile of the nozzle	• Flow rate of the dope • Flow rate of the focusing fluid • Velocity of the take up roller	• Composition of the dope • Composition of the focusing fluid • Composition of the coagulation bath

Table 2.6 – Resume of the geometrical, hydrodynamic and chemical parameters influencing the spinning and coagulation process in the SFS technique.

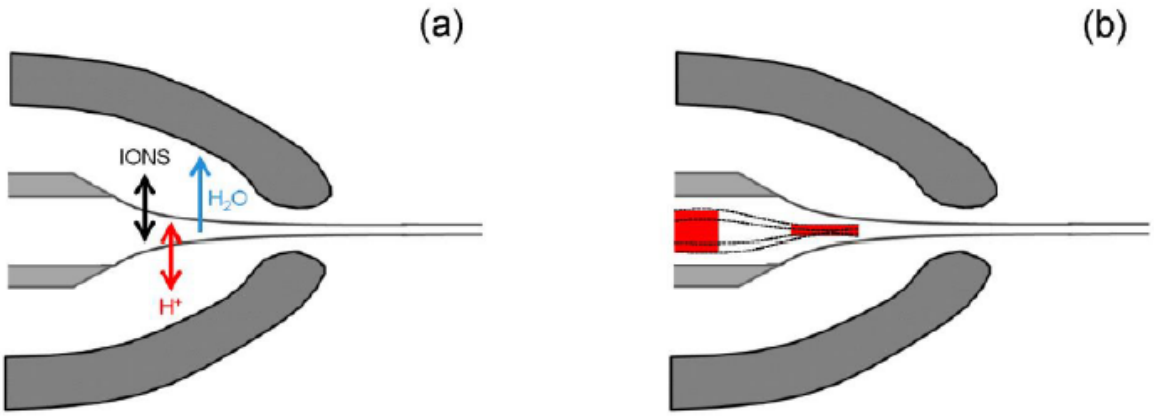

Figure 2.10 - Schematic of the basic processes that result from the interaction between the dope jet and the focusing fluid. (a) Diffusion processes include the exchange of ions, including protons and the removal of water molecules from the dope to the focusing fluid. (b) The hydrodynamic interaction of both fluids results in the deformation of the dope jet.

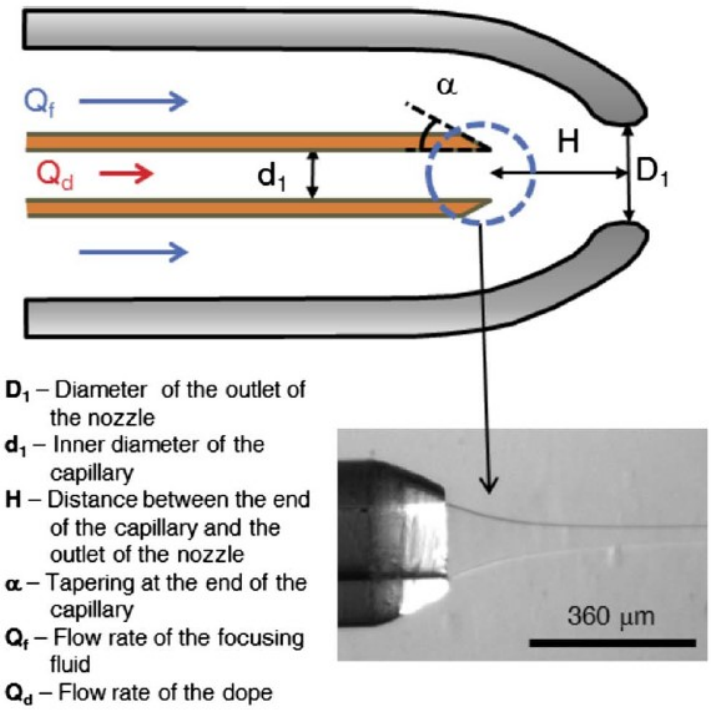

Figure 2.11 – Schematic close look at SFS nozzle-capillary assembly with explanation and abbreviation of all fundamental geometrical and hydrodynamical parameters. A new parameter H is introduced. Fibroin dope grey scale picture is showed to better understand the flow dynamic.

The geometrical and hydrodynamical parameters are determinant factors in triggering the conditions for molecular self-assembly of the SF proteins into a fiber. Thus, a physical understanding on the hydrodynamic process is crucial to achieve a complete understanding of the SFS technique.

It is apparent that the dynamics of the SFS process can be extremely complex. In particular, the dope might show a non-Newtonian behaviour as a consequence of the presence of the fibroin molecules. In addition, the diffusion processes between the dope and the focusing fluid are likely to yield a variation of the hydrodynamic parameters of the fluids throughout the process. In the study conducted by Madurga et al.[18] an attempt to establish a simple model to allow basic understanding of the SFS process is described.

The most important quantity to define is the Draw Ratio (DR), which is also indicated in other spinning techniques, expressed as the ratio between the velocity of the take up roller and the velocity of the dope jet in the extrusion unit. The velocity of the dope is calculated from the flow rate as:

$$V_d = \frac{Q_d}{\pi {d_1}^2} \tag{2.5}$$

Where d_1 and Q_d are the same parameters as explained in Figure 2.11.
DR is a critical parameter in the process since it's used to quantify the elongation rate applied to the fibers during the coagulation process. Contrary to the simple definition of DR in wet spinning, in SFS technique it's mandatory to introduce the focus speed of the dope U_s. Otherwise, it would imply that DR is independent from the behaviour of the focusing fluid. So, U_s is introduced to consider the dependence of the focused dope jet speed on both Q_d, Q_f and the geometrical parameters. Following the calculation reported in the study, the final approximation of U_s is given by:

$$U_s \sim \sqrt[3]{\frac{\rho_f \mu_f {Q_f}^3 Q_d}{{\mu_d}^2 {D_1}^7}} \tag{2.6}$$

Where ρ_f is the focusing fluid density in g/cm^3, μ_f is the focusing fluid dynamic viscosity and μ_d is the dope dynamic viscosity both in Pa·s, and Q_f, Q_d and D1 are as indicated in Figure 2.11. From a dimensional analysis is possible to check that U_s has the unit of a velocity.

The relation (2.6) allows definition of a fundamental draw ratio for the SFS process that considers the flow rates of the focusing fluid and dope and the geometry of the nozzle:

$$DR = \frac{V_{R1}}{U_s} \tag{2.7}$$

By varying the draw ratio is possible to affect the characteristics of the fibers like their diameters and their tensile strength. During this study different parameters have been tested aiming to enhance the mechanical properties of the fibers. This investigation will be discussed later, anyway, the best DR values are comprised between 1 and 10.
Another fundamental quantity to define the parameters influence on the fibers behaviour is the tangential stress applied to the dope jet. It is demonstrated that the coagulation process varies dependently on the stresses exerted on the dope, as in the natural spinning by silkworms.
In this regard, the pressure drop is assumed to represent an estimate of the shear stress supposed to induce coagulation and solidification into the jet. The pressure drop near the nozzle outlet can be estimated by applying Bernoulli's equation as:

$$\Delta P \sim \frac{\rho_f}{2} \frac{\left(4Q_f\right)^2}{\pi^2 {D_1}^4} \tag{2.8}$$

All the parameters are as explained above. This expression may be combined with the Reynold's number of the focusing fluid (Re_f) to yield:

$$\Delta P \sim \frac{8{\mu_f}^2 {Re_f}^2}{\rho_f \pi^2 {D_1}^2} \tag{2.9}$$

It is concluded that in processes in which the Reynold's number of the focusing fluid at the exit of the nozzle is kept constant, the pressure drop increases inversely to the square of the exit orifice of the nozzle. This is important because by changing the nozzle outlet diameter is possible to modify the whole coagulation process, giving the fiber a stronger structural organization.

Once determined the influence of the geometrical and hydrodynamic parameters on the coagulation process, the next step is to analyse the chemical parameters, in particular the composition of the focusing fluid and coagulating bath.

To not introduce another variable, the same composition was initially chosen for both the fluids. Many studies have been conducted on the influence of the coagulants on the regenerated fibers and their coagulating mechanism. Evidence of their influence on the fibers diameter, morphology and mechanical properties, both in air and water, depending on the dope fibroin concentration have been assessed, as well as the differences in solution with dehydrating and acidifying coagulating mechanisms. Combination of the two mechanisms lead to enhanced regenerated silk fibers and it is assumed that this enhancement is the result of a more efficient fibroin aggregation process driven by a pH drop as observed in natural spinning.

In light of the great versatility of the SFS setup, considerations done to select the best solution as a coagulating bath and focusing fluid among a wide choice are listed below:

- Assuming that SFS is a biomimetic technique that aims to easily recreate fibers using mild solvents, all the aggressive and volatile chemical agents that would have required working under aspiration were discarded.

- All the agents that don't provide a sufficient coagulation or an organized morphology of the fibers were discarded.

- Agents that don’t produce enough resistant fibers were discarded.

Considering these points, a mixture of Ethanol 80% and Acetic Acid 1M 20% in distilled water was selected and used all along this work. Ethanol-based solutions leads to a morphology and a secondary structure more similar to those of natural silkworms’ silk. This have been assessed by observing infrared spectra through FTIR technique. Amide I peak of regenerated fibers concurs with that of natural silk fibers and that all samples coagulated with the selected mixture have similar secondary structure. Although these are good findings, natural silk tensile properties are not reflected in the same fashion. It is for this reason that an acidifying agent such as acetic acid is present. The presence of this chemical in the coagulant of the SFS process was observed to improve spinning as the fiber spun broke with less or even null frequency during the drawing.

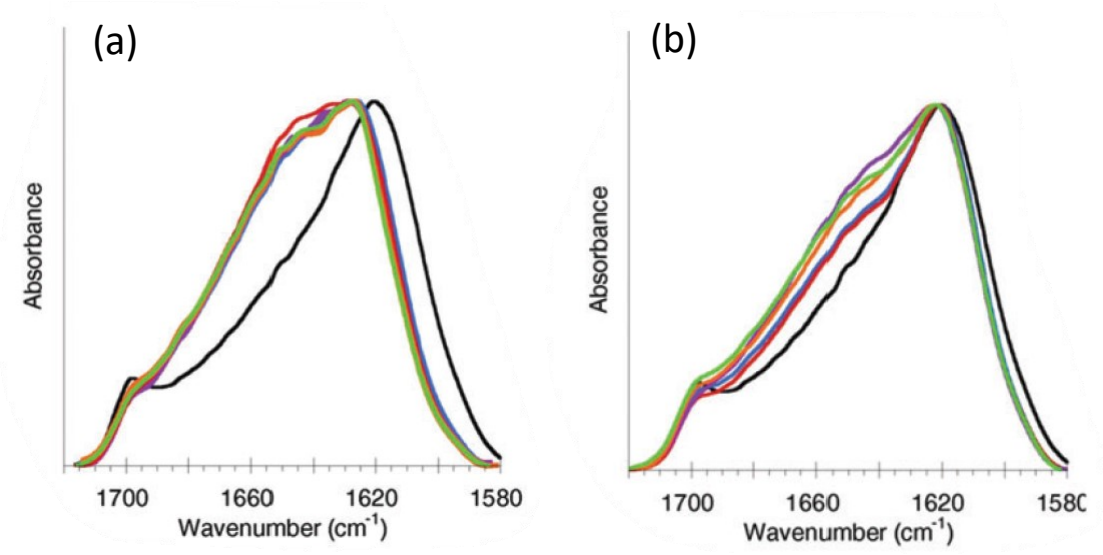

Figure 2.12 - (a) Representative attenuated total reflection-Fourier transform infrared spectroscopy amide I peak of fibers spun from dopes with several fibroin concentration in PEG solutions.
(b) Representative attenuated total reflection-Fourier transform infrared spectroscopy amide I peak of fibers spun from dopes with several fibroin concentration in ethanol and acetic acid solutions.
The spectrum of the degummed natural silkworm silk fiber (black) is shown for comparison. Clearly the secondary structure of the fibers spun in ethanol-acetic acid are more similar to the native silk.

Regarding the proportions of the solution, the following equation have been used to obtain a coagulating bath final volume of two litres.

$$Ethanol\ volume\ [mL] = Solution\ final\ volume * 1000 * \frac{Ethanol\ \%}{100} \quad (2.10)$$

$$Acetic\ acid\ volume\ [mL] = 5 * \frac{C_M * MW_{AA} * 0.2 * Solution\ final\ volume}{\rho_{AA}} \quad (2.11)$$

Where the parameters concerning the properties of acetic acid are listed in the Table 2.7 and solution final volume is reported in L both in (2.10) and (2.11).
Since a solution of only 20% acetic acid in distilled water is used, a multiplying factor of 5 is introduced to correct the calculation in equation (2.11).

Parameters	**Molar concentration C_M [mol/L]**	**Molecular weight MW_{AA} [g/mol]**	**Density ρ_{AA} [g/cm^3]**
Value	1	60.052	1.05

Table 2.7 – Acetic acid constant used in equation (2.11).

Now every parameter influence has been explained and we can introduce the tensile test setup used to describe the mechanical parameters of the strained flow spun fibers.

3 – Mechanical behaviour of regenerated silk fibroin fibers

3.1 – Tensile test setup

The regenerated fibers tensile test to determine the material mechanical behaviour were performed in an Instrom 4411 tensile testing machine, and forces were measured with a precision balance (Precisa XT220A).

The data obtained through the software are the test time in seconds and the mass in grams at a sampling frequency of 4 Hz. The measured mass is negative since the machine is exerting a pulling force on the sample.

To support the sample fiber an aluminium foil, which dimensions are reported in Figure 3.1, is prepared and a fiber is collected singularly from the plastic sheet using small adhesive tape pieces. Then it is fixed on the support using super glue to be sure that the fiber wouldn't slide away during the test. After the pasting procedure, the support is cut in the edges to fit the clamp shape and is fixed by tighten the screws. A small portion of the fiber is saved to measure the diameter after a successful tensile test. The ready to be tested sample is appreciated in Figure 3.2. The stake is then fixed to the Instrom machine, the screws untight and the lateral aluminium pieces cut off. At this point only the fiber is opposing resistance to the tensile force applied during the test. The initial length of the fiber is manually measured by a calibre. Then, the starting point is set and the fiber is stretched up just before the point where the balance measures a mass decrease. In this way we have the exact fiber initial length by adding the calibre measurement to the registered displacement from the initial point. This information, together with the fiber diameter is fundamental to study the material behaviour as it was explained in *Chapter 1*.

Once the whole procedure is performed, the tensile test can start, and a time-mass graphic is displayed by the software to supervise the sample trend. If the latter is correct (for example, without unusual peaks or registering errors during the data acquisition) the saved portion of the fibers is taken to a Leica DMI3000B microscope with a 40x objective to take images of its structure. It is important to take images of the same fiber in different portions of its length since the structure can strongly vary depending on the coagulation process. The procedure used in this study was to take two images near the edges of the aluminium foil. An example of this type of images is showed in Figure 3.3 and Figure 3.4.

The images are elaborated with the software *ImageJ* to digitally measure the micrometric diameter of the fibers. Through the help of a grid specifically designed for the 40x objective, three measures for each image are taken and then the average diameter is assumed as the initial diameter of the fiber. There is a high standard deviation of the diameter measurements that

depend on the coagulating process and the fibers collection on the take up roller. Moreover, many random errors can be made using this procedure and an automatic detection of the diameter should be implemented in the future to have more accurate data. Anyway, once the initial diameter is obtained the data elaboration can start calculating the force by multiplying the mass for $-g$ which represents the gravity acceleration (it is negative to correct the mass data which is negative). Then the elaboration is undertaken following the equations presented in *Chapter 1*.

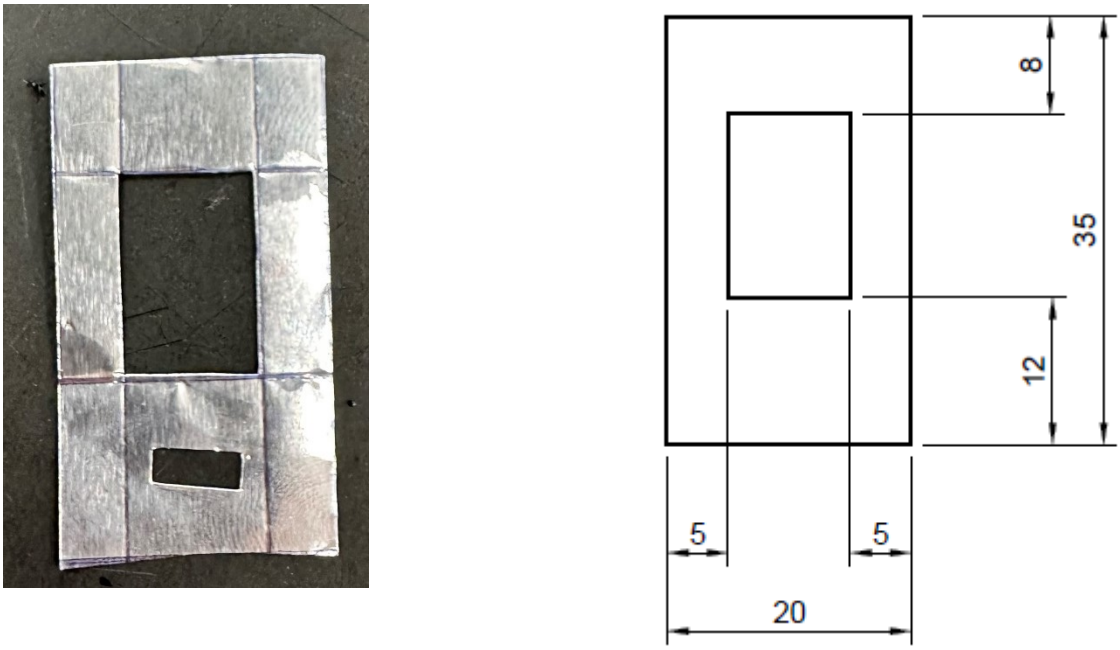

Figure 3.1 – Image of the aluminium foil used as a support to the fibers and its dimensions.

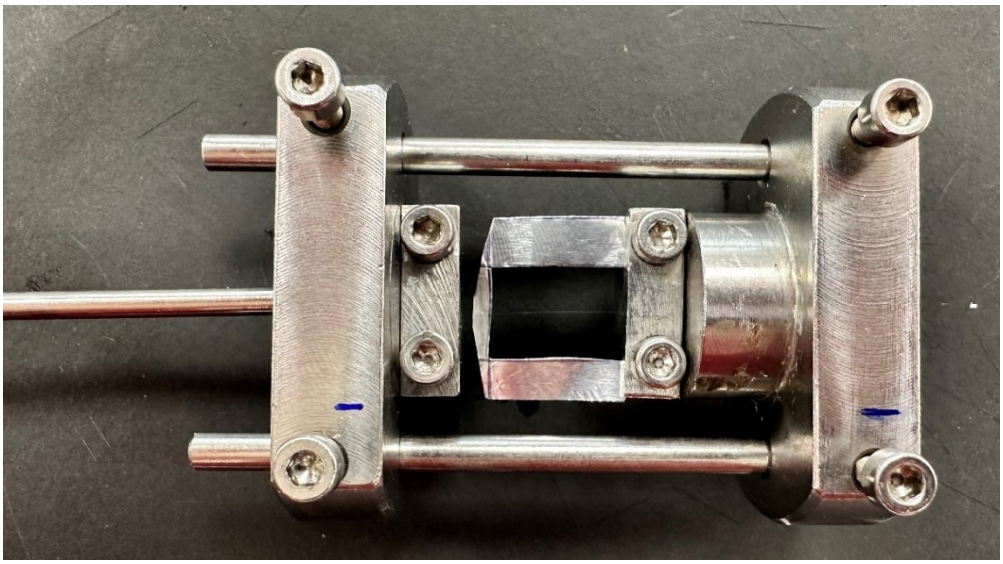

Figure 3.2 – Complete tensile test setup where it can be seen the reflection of the fibroin fiber bonded to the aluminium support. The lateral band will be removed so only the fiber will resist to the tensile force applied.

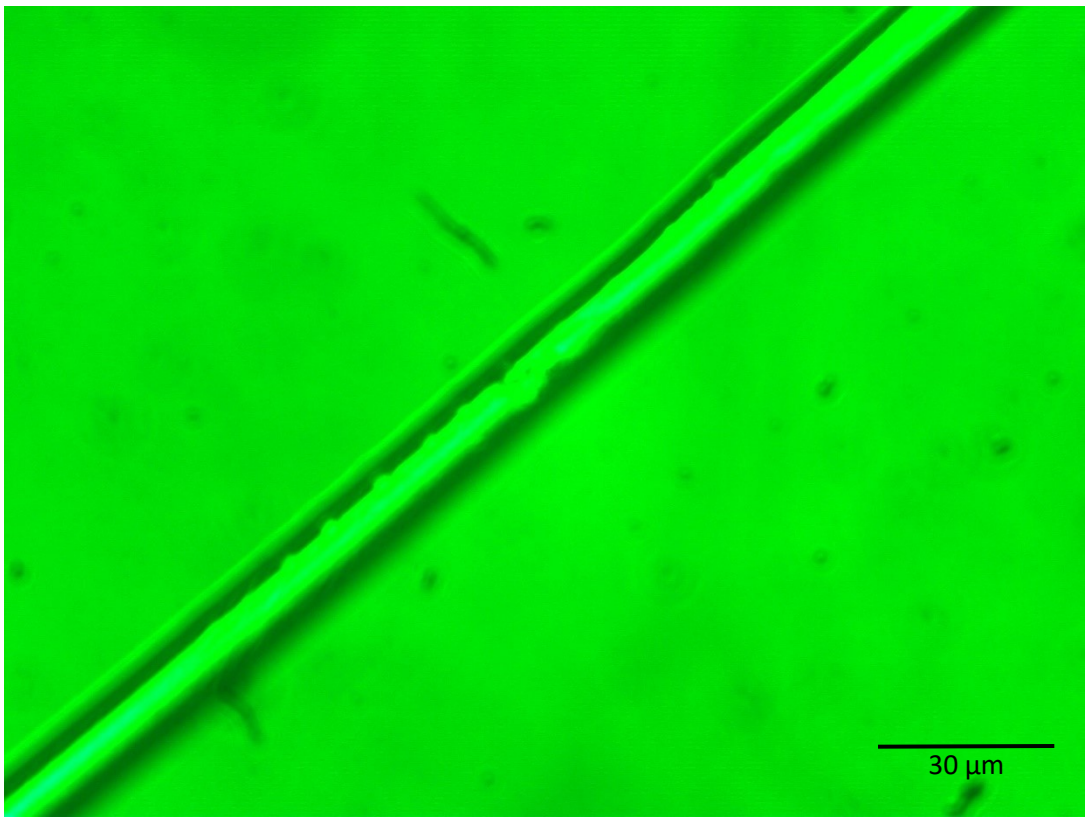

Figure 3.3 – Example of a microscope image of a good, structured fiber with regular shape. A scale for comparison is reported.

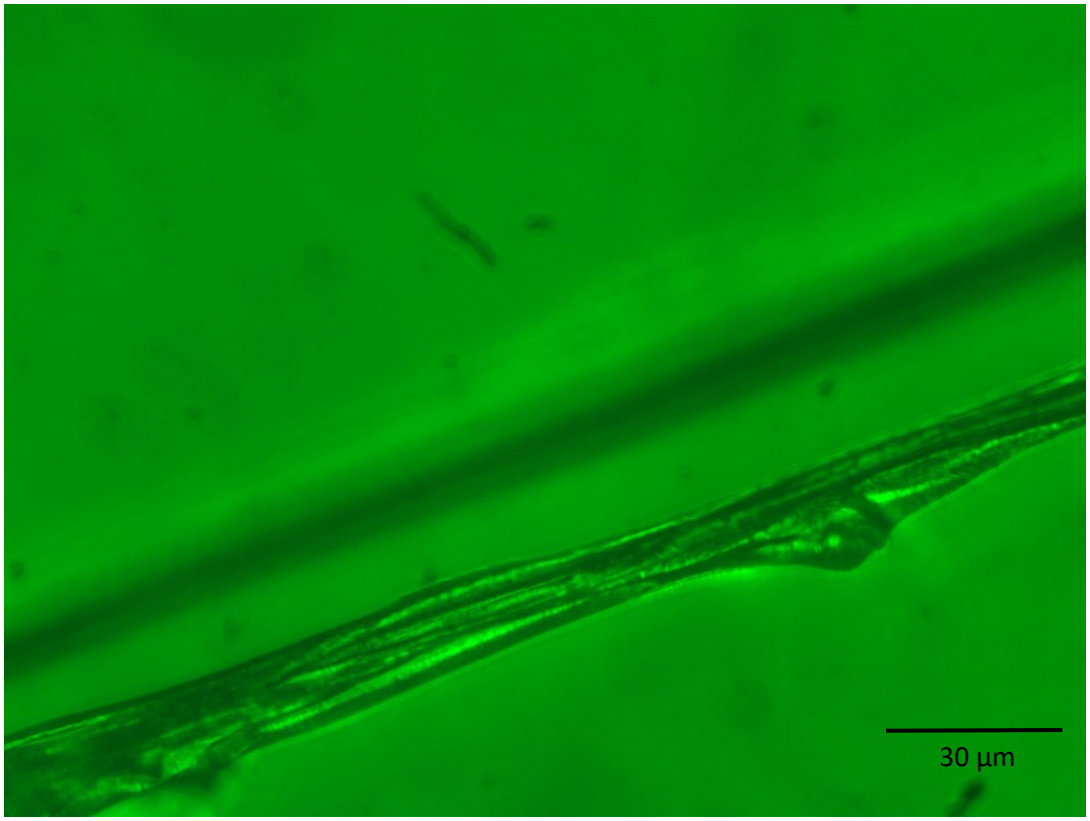

Figure 3.4 – Example of a microscope image of a fiber that presents multiple defects, probably due to poor coagulation during the spinning process. A scale for comparison is reported.

3.2 - Mechanical behaviour in air

In this paragraph the mechanical results obtained during the study will be presented as follows: firstly, a resuming table with the spinning parameters used to produce the fiber batch, a true stress – true strain graphic to show the samples behaviour and a resuming table with the most important parameters.

Starting with the initial test performed to learn the whole spinning and testing procedure, the parameters chosen to spin were the same as indicated in the study by Madurga et al.[19] and reported in Table 3.1. Only Q_f differs since the lowest possible value reachable with the used equipment was 10 mL/min.

Hydrodynamical			Geometrical			Chemical
Dope flow rate Qd [µL/min]	**Focusing fluid flow rate Qf [mL/min]**	**Velocity of take up roller VR1 [m/min]**	**Capillary diameter d1[µm]**	**Nozzle outlet diameter D1[µm]**	**Capillary-Nozzle distance**	**Dope composition and degumming time**
5	10	3.5	150	400	Close to outlet	16% Fibroin w/V 20 minutes

Table 3.1 – List of the SFS parameters used in the spinning process divided into hydrodynamical, geometrical and chemical.

FUNDAMENTAL PARAMETERS	Test1	Test2	Test3	Test4	Test5	AVERAGE	SD
Breaking stress [MPa]	36.33	FAIL	10.07	75.69	79.09	50.30	33.10
Deformation at breaking	0.014	FAIL	0.007	0.006	0.012	0.010	0.004
Elastic Modulus [GPa]	2.88	FAIL	1.45	13.37	7.19	6.22	5.35
Fiber diameter [um]	5.17	FAIL	9.53	4.85	7.37	6.73	2.18
Work to fracture [MJ/m^3]	0.278	FAIL	0.038	0.261	0.517	0.274	0.196

Table 3.2 – Mechanical fundamental parameters listed with average and standard deviation for fibers obtained with set of parameters in Table 3.1. In test 2 the fiber broke as soon as the tensile test was started, so it was considered failed.

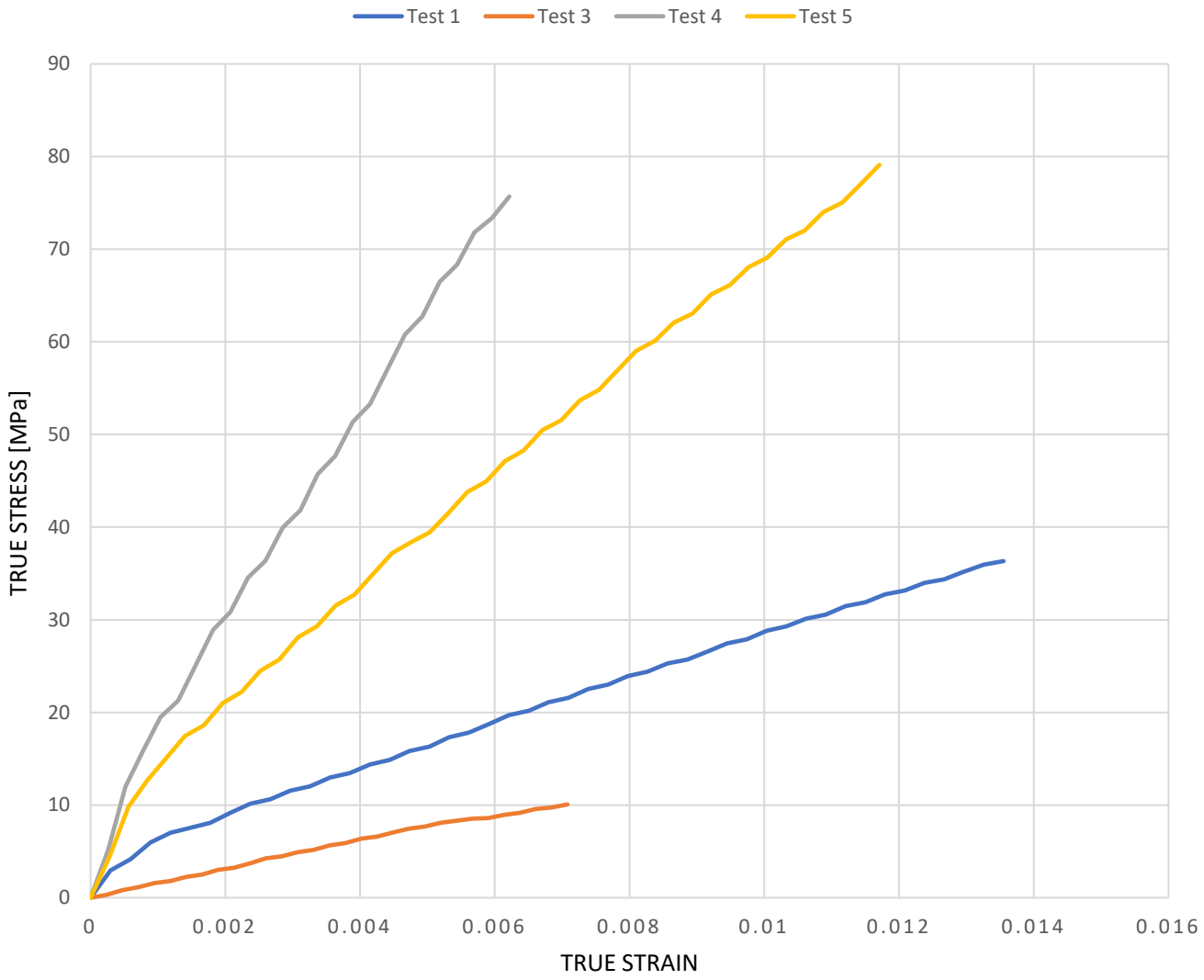

Figure 3.5 – True strain – True stress plot of the samples obtained under the parameter listed in Table 3.1. The evolution of the curves describes the fibroin fibers mechanical behaviour. Good breaking stress are reached while poor deformations suggest a fragile behaviour of the fibers.

REFERENCE N=5	Average	SD	p-value	H0 Rejection
Breaking stress [MPa]	52	2	0.88	0
Deformation at breaking	0.013	0.001	0.08	0
Elastic Modulus [GPa]	4.1	0.1	0.496	0
Work to fracture [MJ/m^3]	0.36	0.03	0.037	1

Table 3.3 – Average and standard deviation of the tensile test carried out on 5 samples by Madurga et al[19]. P-value and statistical independence (null hypothesis H0 rejection) between the reference and the data from Table 3.2 are reported. Only the tenacity of the fiber is statistically significant between the two populations.

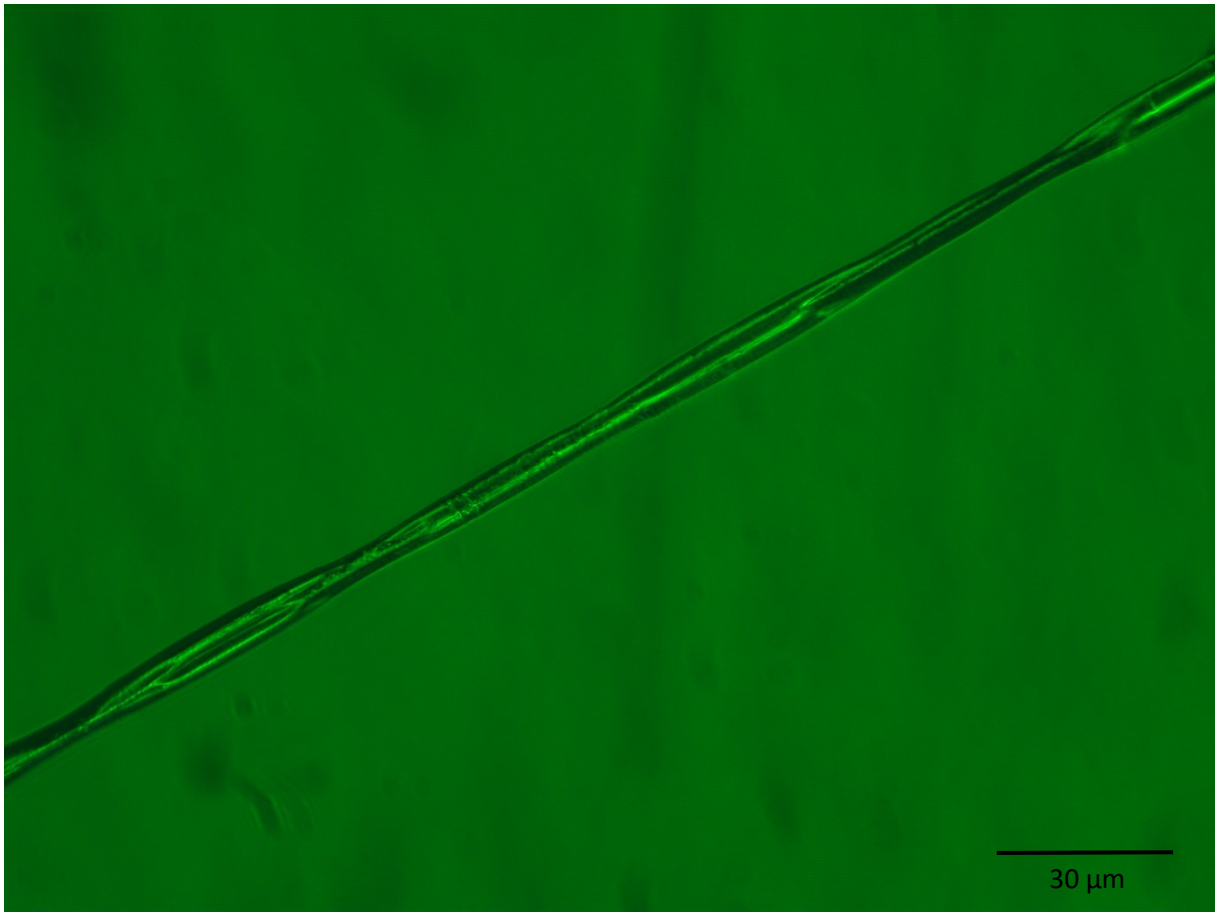

Figure 3.6 – Microscope image of Figure 3.5 test 4 fiber. The structure is devoid of evident defect and quite regular.

Five fiber samples were tested in air. In Figure 3.5 a brittle behaviour is clearly observable since all the fibers break at very low strain percentages, even under 1% of their initial length. The diameters are slightly under the values expected but from the microscope observation no evident defects are noted in the fibers structure. In test 2 no data could be registered since the fiber broke as soon as the tensile force was applied. For the chosen spinning setup, the results match the ones contained in the study conducted by Madurga et al.[19] except for the work to fracture, which is statistically different between the two populations. The fiber diameters weren't reported in the study, so they are excluded from the comparison test. The results of a Student's t-test between the experimental population and the reference dataset is reported in Table 3.3.

The similarity of the results is encouraging since marks that no mistakes were committed during the spinning procedure. Anyway, a high standard deviation is noted which can be associated with the difficulties in the coagulation experimented with this set of parameters. Moreover, the fragile behaviour is not what is seek in this study, highlighting the necessity of changing the parameters to achieve better fibers deformations and works to fracture and a smoother spinning.

Based on these considerations, the second run of spinning was performed under the following parameters.

Hydrodynamical			Geometrical			Chemical
Dope flow rate Qd [µL/min]	**Focusing fluid flow rate Qf [mL/min]**	**Velocity of take up roller VR1 [m/min]**	**Capillary diameter d1[µm]**	**Nozzle outlet diameter D1[µm]**	**Capillary-Nozzle distance**	**Dope composition and degumming time**
5	30	10	150	400	<1 mm	20% Fibroin w/V 20 minutes

Table 3.4 – New SFS parameters set used in the new spinning run.

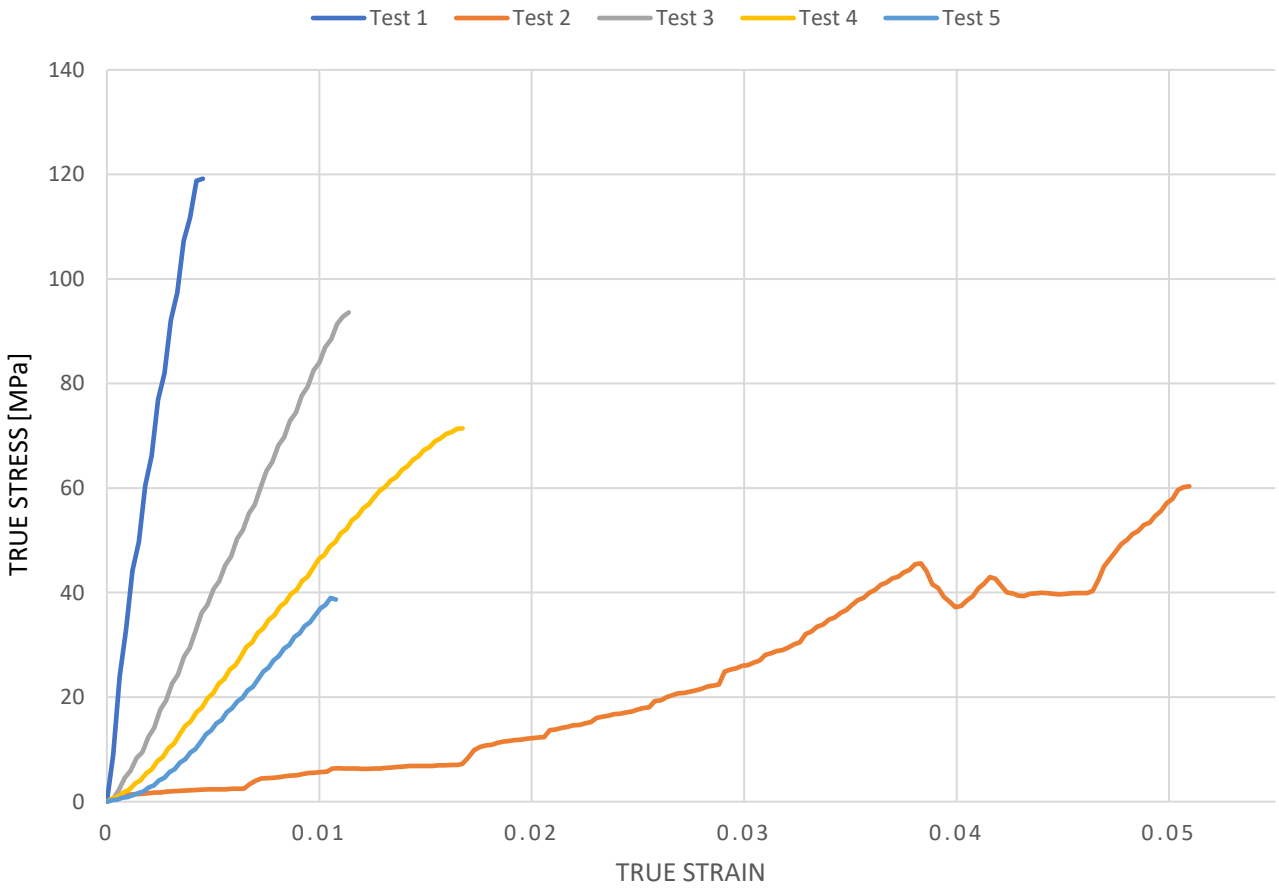

Figure 3.7 – True strain – True stress plot of the fibers mechanical data spun with the parameters set of Table 3.4 with increased focusing fluid flow rate.

FUNDAMENTAL PARAMETERS	Test1	Test2	Test3	Test4	Test5	Average	SD
Breaking stress [MPa]	29.80	60.34	93.60	71.42	38.69	63.79	25.58
Deformation at breaking %	0.452	5.10	1.14	1.67	1.08	2.09	1.84
Elastic Modulus [GPa]	7.38	0.95	7.32	4.50	3.35	5.04	2.74
Fiber diameter [um]	7.48	4.53	9.40	10.78	9.34	8.05	2.41
Work to fracture [MJ/m^3]	0.31	1.15	0.53	0.62	0.18	0.65	0.37

Table 3.5 – Mechanical fundamental parameters listed with average and standard deviation for fibers obtained with set of parameters in Table 3.4. Less variance in the breaking stress and E values is observed.

As it possible to see in Table 3.4, the parameters that have been changed are Q_f, VR_1 and the dope concentration that was increased at 20%. The focusing fluid speed was increased to have more hydrodynamic pressure on the dope jet to permits higher coagulation. Dope concentration was increased too to improve coagulation while the take up roller velocity was increased in consequence of the change of Q_f up to the maximum value at which the fiber could be collected without breaking.

With these parameters it was observed that the spinning process was much easier and long spinning periods were possible. Nevertheless, the fibers behaviour is still fragile, and no statistic difference is achieved with the previous experimental dataset. Anyway, the standard deviation of each parameter is lower than the first fiber batch, suggesting that a more controlled spinning process leads to lower variability in the fibers mechanical properties and structure. Looking at Figure 3.8 is possible to also see that the fibroin microstructure doesn't show significant defect, but it seems thin and poorly resistant, as the mechanical data confirm in test 2.

The conclusion led to the necessity of changing other parameters not yet investigated. Maintaining unchanged the hydrodynamic and geometrical parameters as indicated in Table 3.4, the next results will focus on the analysis of the chemical parameters to determine if the degumming time plays a role in the fibers mechanical behaviour. Several fibroin solutions were prepared at 10, 15 and 20 minutes of degumming, at different concentrations, ranging from the lowest 14% up to 20%. Higher concentrations were not tested as it is reported in bibliography that they show too much coagulation, resulting in nozzle and capillary occlusion.

Not every solution was easily spinnable and in some cases, even if fibers were realized, it was not possible to test them due to their extremely poor resistance.

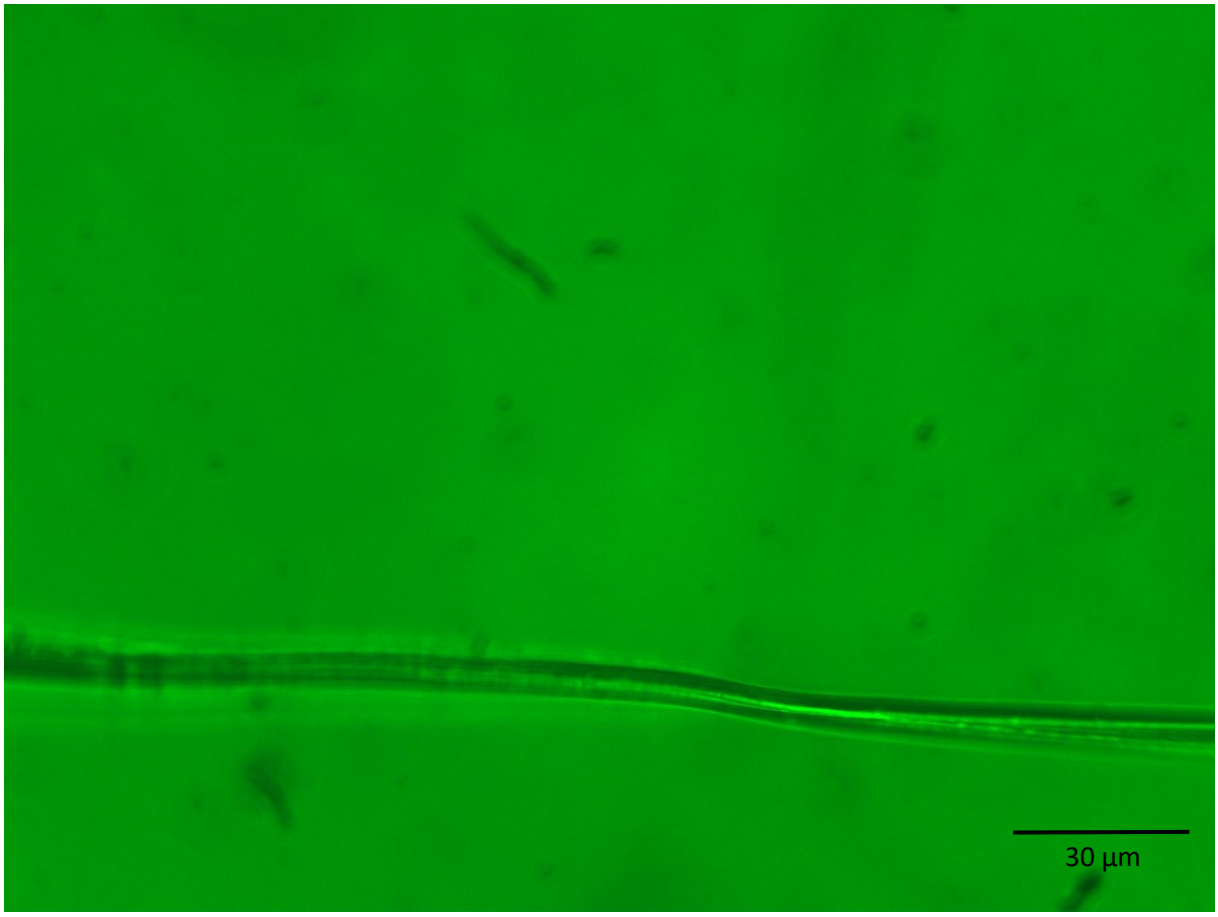

Figure 3.8 - Microscope image of Figure 3.7 test 5 fiber. The structure is devoid of evident defect but it's not regular, justifying the poor mechanical quality.

Degumming time [min]	Fibroin Concentration [w/V %]	Spinnable	Tested
10	16	No – No coagulation	Not possible
10	18	No – No coagulation	Not possible
10	20	Yes	Not possible – Too fragile
15	16	No – No coagulation	Not possible
15	18	Yes	**Possible**
15	20	No – Too much occlusion	**Possible**
20	14	No – No coagulation	Not possible
20	18	Yes	**Possible**
20	20	Yes	**Possible**

Table 3.6 – Resume of all fibroin solutions tested. In the table is indicated whether the solution was spinnable (and the reasons why they weren't) and if the fibers obtained were handleable enough to be tested.

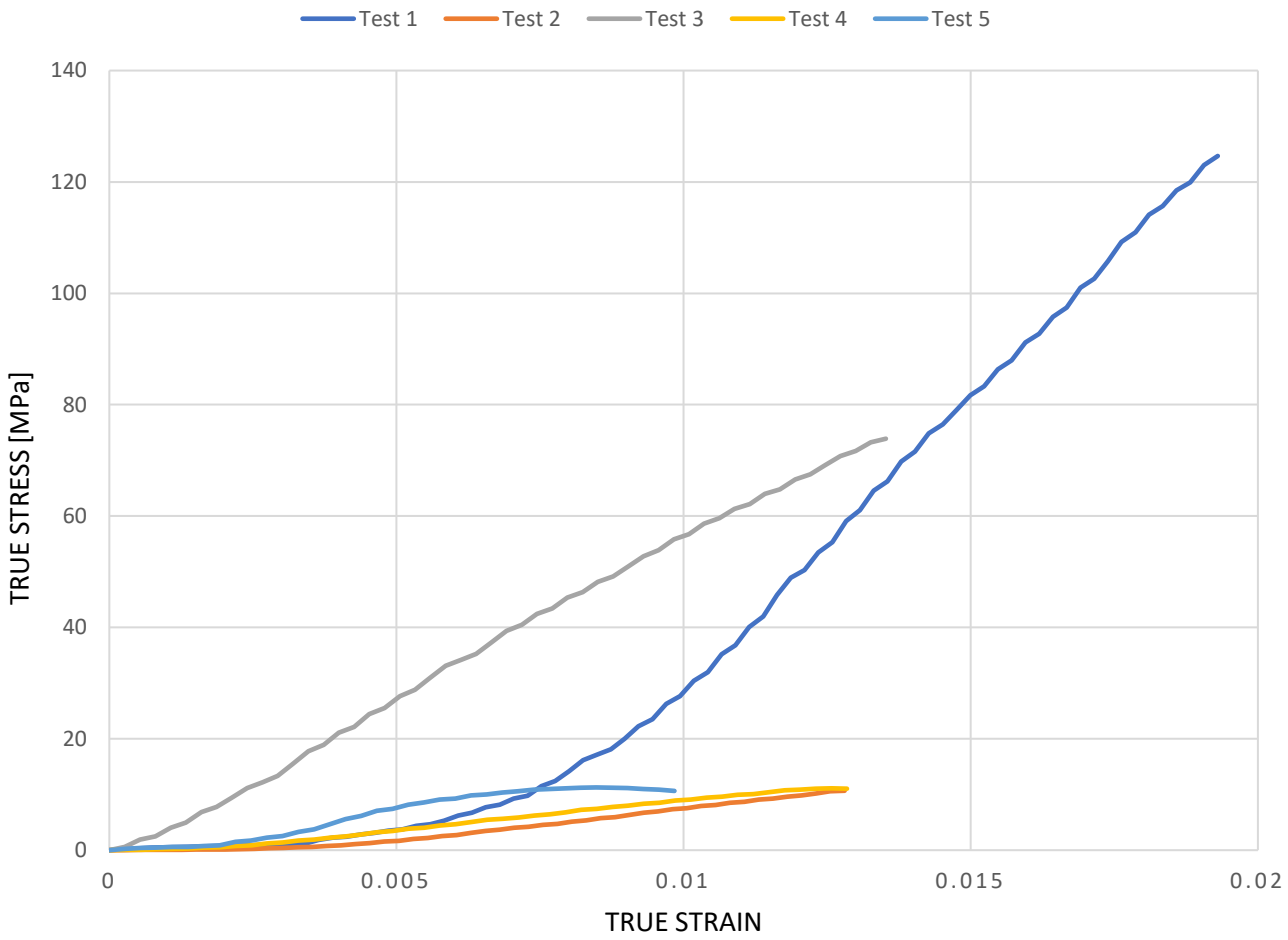

Figure 3.9 – True strain – True stress plot of the samples obtained under the hydrodynamical and geometrical parameter listed in Table 3.4. 15 minutes of degumming time and a fibroin concentration of 18% w/V are the chemical parameters. It is observed that mechanical properties are worse than the other tested fibers.

FUNDAMENTAL PARAMETERS	Test1	Test2	Test3	Test4	Test5	Average	SD
Breaking stress [MPa]	124.66	10.68	72.90	11.03	10.68	45.99	51.55
Deformation at breaking %	1.93	1.28	1.35	1.28	0.98	1.37	0.35
Elastic Modulus [GPa]	10.27	1.19	5.57	0.86	1.33	3.84	4.08
Fiber diameter [um]	10.27	18.78	8.32	20.48	8.76	13.32	5.83
Work to fracture [MJ/m^3]	0.79	0.05	0.50	0.07	0.06	0.29	0.34

Table 3.7 - Mechanical fundamental parameters listed with average and standard deviation for fibers plotted in Figure 3.9. Lower elastic modulus is observed associated with small fibers diameters. The behaviour is still fragile.

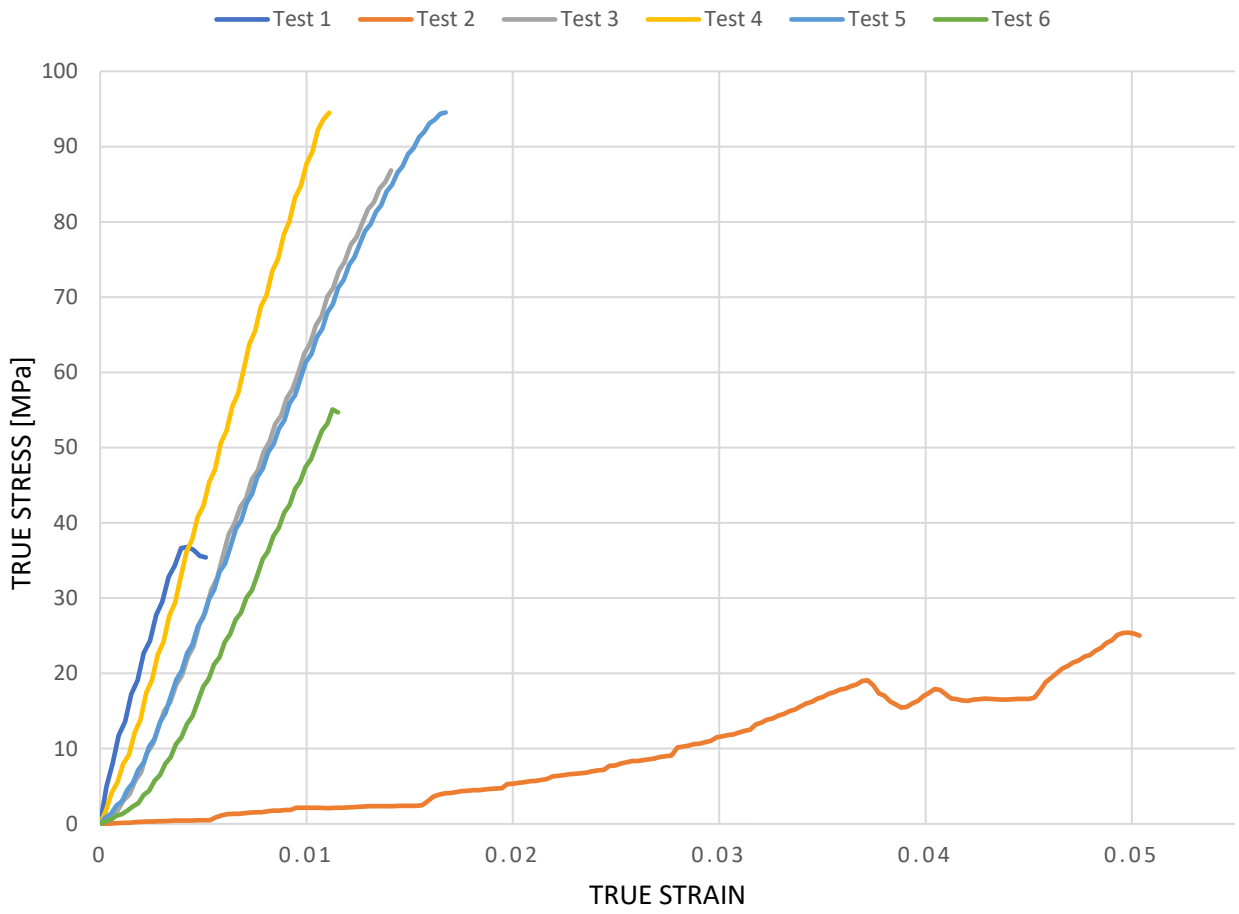

Figure 3.10 - True strain – True stress plot of the samples obtained under the hydrodynamical and geometrical parameter listed in Table 3.4. 20 minutes of degumming time and a fibroin concentration of 16% w/V are the chemical parameters. Similar behaviour between the fibers is appreciable except for test 2, that shows a much lower elastic modulus and higher deformation. Fragile behaviour is still observed.

FUNDAMENTAL PARAMETERS	Test1	Test2	Test3	Test4	Test5	Test6	Average	SD
Breaking stress [MPa]	35.38	25.04	86.83	82.26	94.53	54.67	63.12	29.00
Deformation at breaking %	0.51	5.04	1.41	1.11	1.67	1.15	1.82	1.62
Elastic Modulus [GPa]	8.73	0.41	6.18	8.66	5.95	4.43	5.73	3.09
Fiber diameter [um]	6.47	6.89	13.89	9.33	9.37	7.86	8.97	2.69
Work to fracture [MJ/m^3]	0.12	0.48	0.60	0.53	0.82	0.27	0.43	0.25

Table 3.8 - Mechanical fundamental parameters listed with average and standard deviation for fibers plotted in Figure 3.10. If test 2 is not considered, the results show little variance in elastic modulus and breaking stress.

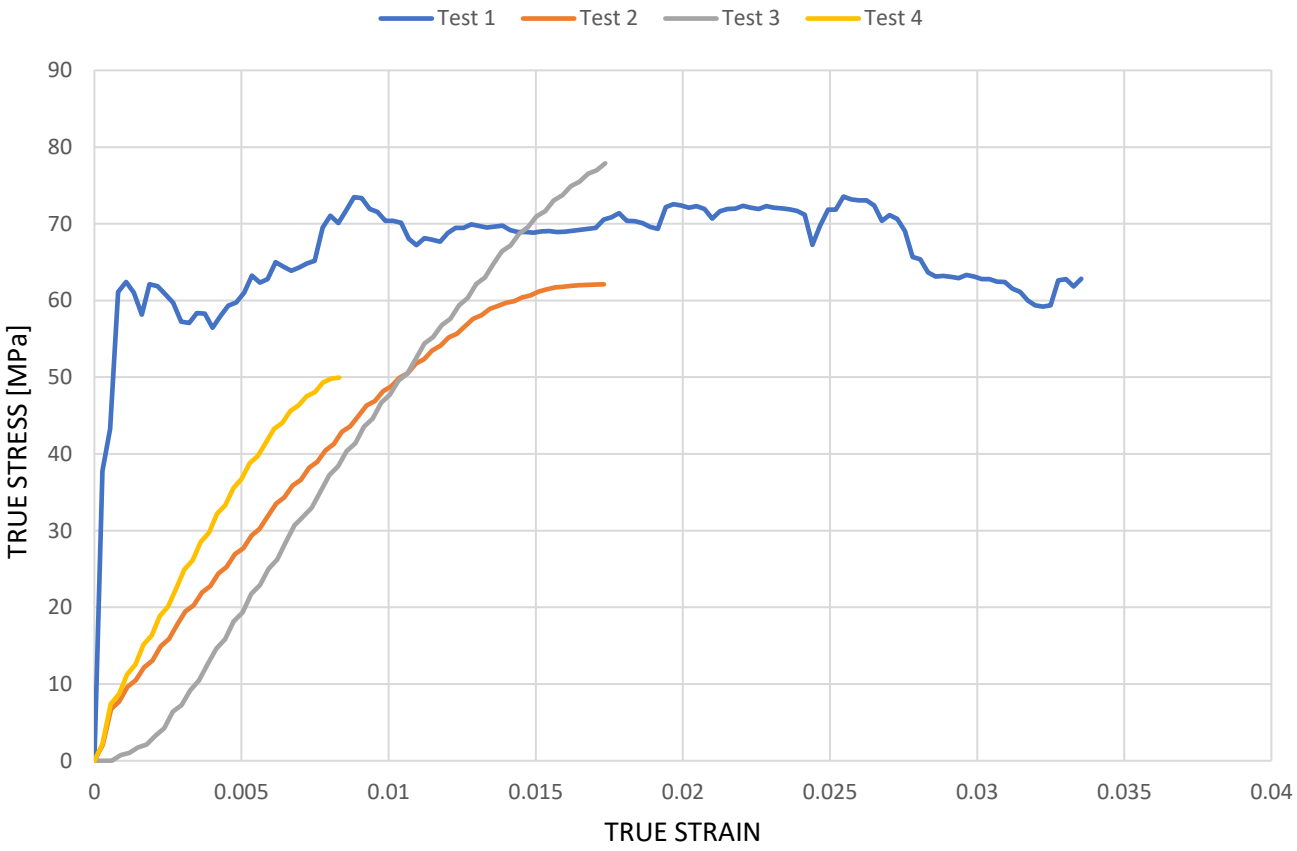

Figure 3.11 - True strain – True stress plot of the samples obtained under the hydrodynamical and geometrical parameter listed in Table 3.4. 20 minutes of degumming time and a fibroin concentration of 18% w/V are the chemical parameters. Test 1 show a good, plastic mechanical behaviour while other tests keep showing a fragile behaviour. This suggest that there might be other parameters influencing the mechanical properties.

FUNDAMENTAL PARAMETERS	Test1	Test2	Test3	Test4	Average	SD
Breaking stress [MPa]	62.83	62.11	77.88	49.94	63.19	11.44
Deformation at breaking %	3.35	1.73	1.74	0.83	1.91	1.05
Elastic Modulus [GPa]	69.21	4.90	4.63	6.88	21.41	31.89
Fiber diameter [um]	11.34	8.98	7.47	8.46	9.06	1.64
Work to fracture [MJ/m^3]	2.23	0.69	0.68	0.25	0.96	0.87

Table 3.9 - Mechanical fundamental parameters listed with average and standard deviation for fibers plotted in Figure 3.11. A clear disproportion and different behaviour are present in test 1 respect to the others. Likely, errors during the tensile test procedure in test 1 were committed.

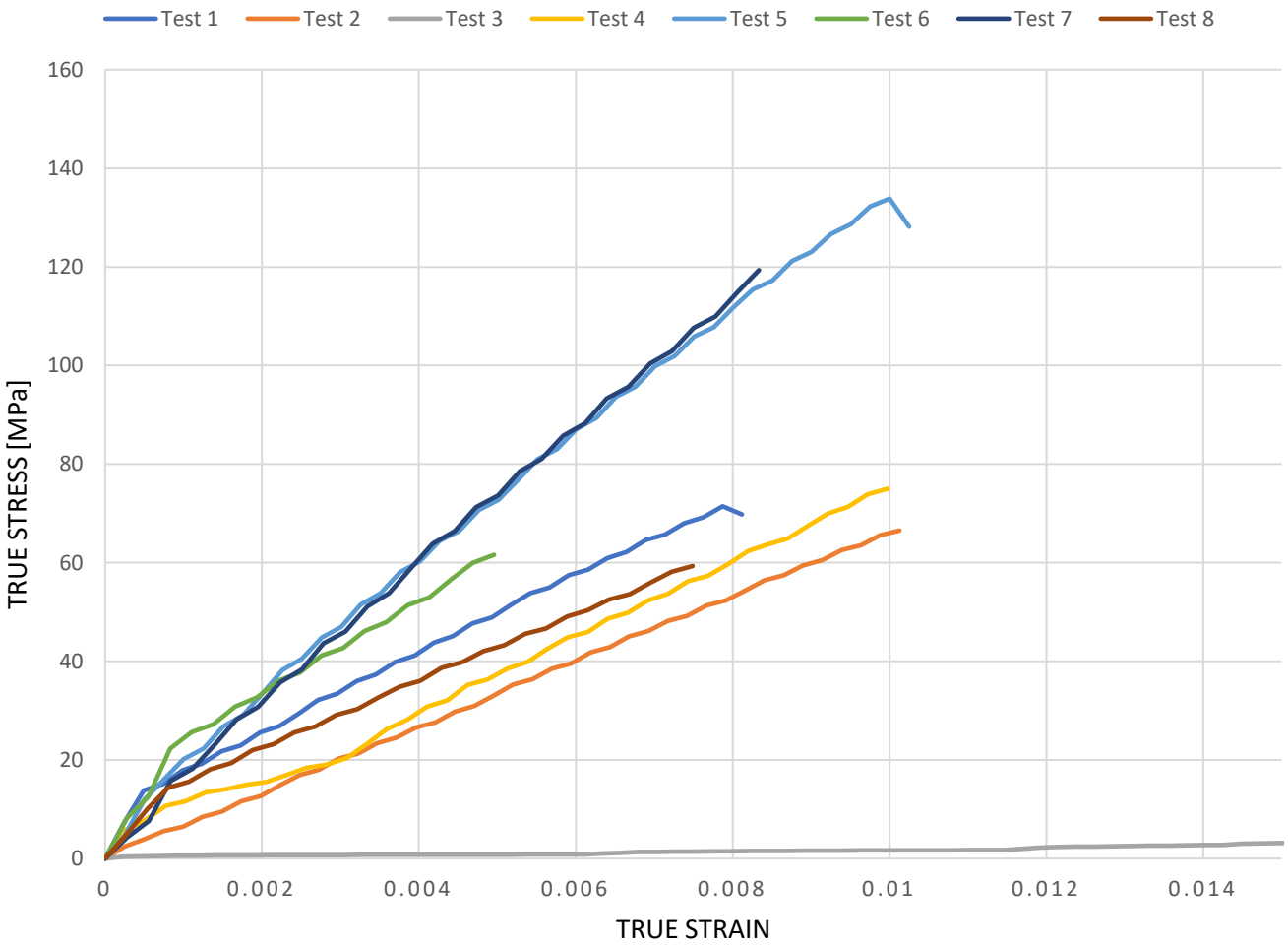

Figure 3.12 – True strain – True stress plot of the samples obtained under the hydrodynamical and geometrical parameter listed in Table 3.4. 20 minutes of degumming time and a fibroin concentration of 20% w/V are the chemical parameters. Excluding test 3 (in which probably the fiber was not completely dry) a similar behaviour is achieved among all tests. These results show the potential repeatability of the SFS spinning under the spinning parameters chosen.

FUNDAMENTAL PARAMETERS	Test1	Test2	Test4	Test5	Test6	Test7	Test8
Breaking stress [MPa]	69.78	68.18	75.02	133.85	61.60	119.34	59.32
Deformation at breaking %	0.79	1.09	1.00	1.00	0.50	0.83	0.75
Elastic Modulus [GPa]	9.78	6.21	7.52	14.09	13.74	14.56	8.53
Fiber diameter [um]	8.62	7.04	3.37	4.61	4.33	7.04	3.81
Work to fracture [MJ/m^3]	0.351	0.373	0.379	0.756	0.182	0.513	0.253

Table 3.10 - Mechanical fundamental parameters listed for fibers plotted in Figure 3.12. Fragile fibers are still detected but all samples show the same behaviour excluding test 3.

FUNDAMENTAL PARAMETERS	Average	SD
Breaking stress [MPa]	83.87	29.94
Deformation at breaking %	0.9	0.2
Elastic Modulus [GPa]	10.63	3.45
Fiber diameter [um]	5.86	2.06
Work to fracture [MJ/m^3]	0.40	0.19

Table 3.11 -Average and standard deviation for mechanical data reported in table 3.10. Low variance in every parameter is appreciable.

As reported in Table 3.6, two of the solutions obtained after 10 minutes of degumming weren't spinnable, while the most concentrated one didn't lead to good quality fibers. In fact, they didn't show enough coagulation at 16% and 18% and managing the fibers obtained from the last solution was extremely difficult, highlighting their extremely poor resistance. A possible reason for this phenomenon is that boiling for only ten minutes creates solutions with larger molecules respect to higher times. Therefore, these solutions might need more tangential stress to start coagulating the molecules into a fiber. It is possible to obtain this increasing by varying the focusing fluid flow rate or the dimension of the nozzle outlet. Anyway, there was no reason to focus on the 10 minutes degummed solutions since discrete results were obtained with higher degumming times.

Regarding the solutions at 15 minutes of degumming, results were obtained only from the solution at 18% and they are represented in Figure 3.9. A fragile behaviour is still observable and the variance in the sample seems to be higher. Three fibers show a very low elastic modulus compared to the previous results. This lead to think that under the chosen parameters 15 minutes of degumming doesn't show any relevant improvement, on the contrary it seems to worsen the fibroin mechanical properties.

Moving on to analyse the solutions at a classic 20 minutes degumming time, the lowest fibroin concentration solution (14%) didn't show any coagulation while appreciable results were obtained using fibroin concentrations at 18% and 20%. Figure 3.11 test 1 show a good evolution of the true strain - true stress curve as it should be expected when testing fibroin fibers but, once again, with low deformation at breaking. Nevertheless, it's likely to think that something went wrong during the testing procedure since the elastic modulus is clearly disproportionate to any other sample or data reported in other studies.

Encouraging results are obtained and plotted in Figure 3.12 with solutions at fibroin concentration of 20%. Although in Table 3.5 the mechanical data of the same solutions type spun under the same parameters are reported, results listed in Table 3.10 show higher elastic modulus associated with an acceptable variance. This finding arises questions about spinning fibroin fiber in a repeatable way. Moreover, even if these results have improved in some aspect, the main problem remains that every fiber show poor deformation at breaking.

Under these considerations and after all the parameters tested, the choice was to carry on the optimization process with solution degummed for 20 minutes at fibroin concentration of 20% in w/V. In fact, not only this kind of solution is the easiest to spin, but also the fibers are handleable and manageable to perform the tensile test without experimenting problems.

In the whole study conducted, only one parameter was not indagated until now. The nozzle outlet was always left untouched since in any study reported in bibliography an outlet diameter of 400 μm was assumed. At this point, there is no reason not to investigate a smaller outlet diameter to increase the tangential stress and hopefully the fibers structural integrity. It was chosen to reduce the diameter around 250 μm and the correct dimension was checked in the same way the fibers diameters were measured. The parameters used for this run are reported below as well as the mechanical parameters.

Hydrodynamical			**Geometrical**			**Chemical**
Dope flow rate Qd [μL/min]	**Focusing fluid flow rate Qf [mL/min]**	**Velocity of take up roller VR1 [m/min]**	**Capillary diameter d1[μm]**	**Nozzle outlet diameter D1[μm]**	**Capillary-Nozzle distance**	**Dope composition and degumming time**
5	30	10	150	250	<1 mm	20% Fibroin w/V 20 minutes

Table 3.12 – New spinning parameters that include the nozzle outlet diameter reduction.

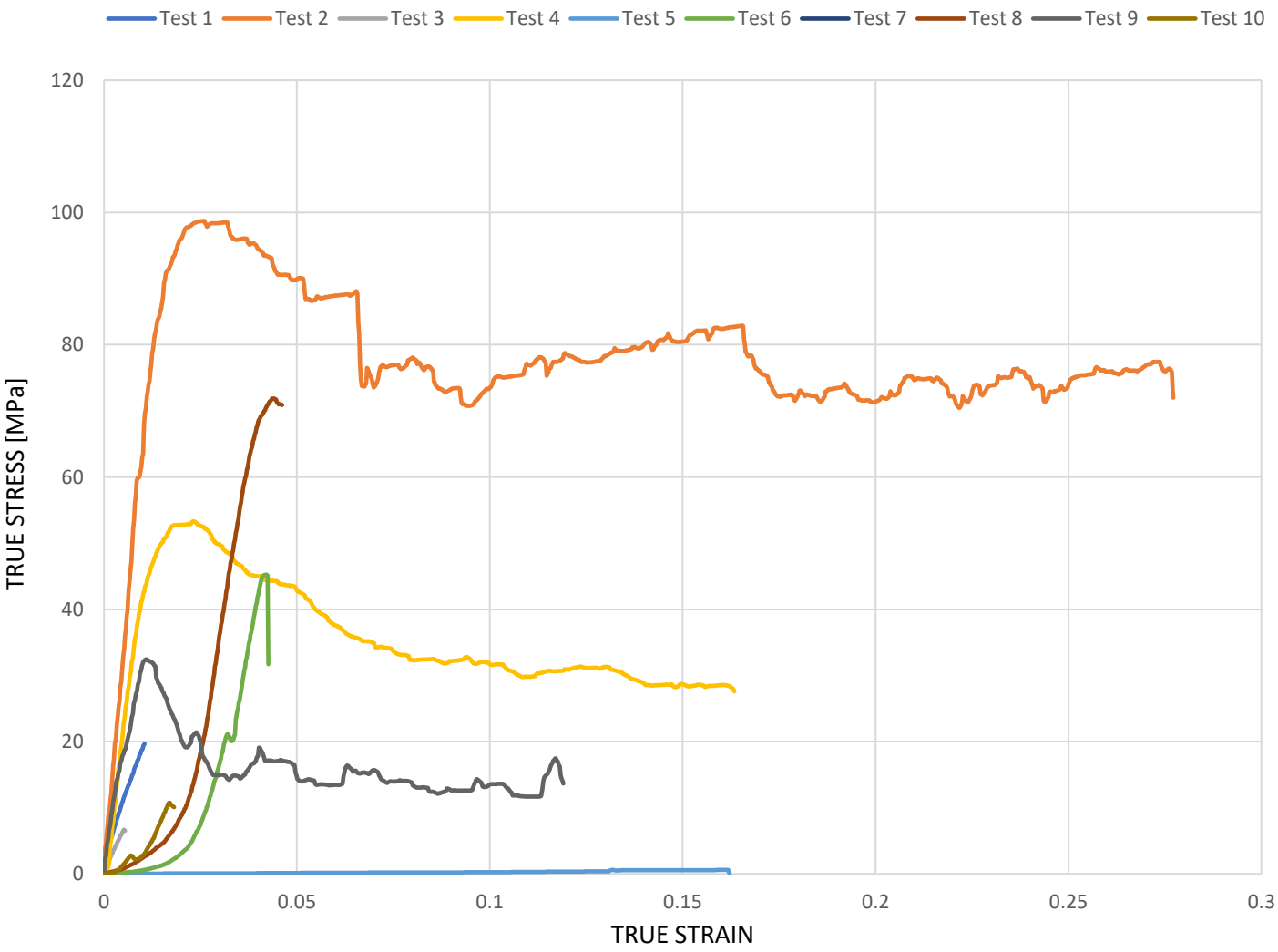

Figure 3.13 - True strain – True stress plot of the samples obtained under the parameters listed in Table 3.12. Finally plastic behaviour associated with good mechanical characteristic is observed in tests 2, 4 and 9. The process of optimization have led to the expected result.

FUNDAMENTAL PARAMETERS	Test1	Test2	Test3	Test4	Test6	Test7	Test8	Test9	Test10
Breaking stress [MPa]	19.63	72.00	25.88	27.58	45.08	12.57	70.72	13.65	10.09
Deformation at breaking %	1.05	27.72	0.54	16.34	4.24	1.23	4.66	11.91	1.82
Elastic Modulus [GPa]	2.03	5.56	5.28	3.50	3.25	1.03	3.65	3.33	0.48
Fiber diameter [um]	11.54	14.22	14.11	27.22	29.2	19.82	31.62	12.95	22.13
Work to fracture [MJ/m^3]	0.12	21.44	0.08	5.77	0.49	0.07	1.26	1.90	0.07

Table 3.13 - Mechanical fundamental parameters listed for fibers plotted in Figure 3.13. Fragile fibers are still detected but three results are extremely positive showing good fibers tenacity. Moreover, test 2 show the possibility to spin fiber having outstanding property if the SFS device is tuned properly.

FUNDAMENTAL PARAMETERS	AVERAGE	SD
Breaking stress [MPa]	33.02	24.15
Deformation at breaking %	7.72	9.26
Elastic Modulus [GPa]	3.12	1.72
Fiber diameter [um]	20.31	7.62
Work to fracture [MJ/m^3]	3.47	6.98

Table 3.14 – Average and standard deviation reported for the mechanical data contained in table 3.13. The most improved results are the work to fracture and the low variance in the elastic modulus. It is noted that higher diameters lead to improved results.

Finally, a plastic behaviour is achieved as is possible to observe in Figure 3.13, especially in tests 2, 4 and 9. These three tests show an initial linear region common to all other tests, but also a sort of stress relaxation as the deformation increases. This is typical of ductile materials, and it represents exactly the mechanical characteristic that is seek in this study. By associating a great breaking stress and good deformation at breaking, fibers with perfect mechanical characteristics to create tubular guides have been obtained through the SFS technique. The good behaviour is also found in the good fibers handleability during the manipulation to prepare the tensile test samples.

Focusing on the fundamental parameters, in test 2 the work to fracture reaches the value of 21.44 MJ/m^3 which represents the 30.6 % of the natural silk tenacity according to Table 1.1. This is a great achievement compared to all the other fibers obtained and confronted to the data of fibers spun with other techniques. Having other two test that confirm this behaviour is encouraging if related to the poor repeatability experimented in other runs. Moreover, the initial elastic modulus of almost all fibers is contained in a small range. This also confirms the improvement in the results repeatability.

In conclusion, through the whole process of parameter optimization it is possible to achieve silk fibroin fibers that show outstanding mechanical quality, especially if compared to simple wet spinning. Nevertheless, the optimization is a heavily time demanding process that may also be influenced by the raw silk initial quality and storage. Therefore, this procedure should be repeated for every different silk batch. Anyway, the optimization process described is sufficient to obtain good quality fibers, which are essential to this work's next steps.

3.3 – Mechanical behaviour in water

The second step after obtaining silk fibroin fibers that meet the essential mechanical requirements is testing their behaviour submerged in water. In fact, the biological environment is not dry and fibroin's chemical structure is sensitive to hydrolysis. This indicates that is likely to have a change of the mechanical properties when the fibers are exposed at humidity.

Fibers collected directly from the same batch spun under Table 3.12 parameters were mounted in the experimental setup. The latter was submerged completely for five minutes before taking the test without removing the water. In this way the hydrolysis cleavage has time to interact with the silk fibroin structure, starting to break hydrogen bonds. Mechanical data are presented as for the tests performed in air. The experimental setup is showed in Figure 3.16.

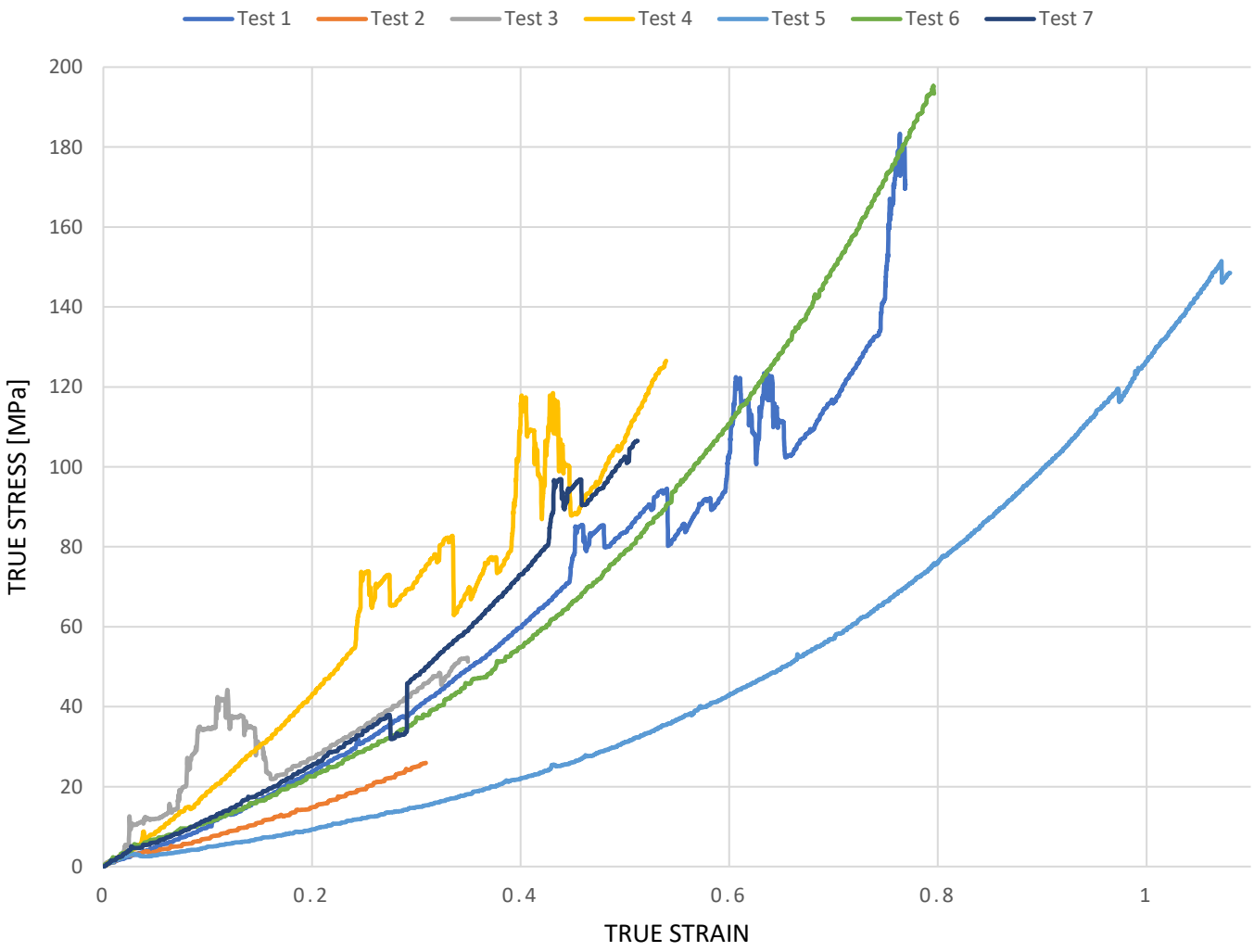

Figure 3.14 – True strain – True stress plot of the submerged samples obtained under the parameters listed in Table 3.12. The fibers show a different behaviour respect to the in-air tests. Some tests show disturbs in the evolution that might be due to balance related errors. Anyway, some good tests are appreciable, giving a good idea of the silk fibroin SFS fibers mechanical behaviour in water.

FUNDAMENTAL PARAMETERS	Test1	Test2	Test3	Test4	Test5	Test6	Test7	AVERAGE	SD
Breaking stress [MPa]	170.66	25.93	51.28	126.57	148.54	193.38	106.48	117.55	61.26
Deformation at breaking %	76.91	30.93	34.96	53.94	108.00	79.63	51.23	62.23	27.47
Fiber diameter [um]	10.96	9.32	9.04	8.43	16.31	10.36	10.08	10.64	2.64
Work to fracture [MJ/m^3]	47.36	3.70	10.39	32.33	53.11	55.28	22.02	32.03	20.78

Table 3.15 – Mechanical fundamental parameters along with average and standard deviation listed for fibers plotted in Figure 3.14. High tenacity and plastic behaviours are evident in the data. Elastic modulus is not reported since no linear region is present.

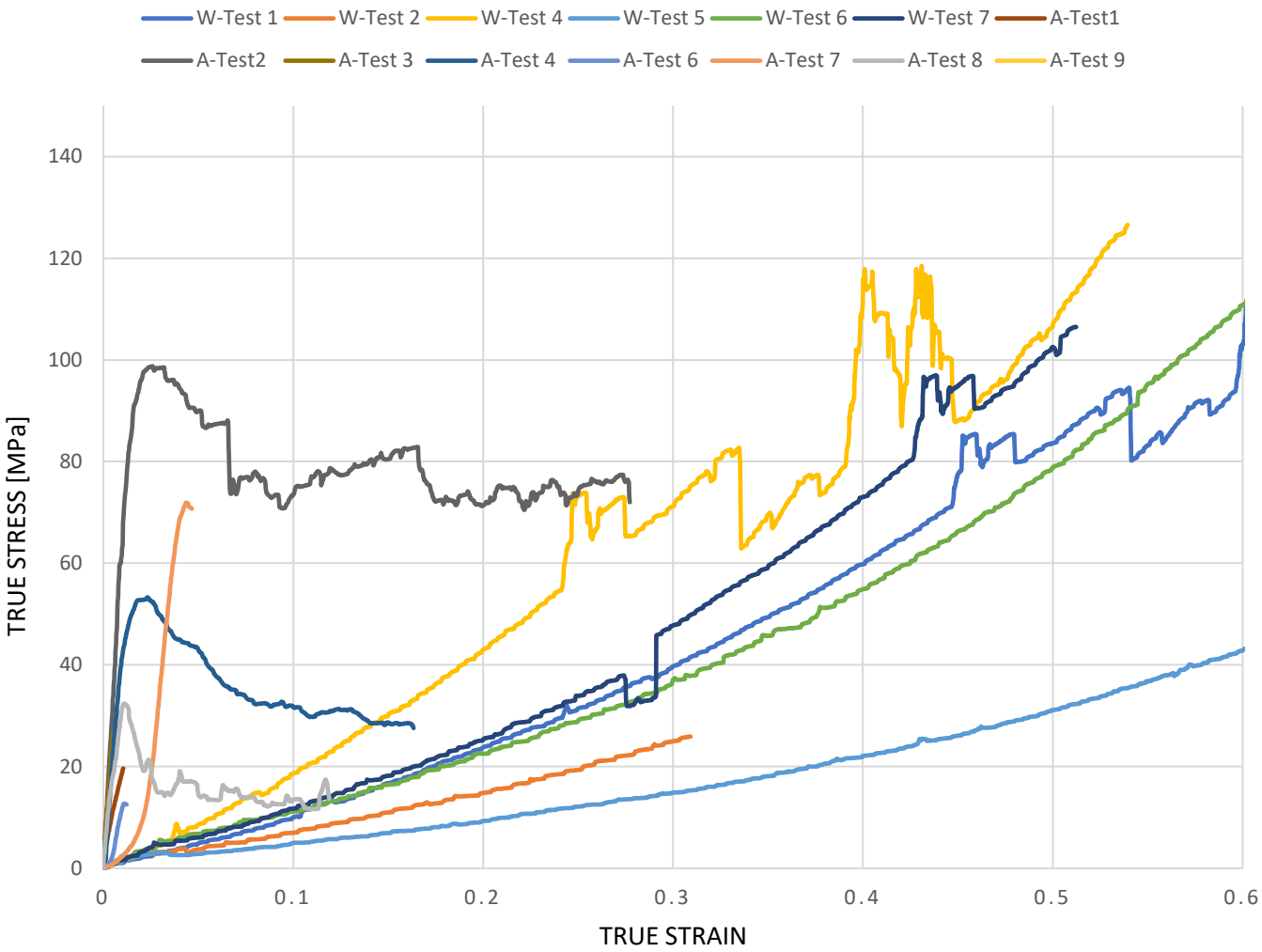

Figure 3.15 – Comparative plot of all in-air and in-water curves for silk fibroin fibers after 20 minutes of degumming at 20% fibroin concentration in w/V. In legend the letter "W" stands for water, while letter "A" stands for air. Plotted data are relative to Table 3.15 for in-water tests and Table 3.13 for in-air tests. A couple of problematic tests were removed from the plot. A limitation on the true strain axis was applied to allow better visualization of the plot initial region.

As expected, an evident change is observed in Figure 3.15 compared to the air testing. Outstanding fiber deformation are achieved up to a maximum of 108% the initial length of test 5 fiber. The elastic modulus values are estimated by taking the tangential values in initial region of each test and an average modulus of 154 MPa is found. At the same time, the submersion in water does not seem to affect too much the resistance at breaking. This evidence leads to think that the cleavage of the hydrogen bonds changes the fragile fibers behaviour into a ductile one. This is interesting when related to silk fibroin-based guides implantation, since it could mean that the constructs will easily bear the deformations caused by blood flow. In the Figure 3.14 plot there are some peaks that might be related to balance errors during the test evolution. Changing in the fiber organization during the test might also be an explanation.

Comparing the in-water behaviour of SFS fibers to wet-spun fibers results contained in the work of Plaza et al[20], is evident that this technique greatly improves the mechanical resistance of silk fibroin fibers even when submerged.

The reduction in the elastic modulus and the behaviour change to a more ductile one, are promising observations since they resemble much more the mechanical characteristics of natural blood vessel structure.

Concluding this chapter, it is possible to say that mechanical data obtained both in air and in water tests, let think that all the mechanical requirements to create silk fibroin fibers based tubular guides are met, even if difficulties were experienced during this work. Established that, the enzymatic degradation kinetics of good quality silk fibroin fibers will be this work focus from now on, since the ultimate objective is to determine a way to join one or more tubular guides.

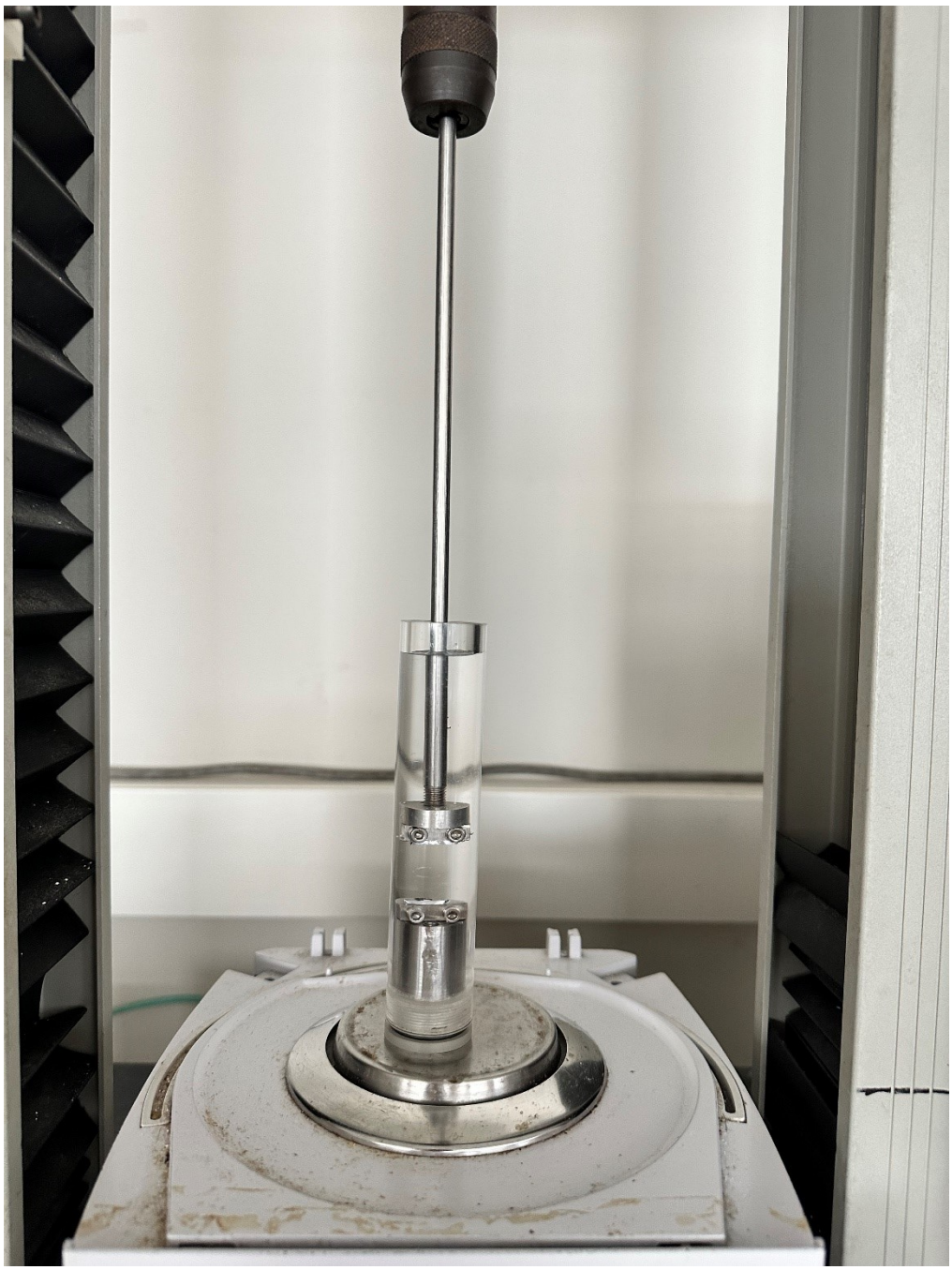

Figure 3.16 – Experimental setup for the tensile test conducted with the fiber submerged by water. Since great deformation is expected, the tube is filled completely with water whatever fiber initial length is.

4 – Enzymatic degradation kinetics of SFS silk fibroin fibers

4.1 – Introduction to enzymatic degradation of silk fibroin

Silk fibroin has promising advantages over synthetic polymers due to its favourable properties, including good biocompatibility, biodegradability and bioresorbability. These last two properties will be the focus of this paragraph where the enzymatic degradation of regenerated silk fibroin fibers will be investigated.

A brief introduction to the degradation mechanism of different enzymes must be made to understand the choices taken in the experimental setup.

Factors dictating the enzymatic degradation of regenerated silk materials can be categorized into two main groups: (a) structure-related and (b) morphology-related. Structure-related factors include molecular weight, protein secondary structures, crystallinity, and hierarchical structure. Morphology-related factors include material format, porosity and surface morphology. All these factors must be considered when assessing the degradation properties of regenerated silk materials. Generally, the main secondary structures of fibroin are random coils and amorphous type (silk I) and the antiparallel β-sheet type (silk II) which is formed through hydrogen bonds between adjacent peptide chains in a self-assembly process. The silk I structure is water-soluble while the silk II one is insoluble in several solvents including mild acid conditions adopted during this study. It appears clear that, in the final molecular assembly, the hydrophobic domains play a fundamental role by determining silk fibroin biodegradability and biocompatibility. Harsher degumming conditions and longer degumming times lead to lower molecular weight since silk fibroin is susceptible to slow hydrolysis due to the alkaline conditions utilized during the process. Thus, the protein structures of regenerated silk fibroin change compared to the native fiber features, which leads to changes in susceptibility to enzymatic degradation. Regardless of enzyme preference, the processing methods used to make regenerated silk materials dictates the degradation properties of the products, since the structures and morphologies of these silk materials vary based on the processing method utilized. Knowing this, the first step is to identify a good enzyme for this study purpose.

Many studies in the past have focused on investigating the biodegradation of silk fibroin-based materials. As a protein, silk fibroin is susceptible to biological degradation by proteolytic enzymes such as chymotrypsin, actinase and carboxylase[22]. Examples of proteolytic enzymes can be found in Table 4.1.

Generally, the biodegradation behaviour is a two-step process. The first step is adsorption of the enzyme on the substrate surface through surface-binding domain and the second step is hydrolysis of the ester bond. The final wastes of silk fibroins are the corresponding amino acids,

which are easily absorbed *in vivo*. The characteristics of silk degradation behaviours vary with different enzymes. One of the first investigation regarding the biodegradation of silk fibroin fibers and films was conducted by Arai et al.[23] who tested the action of collagenase type F, α-chymotrypsin and protease type XXI. Silk fibroin fibers were obtained directly after a degumming procedure, while films were obtained by dissolving the fibroin in a LiBr solution previously. Both constructs were incubated in enzymatic solutions and the changes in sample weight were measured at different type.

The first discovery was the low amount of mass loss of fibroin fibers (only 2% respect to the initial mass) while significant changes were observed in films with high amorphous regions when they were immersed in collagenase and protease solutions. Among the enzymes used, they found out that protease was more aggressive respect to the other two enzymes tested and it always caused greater weight loss. Other study conducted by Li et al.[24] and Horan et al.[25] find that α-chymotrypsin could degrade the dissolved fibroin proteins but not the fibroin sheets. This confirms how this enzyme is more prone to degrade amorphous regions of fibroin fibers. The motivation is related to the silk II structure steric hindrance that limits the enzyme diffusion into the packed texture.

Such information leads to a first selection in the enzyme choice to degrade the SFS fibers. In fact, it is assessed that, thanks to the innovative spinning technique, the regenerated fibroin fibers show good degree of crystallinity, which is represented by silk II domains. Since the aim of this section is the determination of an enzymatic solution that can rapidly degrade the fiber structure, there is no reason to work with chymotrypsin.

On the other hand, proteases are highlighted as a good candidate to rapidly digest silk fibroin regenerated fibers. Although protease is the less specific compared to other enzymes, it is assessed that after exposing fibroin film to its action silk II almost disappears while a large amount of silk I is formed. This shows the strong protease ability to degrade silk fibroin.

Among the literature many proteases have been investigating like protease XIV, protease E, protease XXI, protease XXIII and proteinase K[22-27]. In the review proposed by Guo et al.[26] it is reported how proteinase K shows better degradation efficiency on silk films than protease XIV which is one of the best proteolytic enzymes to digest silk fibroin. This is also due to the difference between the two that consists in the evidence that proteases are involved in the cleavage of the peptide bond in proteins, while proteinases are a type of protease capable of cleaving internal peptide bonds. Moreover, a recent study conducted by Jameson et al.[28] compares the degradation performance of protease K and protease XIV on silk fibroin sponges. It is found that incubating the sponges in same concentration enzymatic solutions of the two proteases led to complete degradation of the sponges in 11 days for protease XIV and in 2 days

for proteinase K. Supporting this experimental data, in Table 4.2 the proteinase K and protease XIV cleavage sites and their theoretical number for silk fibroin protein are observable. Then is clear why proteinase K show the greatest extent of degradation compared to any other protease. This characteristic is exactly what it was sought to start the degradation experiment. The choice then was to continue the study using proteinase K as biodegradation agent.

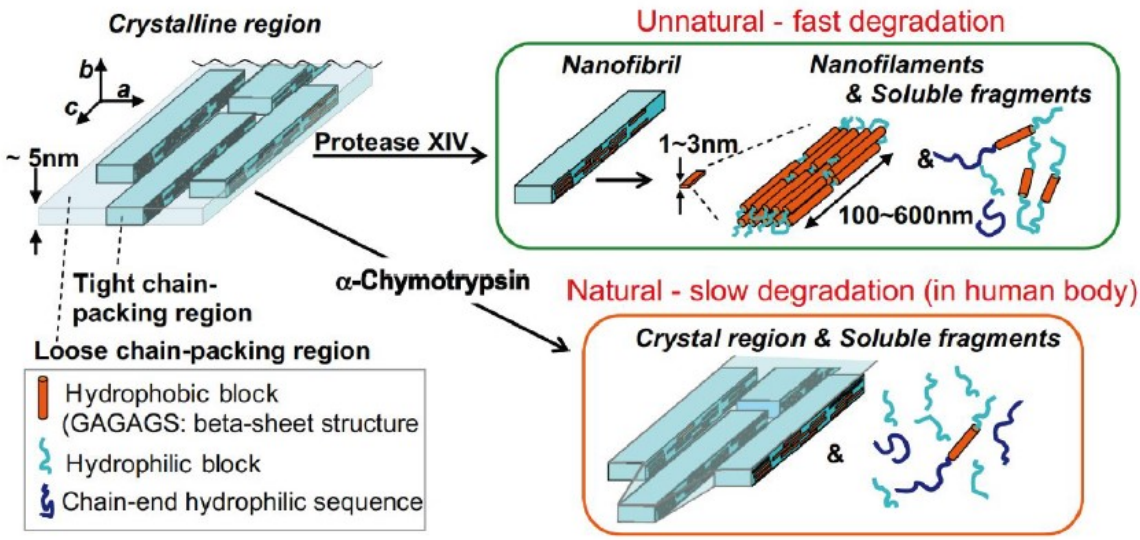

Figure 4.1 – Model of enzymatic degradation of β-sheet crystalline regions of silk fibroin. Upon enzymatic degradation by protease XIV, the loosely chain-packing regions are degraded first, followed by degradation of tightly chain-packing structures. Upon enzymatic degradation by α-chymotrypsin, the edges and ends of loosely chain-packed regions are degraded.

Enzyme	Cleavage sites	No. of cleavage sites in silk fibroin
Protease XIV	Tyr, Phe, Trp, His, Lys, Arg	~390
α-chymotrypsin	Tyr, Phe, Trp, Val, Ile, Leu	~520
Proteinase K	His, Phe, Trp, Tyr, Ala, Ile, Leu, Pro, Val, Met	~2200
Papain	Lys, Arg	~40
Matrix metalloproteinases 1	Gly-Ile, Gly-Leu	<10
Matrix metalloproteinases 2	Gly-Ile, Gly-Leu, Gly-Val, Gly-Phe, Gly-Asn, Gly-Ser	~600
Collagenase	X-Gly-Pro	~15

Table 4.1 Examples of proteolytic enzymes for degrading silk fibroin presented with aminoacidic cleavage sites and their estimated number for silk fibroin protein.

4.2 - Degradation trials and results

To develop a first model on the degradation rate of straining flow spun silk fibroin fibers, a similar approach to the one adopted by Jameson et al.[28] was selected. The concentration of the enzyme proteinase K in phosphate buffered saline (PBS) solutions was varied between 0.001 and 0.1 U/mL. The unit U called "activity" is defined as it follows: unit for the amount of a particular enzyme that produces a certain amount of enzymatic activity. In other words, it quantifies the enzyme amount that catalyses the conversion of 1 micro mole of substrate per minute. The solutions were prepared in 0.5 mL eppendorfs from a starting proteinase K solution of 0.6 U/mL following the elution equation.

$$C_0 * V_0 = C * V \tag{4.1}$$

Where C_0 and V_0 are the initial concentration in U/mL and the initial volume in mL respectively. Knowing the target solution volume which is constant at 0.5 mL and the initial concentration, constant as well at 0.6 U/mL the only thing to arbitrarily choose are the different final concentrations to test. In this study concentrations studied were 0 (pure PBS), 0.005, 0.01, 0.05 0.1 and 0.5 U/mL. Calculations based on equation (4.1) are reported in Table 4.2.

Concentration [U/mL]	Volume of PBS [uL]	Volume of Proteinase K solution [uL]
0.5	83	417
0.1	417	83
0.05	458	42
0.01	492	8
0.005	496	4
0	500	0

Table 4.2 – Proteinase K volume collected from a 0.6 U/mL original solution to be add to PBS volume to obtain the desired dilution.

To collect such small amounts of solutions, different laboratory pipettes were used, in particular it was used a P10 pipette (0.1 – 10 uL) to collect the smallest enzyme volumes.
Incubation time for the first trial was set around 24h at 37°C since, as previously seen, for proteinase K 48h are sufficient to completely degrade more complex structure as sponges at the set temperature. To study the degradation effect, the following equation was used to determine the residual mass in percentage:

$$Residual\ mass\ \% = \frac{Residual\ mass\ after\ degradation}{Initial\ mass} * 100 \qquad (4.2)$$

Both fibers initial and residual masses were measured in a completely dry state. To ensure this, fibers were dried at 65°C for 24h. Moreover, higher temperatures inhibit residual proteinase K activity.

Although at first some attempts were made to analyse the degradation directly on single fibers, the mass loss data were influenced by the presence of the aluminium support, or the fiber was so damaged that it wasn't observable anymore. Moreover, weighting single fibers requires high resolution and sensitivity instrumentation and clean the fibers from proteinase K was difficult to realize.

Trying to resolve these problems, fibroin fibers balls of approximately 2-3 mg in weight were realized with fibers collected from in air good mechanical quality batches. To assess the silk II packing of the fibroin, few fibers were aligned on a laboratory glass and a drop of water was put over the fibers. If after 1h the fibers were still observable (or the light reflection produced by a torchlight) then they are insoluble and can be submerged in the enzymatic solutions. An example of insoluble fibers can be found in Figure 4.2.

Figure 4.2 – Silk fibroin fibers aligned in a laboratory glass. A drop of water is made to fall on the fibers. Although is difficult to see, from a closer look fibers are still visible even in contact with water. This assesses the insoluble state of fibroin fibers.

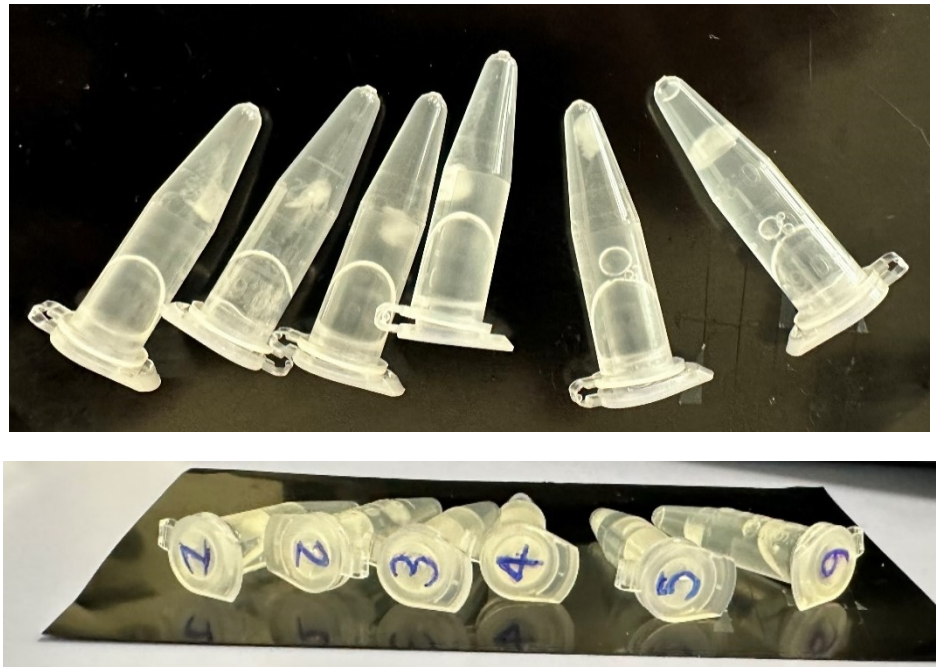

Figure 4.3 – Eppendorfs with fiber balls submerged in different concentration enzymatic solutions. 1 stands for the highest concentration used in the trial, while C stands for control.

Once created, the fibroin balls were put into the eppendorfs filled with enzymatic solutions at different concentrations. In Figure 4.3 the eppendorfs are showed and classified by a number, where 1 represents the highest enzymatic concentration and the C the control of pure PBS. To dry the fibroin masses, they were extracted from the enzymatic solution and distributed on a laboratory glass as in Figure 4.4. Then they were left to dry in the same way applied to the fibers. As already mentioned, the first trial incubation was 22h. Results are listed in Table 4.3.

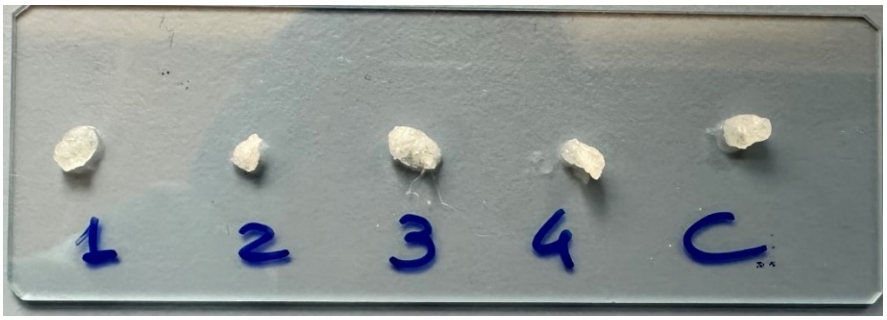

Figure 4.4 – Laboratory glass where wet fibroin balls are collected after the incubation time and left to dry in the oven. The numbers are written to recognize each sample.

Enzyme solution concentrations [U/mL]	Fibroin initial mass [mg]	Residual mass [mg]	Residual mass %
0.5	2.15	0.54	25.12
0.1	2.14	1.07	50
0.01	2.47	1.56	63.16
0.005	2.08	1.51	72.60
0	2.06	1.66	80.58

Table 4.3 – Fibroin initial mass, residual mass after degradation and drying and residual mass percentage from 22 hours incubation trial.

From a first simple plot a negative exponential evolution is detected. Thanks to *Matlab* tools, an explorative first fit is applied to the experimental data following the general equation (4.3) and its plot is showed in Figure 4.5.

$$y = ae^{-\alpha x} \tag{4.3}$$

y represents the studied quantity, in this case the residual mass percentage, while x is represented by enzyme solution concentrations. The other letters are model parameters that must be determined computationally. A first set of parameters is listed in Table 4.4. Only final parameters will be presented to not burden the result presentation.

The model doesn't represent well the data as it is confirmed by its R^2 coefficient, which represents the percentage of the dataset explained by the model. For this reason, a second negative exponential is added to the model as indicated in equation (4.4). This improves largely the model accuracy, with a R^2 value equal to 0.996.

$$y = ae^{-\alpha x} + be^{-\beta x} \tag{4.4}$$

Model parameters	Single exponential	Double exponential
a	71.74	22.4
α	2.42	115.3
b	/	58.69
β	/	1.689

Table 4.4 – First explorative set of parameters for the one exponential model and double exponential model. In the more complete model, the first term rapidly decreases to leave more importance to the second exponential.

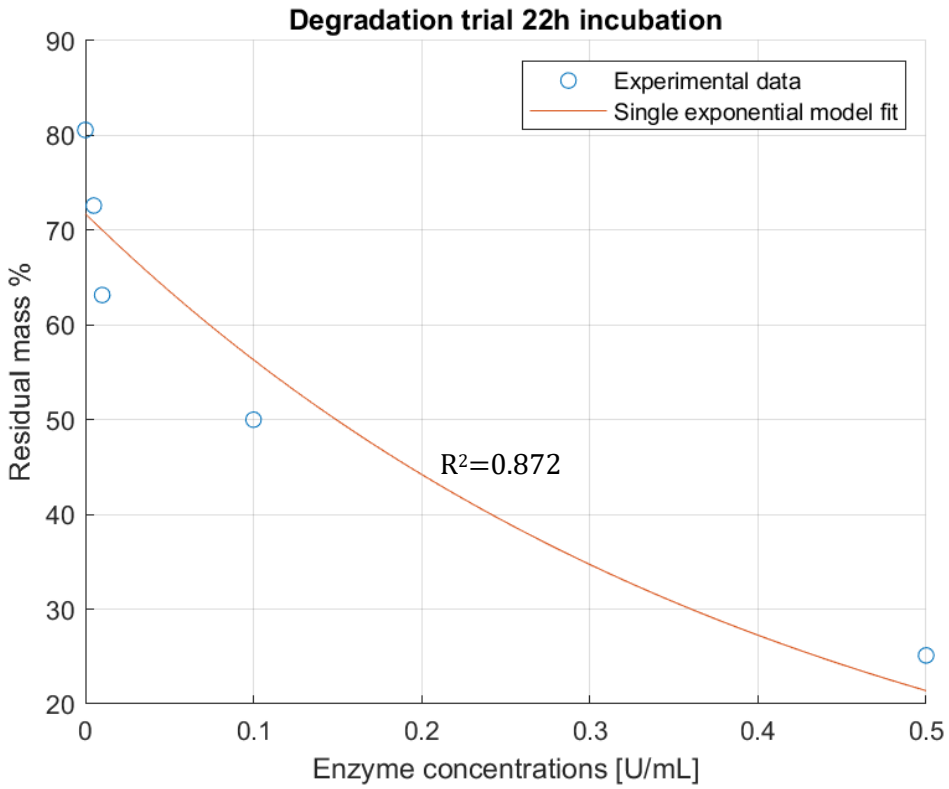

Figure 4.4 – Plot of the experimental data and single exponential model fit for the 22 hours incubation time trial. The model doesn't fit well the dataset, especially in the initial region where a lot of information are lost. R^2 coefficient confirms the loss of information.

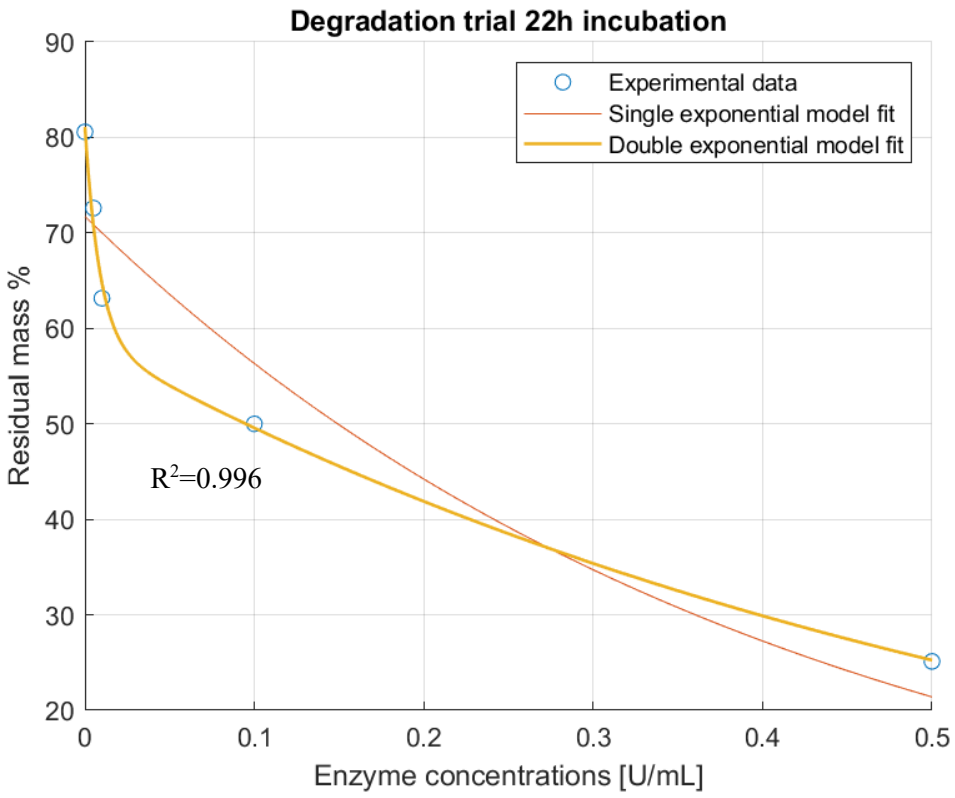

Figure 4.5 – Overlaid plot of the fit by the double exponential model. The single exponential curve fit is still represented to appreciate the significant difference in data interpretation. In this case too, R^2 coefficient confirms the good model approximation of the experimental data.

Observing the plot in Figure 4.5, the first exponential rapidly tends to decrease and gives its bigger contribution for low levels of proteinase K concentration, while the second exponential takes over in the second half of the plot. These considerations are based on only one trial and others must be performed to confirm them.

Apparently strong degradation is found to happened even for low concentrations. It's interesting to note that even in the control solution composed by only PBS, mass loss is visible, meaning that simple hydrolysis plays a role in the degradation process and creates a mass loss of almost 20% in this trial.

To study the effect of incubation time in the silk fibroin fibers degradation, a second trial was carried out with an incubation time of 90 minutes. Results are reported in Table 4.5

This time evident greater degradation is appreciable starting from the lowest enzyme concentration. This might be because these fiber balls, even if belonging to the first trial batch, were tested after some days they were produced. As a consequence, this might have an influence in the proteinase K attack effectiveness and need to be remembered for future tests. However, the double negative exponential model suits the experimental data. This shows the versatility of the model and its possible application to describe the phenomenon. Interestingly, in this case the degradation effect does not seem to highly increase at higher concentration levels, varying from 0.1 to 0.5 U/mL for only a 10%. This suggests that it is better to focus on low enzyme levels since this is the condition corresponding to major degradation potential.

More trials are needed to build a complete dataset to reduce the statistical uncertainty and to obtain more convincing results.

Since one of the objectives was to observe a fast degradation method and high degradation is found also for the 90 minutes trial, it was decided to perform the successive trials at 1h incubation. Moreover, to have more information on the residual mass for low concentrations, a new enzyme concentration solution is introduced at 0.05 U/mL.

For the next results to be presented, since a great amount of fiber was spun, three trials were taken simultaneously with only one control sample.

Enzyme solution concentrations [U/mL]	Fibroin mass [mg]	Residual mass [mg]	Residual mass %
0.5	2.07	0.14	6.76
0.1	1.79	0.29	16.20
0.01	2.03	0.48	23.64
0.005	1.85	0.67	36.22
0	1.57	1.22	77.71

Table 4.5 – Fibroin initial mass, residual mass after degradation and drying and residual mass percentage from 1.5 hours incubation trial.

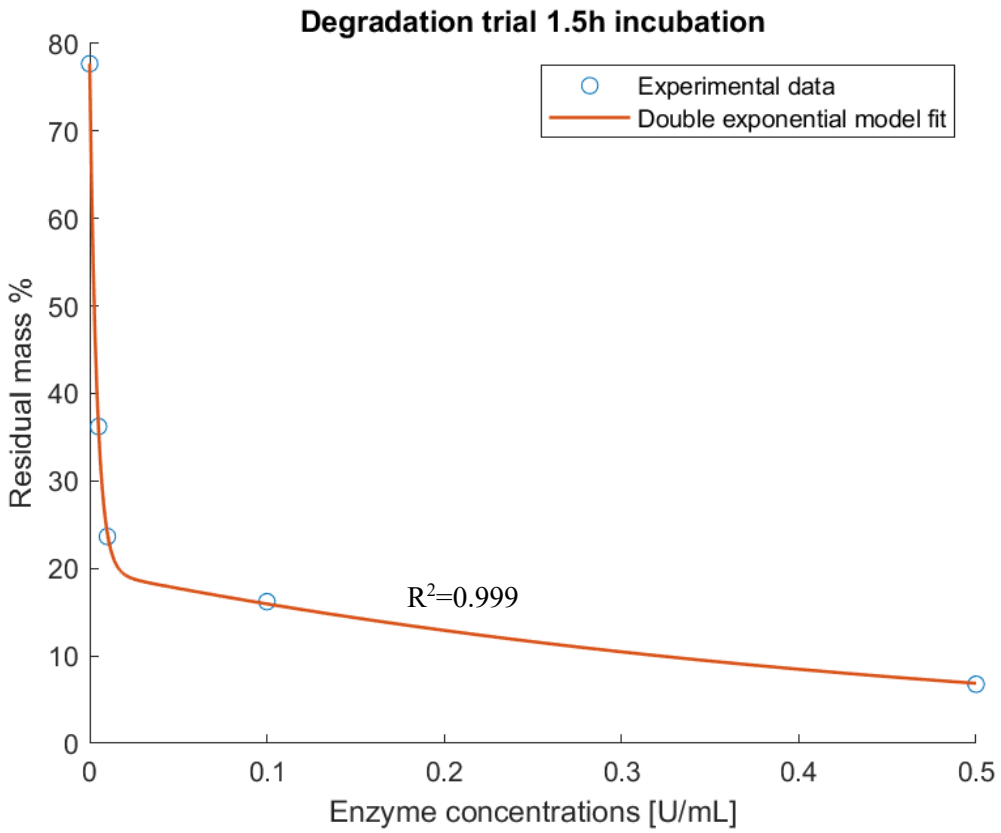

Figure 4.6 - Plot of the experimental data and double exponential model fit for the 1.5 hours incubation time trial with R^2 coefficient reported. The approximation is almost perfect.

1 - Trial 1h	Enzyme concentrations [U/mL]	Fibroin mass [mg]	Residual mass [mg]	Residual mass %
T1	0.1	2.82	0.72	25.53
	0.05	2.44	0.73	29.93
	0.01	2.61	0.95	36.40
	0.005	2.89	1.12	38.75
T2	0.1	2.22	0.64	28.83
	0.05	2.58	1.02	39.53
	0.01	2.25	1.05	46.67
	0.005	2.18	1.05	48.17
T3	0.1	1.5	0.4	26.67
	0.05	1.45	0.49	33.79
	0.01	1.6	0.905	56.56
	0.005	1.45	0.877	60.48
CONTROL	0	2.96	2.3	77.70

Table 4.6 - Fibroin initial mass, residual mass after degradation and drying and residual mass percentage from first 1-hour incubation trials divided into repetitions named T1, T2 and T3. The control corresponds to the pure PBS solution.

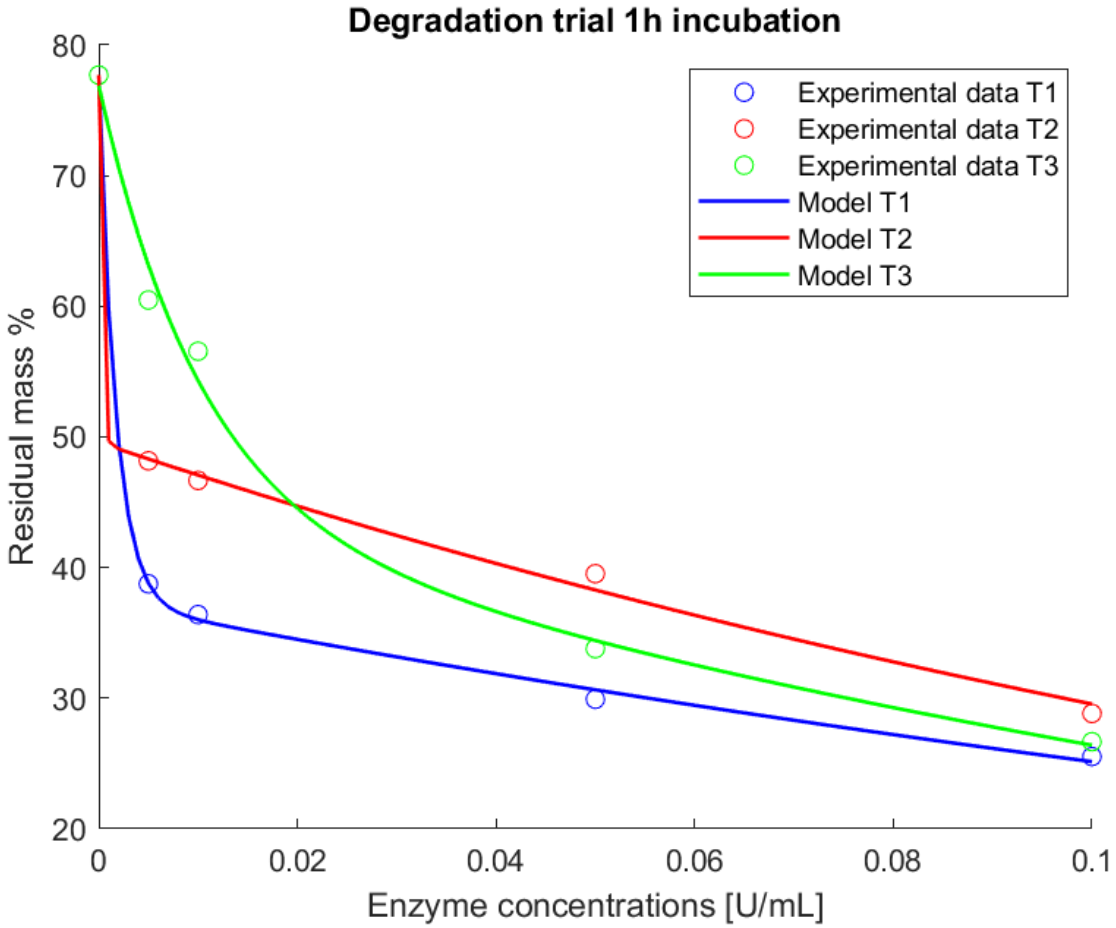

Figure 4.7 – Plot of the experimental data and double exponential model fit for the first run of 1 hour incubation time trials T1, T2 and T3 represented in different colours. All datasets seem to be well represented by the double exponential model.

Trial 1 – 1h Incubation time	**Model R^2 coefficient**
T1	0.998
T2	0.993
T3	0.969

Table 4.7 – List of models R^2 coefficients for the trials T1, T2 and T3 represented in Figure 4.7. The coefficients confirm the good model approximation.

From the plot in Figure 4.7 and the R^2 coefficients of Table 4.7 is possible to deduce that the model suits the data in a good way. This confirms the goodness of the model. The degradation

evolution is similar to the previous trials with T1 and T3 showing a regular behaviour. Only T2 seems to have an extremely rapid decrease in residual mass and then a linear-like evolution. It is noted that for highest enzyme concentrations the variance in the experimental data is lower. This suggests that if we want a fast and reliable degradation, concentrations between 0.05 and 0.5 should be used.

For the last batch of fibers, other three trials were conducted, reaching a final number of trials of 8.

2 - Trial 1h	Enzyme concentrations [U/mL]	Fibroin mass [mg]	Residual mass [mg]	Residual mass %
T1	0.1	2.58	0.91	35.27
	0.05	2.98	1.28	42.95
	0.01	2.95	1.36	46.10
	0.005	2.85	0.89	31.23
T2	0.1	2.79	0.6	21.51
	0.05	2.92	0.68	23.29
	0.01	2.97	1.12	37.71
	0.005	2.63	1.15	43.73
T3	0.1	2.93	0.91	31.06
	0.05	2.88	0.96	33.33
	0.01	2.75	1.44	52.36
	0.005	2.63	1.06	40.30
CONTROL	0	2.85	1.85	64.86

Table 4.8 – Fibroin initial mass, residual mass after degradation and drying and residual mass percentage from second 1-hour incubation trials divided into repetitions named T1, T2 and T3. The control corresponds to the pure PBS solution. Some oddities are found in the residual mass percentage of T1 and T3 since the values corresponding to 0.005 U/mL concentration are lower than the residual mass corresponding to 0.01 U/mL concentration.

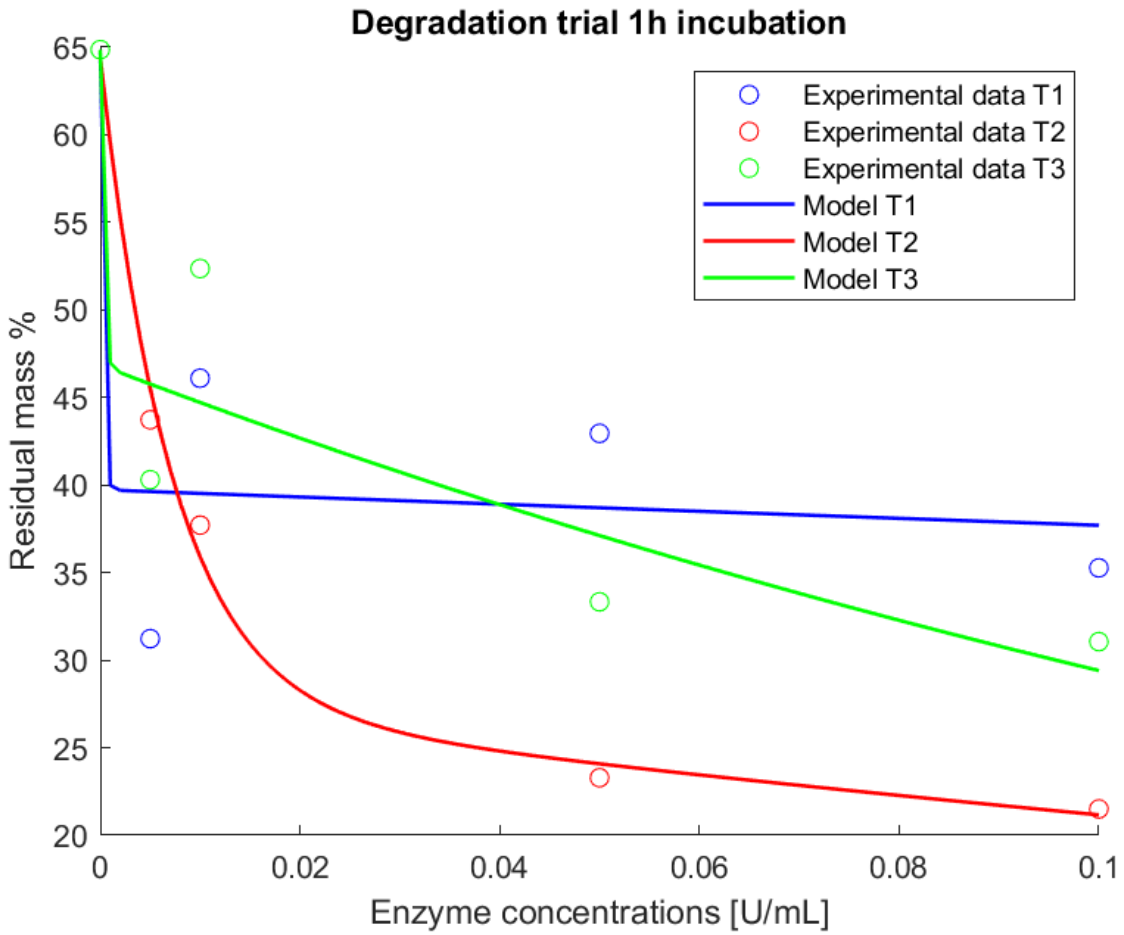

Figure 4.8 – Plot of the experimental data and double exponential model fit for the second run of 1 hour incubation time trials T1, T2 and T3 represented in different colours. Contrary to the first run, in this case the model seems incapable of fitting T1 and T3 datasets. Nevertheless, the experimental data show a strange behaviour, justifying the bad model approximation.

Trial 2 – 1h Incubation time	**Model R^2 coefficient**
T1	0.189
T2	0.976
T3	0.472

Table 4.9 - List of models R^2 coefficients for the trials T1, T2 and T3 represented in Figure 4.8.

Unlikely the other results obtained, this run shows different problems, starting from the experimental data measured. As it possible to see both in T1 and T3 the residual mass at 0.01 U/mL is higher than the one measured at 0.005 U/mL. This of course is not what is normally expected and disagrees with the other runs performed. Then it's clear that the model can't interpret these datasets, justifying the poor R^2 coefficients when applied to T1 and T3. The reasons behind these errors could be multiple, but probably in this fiber batch the chemical

organization varied deeply between the fibers. Anyway, T2 shows a normal behaviour and is well fitted by the model.

At this point, summarizing all the experimental data acquired, the final version of the model parameters can be obtained. For the trials where one enzymatic calculation is missing, the corresponding value gained by the model was used to fill the dataset. To resume the variance in the different trials, a boxplot is presented in Figure 4.9.

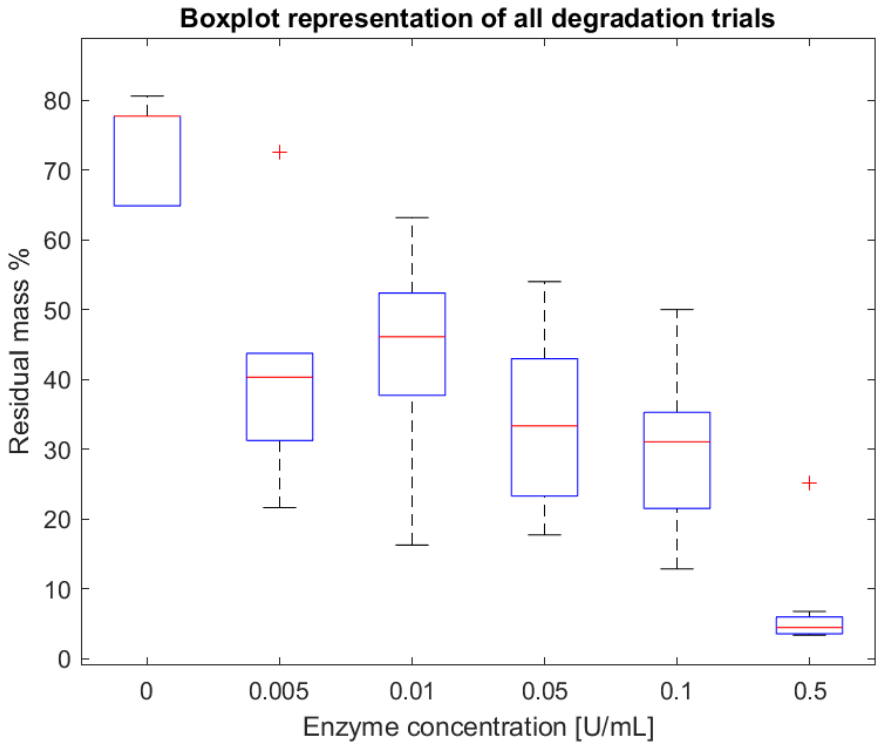

Figure 4.9 – Boxplot representation of the experimental data obtained from all 8 degradation trials performed in the study. Only two outliers are detected, relative to the same trial. The global behaviour is coherent to what was expected, except for the residual masses relative to 0.005 U/mL concentration. This is certainly due to the odd data obtained by the second 1h hour incubation time trials.

Enzyme concentration [U/mL]	Residual mass % average	Standard Deviation
0.5	4.47	1.28
0.1	26.93	8.47
0.05	30.98	9.93
0.01	41.23	12.54
0.005	36.02	8.25
CONTROL	72.20	6.84

Table 4.10 – Average and standard deviation of the whole experimental data collected.

Observable outliers related to the same trial (22h incubation time) are detected and not considered in model final formulation nor in the data listed in table 4.10.
Finally, the final parameters of the model are presented in the following equation:

$$Model\ residual\ mass\ \% = 32.61e^{-3553*C} + 39.59e^{-4.175*C} \quad (4.5)$$

Where C stands for the enzyme concentration in U/mL. It appears clear that the two negative exponentials have a different behaviour, where the first one tends to give a contribution only for concentration values that are relay close to zero. The second term contains the biggest part of the information, tracing the model evolution.
Observing the model evolution in Figure 4.10, three different regions are detected:

- The initial region, where both terms give their contribution and rapidly decreases. This region confirms that heavy degradation effect is present even for almost null proteinase K concentrations.

- The middle region where a change of pendant is observed and where degradation is slower as concentration is higher. This might mean that the enzymatic sites are already almost fully occupied by lower enzyme concentration, leaving the excessive proteinase K unemployed.

- The final region where a sort of plateau is visible. Concentrations over 0.5 U/mL don't produce significant differences in mass loss respect to lesser ones. On the contrary, the effect of low concentrations degradation compared to pure PBS (simple hydrolysis) solution is evident.

Knowing the mechanisms about how silk fibroin regenerated fibers are attacked by proteinase K and the evolution of the degradation depending on the enzyme concentration, it is possible to conclude that low amount of proteinase K create sufficient mass loss to degrade silk fibroin straining flow spun fiber in a limited amount of time. Of course, the incubation time plays a role in this phenomenon and, for more complex structures respect to fiber balls it should be increased to observe relevant mass loss.

The original question driving this paragraph study was if it is possible to obtain appreciable degradation effect on fibroin fibers, therefore to create a hole on the surface of a silk fibroin based tubular guide. Based on the findings presented, it is possible to say that the degradation effect is sufficiently strong to hypothesize that, if the tubular structure is put in contact with enzymatic solution at concentrations of at least 0.1 U/mL, a hole can be created. However, it must be considered that tubular guides are definitely more complex structures formed by several layers of fibroin fibers. Then, as shown also by the literature, enzymatic concentrations and incubation time can vary largely from the ones adopted in this study.

To further deepening the knowledge of the degrading effects of proteinase K on silk fibroin, it was decided to perform a spectroscopic analysis with FTIR (Fourier-Transform Infrared spectroscopy) technique.

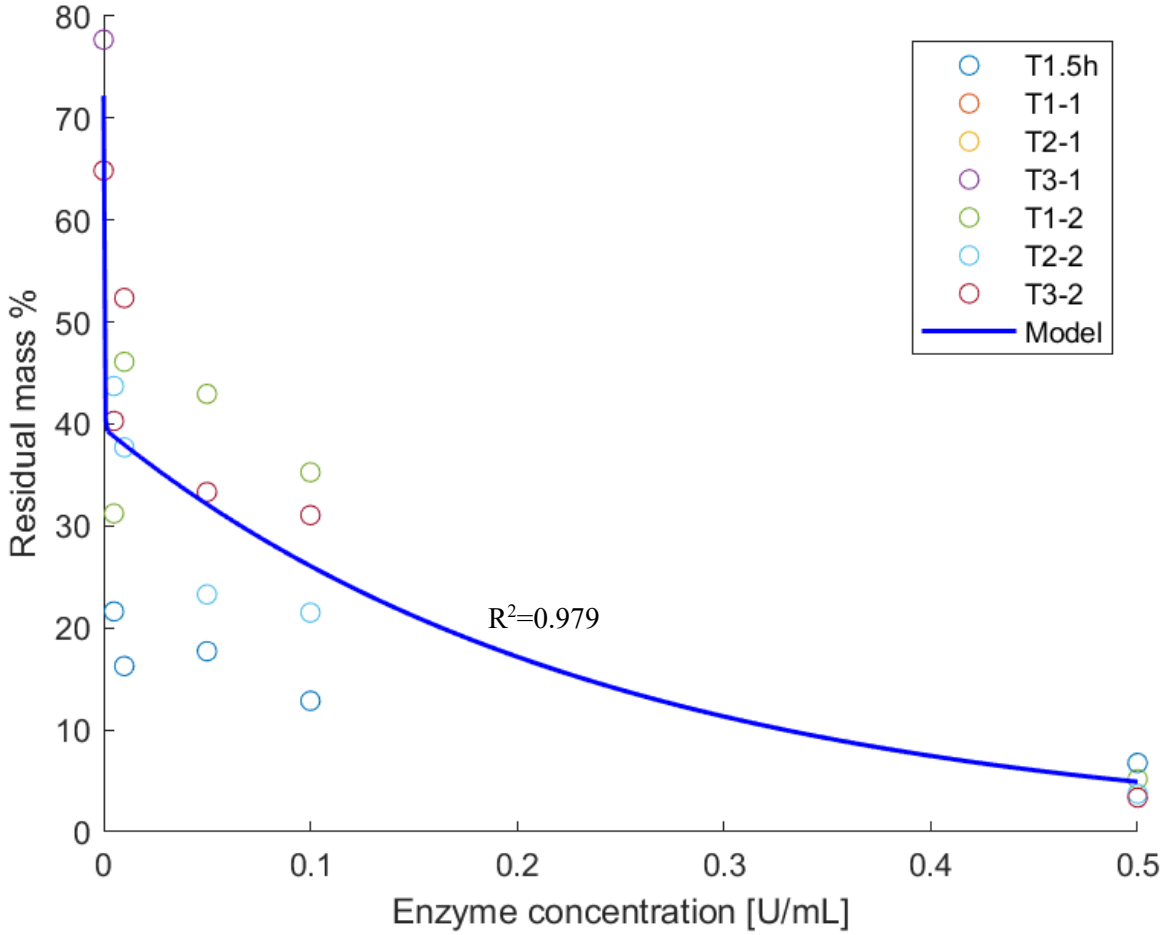

Figure 4.10 – Final plot of the experimental data used to determine the double exponential model parameters and model fit to them. R^2 is reported and assesses the fit good quality. A strong decreasing behaviour is found in the graphic first section, then the decreasing becomes slower. This plot suggests that degradation effects are lower for higher concentration at the same incubation time.

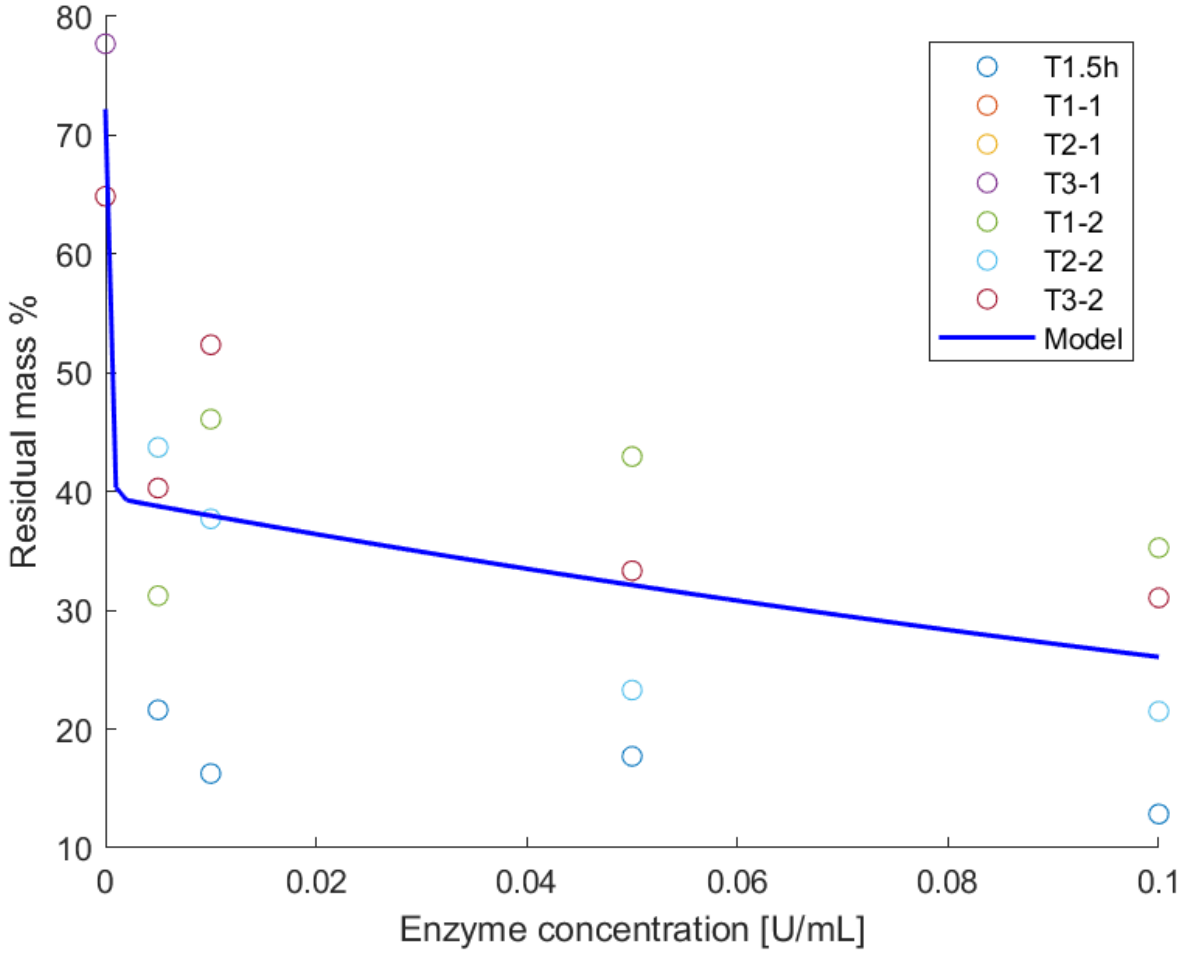

Figure 4.11 – Enlargement of Figure 4.10 plot by limiting the graphic to 0.1 U/mL to appreciate better the behaviour around the pendant change.

4.3 Post degradation fibroin secondary structure analysis by FTIR spectroscopy

Mass loss produced by proteinase K is the most evident effect of macroscopical degradation but for sure it affects the microstructure of the fibroin protein. To investigate how the enzyme affects the organization of the protein, a Fourier Transform Infrared spectroscopy (FTIR) analysis was performed on the dry fibroin balls after being weighted.

FTIR is a technique used to obtain an infrared spectrum of absorption or emission of a solid, liquid, or gas. An FTIR spectrometer simultaneously collects high-resolution spectral data over a wide spectral range. The goal of absorption spectroscopy techniques is to measure how much light a sample absorbs at each wavelength. The FTIR technique shines a beam containing many frequencies of light at once and measures how much of that beam is absorbed by the sample. Next, the beam is modified to contain a different combination of frequencies, giving a second data point. This process is rapidly repeated many times over a short time span. Afterwards, a computer takes all this data and applies the Fourier transform to infer what the absorption is at each wavelength. From a wavelength database is possible to deduce the secondary organization of the silk fibroin crystallites.

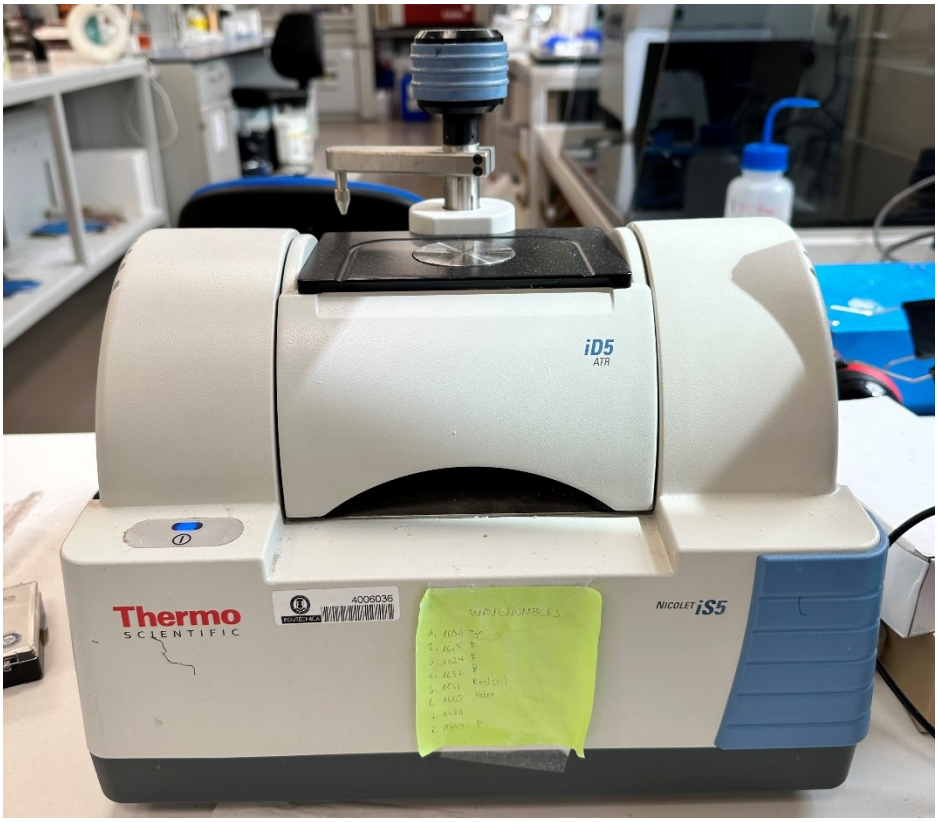

Figure 4.12 – Nicolet iS5 spectrometer used in laboratory.

Spectra were obtained by using a Nicolet iS5 spectrometer (Figure 4.12) equipped with an iD5 ATR complement. Each spectrum was obtained from a bundle of fibers and a background spectrum measured previously was subtracted from the experimental data. Spectra were determined as the average of 64 measurements in the range 550-4000 cm^{-1} as observable in Figure 4.14. Vibrational and assignment in the amide I region, that contains information on the secondary structure of the proteins, are listed in Table 4.11 to indicate which peaks determine the fibroin packing structure.

Wavenumber [cm^{-1}]	**Assignment**
1594-1609	Tyr side chain/aggregated strand
1610-1620	Aggregate β-strand/intermolecular β-sheet
1621-1627	Intermolecular β-sheet
1628-1637	Intramolecular β-sheet
1638-1655	Random coil
1656-1662	Helical structures
1663-1694	β-turn
1696-1703	Intermolecular β-sheet

Table 4.11 – Secondary structure assignment to wavenumbers obtained by FTIR spectroscopy.

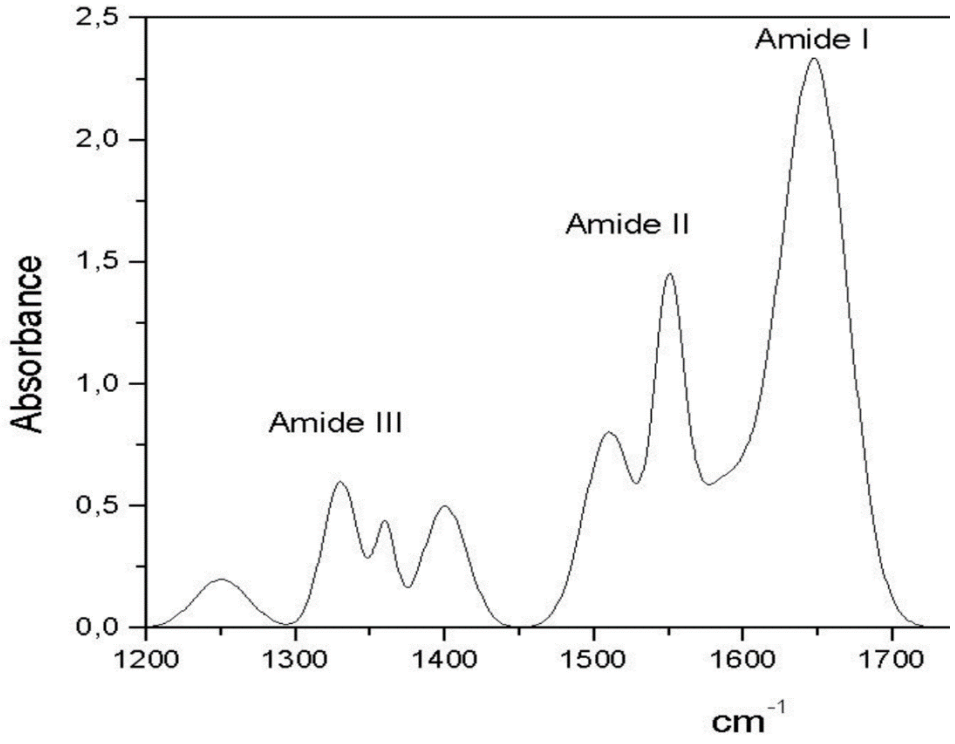

Figure 4.13 – Amide I, II and II typical peaks.

Intense amide I and amide II bands are typical of crystalline silk fibroin. Peaks around 1621-1637 cm^{-1} [29-31] indicate a β-sheet packing, characteristic of silk II state, while peaks around 1647 cm^{-1} [32] indicate prevailing random coil molecular conformation, typical of silk I configuration.

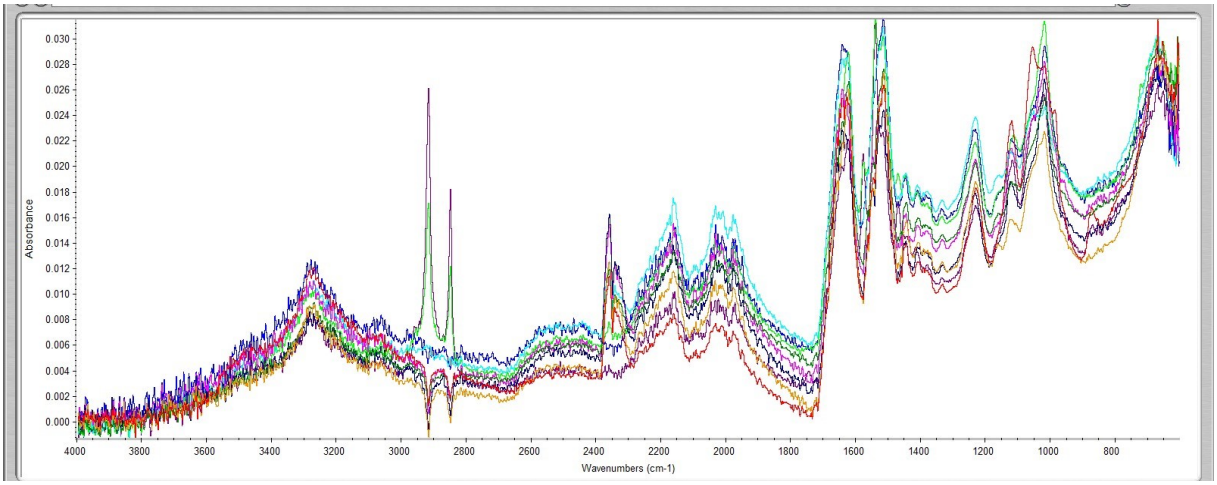

Figure 4.14 – Full experimental spectra obtained by the left fibroin balls after degradation trials. All spectra follow the same path except some irregularities around 2900 cm^{-1}. Anyway, they are not significant since the important region is in the amide I interval.

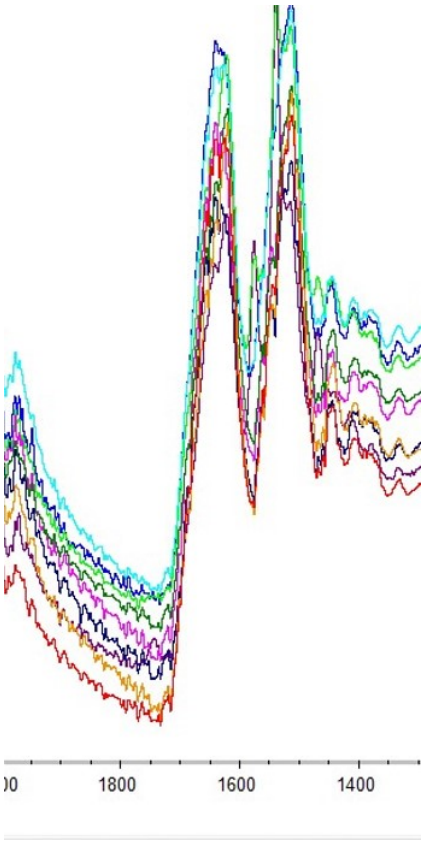

Figure 4.15 – Enlargement of the amide I wavenumber region. Peaks are detected corresponding to random coil conformation 1630 cm^{-1} and around 1530 cm^{-1}.

All the residual fiber bundles after the degradation trial were examined in the FTIR spectroscopy. Recalling the fiber chemical properties, they were degummed for 20 minutes and spun from a solution at 20% fibroin in w/V. Peaks around 1630 and 1530 cm^{-1} are found, corresponding to the amide I and II typical peaks. The conclusion is that even after heavy degradation, especially in samples where the residual mass percentage was less than 10%, the residual fibers maintain their original secondary structure and the action of proteinase K doesn't change it in any way.

Overall, this result could be predicted since the fibers did not dissolve in the enzymatic solutions, but it also confirms that the fibers maintain the packing into β-sheet structures and don't reorganize themselves into other insoluble structures.

5 - CONCLUSIONS

5.1 – Discussion about this work objectives and its limitations

This study was aimed was to investigate the mechanical and chemical characteristics of silk fibroin, in particular of regenerated fibers produced thanks to an innovative and biomimetic technique called Straining Flow Spinning.

The motivation behind this research was to investigate whether it was possible to create polybranched tubular guides based on silk fibroin that could be used in tissue engineering applications for peripheral vasculature regeneration. To partially answer to this question, several tensile tests were conducted on single fibers both in air and in wet conditions. Even if some difficulties in the spinning of good mechanical quality fiber were encountered, it was found that producing high performance fibers through SFS technique is a possible and relatively simple process that implies only mild chemical condition. By comparing obtained fibroin fibers with others recreated from other spinning techniques, an evident improvement in strain at breaking and toughness is observed.

It is noted that a post spinning process as described in several literature papers[3, 10, 18, 19] can largely improve the fibers global mechanical quality and reproducibility. During this study it was chosen to maintain the spinning process as simple as possible, so no post spinning was present.

Anyway, good fibers were obtained even with the simplest spinning option, meaning that the SFS technique is a great improvement in regenerated silk fibroin fiber production. Thinking about creating tubular guides based on regenerated silk fibroin SFS produced fibers is then possible basing on the evidence presented in this study. It must be said that the analytical process of the tensile tests data might have been influenced by some errors during the evolution of the tests themselves and regarding the fiber diameter estimation procedure as it was discussed in the result presentation paragraphs. A more precise procedure utilizing more accurate instrumentation can provide improvements in fibroin fibers behaviour analysis.

The second question this study aimed to answer is if it is possible to experiment sufficient degradation in a fast way to create a hole in a guide tubular structure to use it as a junction site for another guide. Through an initial enzyme selection process based in literature, the most effective proteolytic enzyme for fibroin protein was found to be proteinase K and chosen to carry on the study. Multiple enzymatic concentrations were tested in different incubation time trials. The whole data collected resulted in the construction of a double negative exponential model able to estimate the residual mass percentage in dependence of the concentration. It was found out that proteinase K concentration of at least 0.1 U/mL rapidly degrade fibroin fiber balls structure. Therefore, by delivering the solutions directly on the surface of a guide is

possible to create higher enough degradation to open a hole. Moreover, an FTIR spectroscopy on the post degradation fibers revealed that the secondary structure isn't changed by proteinase K activity. Although during the degradation study many difficulties were experimented, several simplifications were made in the experimental procedure. The most important one was testing fibers aggregates that didn't show a proper structure while a tubular guide is made of multiple organized layers of fibers. As already mentioned during the result analysis, this could result in much higher incubation time and enzyme concentrations to experiment decent degradation. Secondly, only eight degradation trials were performed and only seven were considered for the model construction. More information should be collected since the degradation process is strongly influenced by the fibers microstructure and sensitivity to hydrolysis. This limitation can be solved by improving the SFS spinning reliability in creating fibers that show the same characteristics.

It is clear then that this works only can be taken as an explorative approach in the realization of tubular branched silk fibroin-based guides and it should be refined with other degradation trials to improve the model ability to interpret the experimental data. Nevertheless, the whole study confirms the possibility to realize the original research question, validating further research on this topic. That could bring precious information by ultimately upscaling scaffolds geometrical complexity in cardiovascular tissue regeneration applications.

5.2 – Future development and improvements

Many improvements can be applied to this work in different aspects. Great attention must be put on finding a way to fast optimize the SFS parameters to obtain good mechanical quality fibers in a repeatability way. Guides obtained by fibers with high variance in their mechanical properties wouldn't be used in any application. A possible solution is implementing a second take up roller or a post spinning treatment that can ensure more repeatability to the fibers by stretching more the fiber microstructure obtaining a more crystalline structure. Variance is intrinsic in any biopolymer so it is normal to expect hovering results, but the variations found in this study must be limited to tighter ranges.

Then the guide production is still to be explored. Direct collection of SFS fibers can be an option if a small diameter second roller is used to build the tubular structure. A way to extract the support and only leave the fibers must be studied in this eventuality.

Another point where next studies can focus on is the enzymatic delivery to the guide surface. In this study the focus was put on understanding and characterizing the proteinase K degradation action in solutions, but in the future a way to deposit and then inhibit the enzyme must be studied.

Ultimately, after realizing the guides, an in vitro study on the adhesion and proliferation of fibroblast should be conducted to observe how the SFS silk fibroin fibers work as support.

A lot of work is still needed to finally achieve the ultimate objective of creating silk fibroin branched tubular guide, but this study traces the initial line to develop this research.

BIBLIOGRAPHY

[1] Sun W, Gregory DA, Tomeh MA, Zhao X. Silk Fibroin as a Functional Biomaterial for Tissue Engineering. Int J Mol Sci. 2021 Feb 2;22(3):1499. doi: 10.3390/ijms22031499. PMID: 33540895; PMCID: PMC7867316.

[2] Leng-Duei Koh, Yuan Cheng, Choon-Peng Teng, Yin-Win Khin, Xian-Jun Loh, Si-Yin Tee, Michelle Low, Enyi Ye, Hai-Dong Yu, Yong-Wei Zhang, Ming-Yong Han. Structures, mechanical properties and applications of silk fibroin materials. Progress in Polymer Science, Volume 46, 2015, Pages 86-110, ISSN 0079-6700. https://doi.org/10.1016/j.progpolymsci.2015.02.001

[3] Madurga R, Gañán-Calvo AM, Plaza GR, Guinea GV, Elices M, Pérez-Rigueiro J. Production of High Performance Bioinspired Silk Fibers by Straining Flow Spinning. Biomacromolecules. 2017 Apr 10;18(4):1127-1133. doi: 10.1021/acs.biomac.6b01757. Epub 2017 Mar 3. PMID: 28226209.

[4] Bin Liu, Yu-wei Song, Li Jin, Zhi-jian Wang, De-yong Pu, Shao-qiang Lin, Chan Zhou, Hua-jian You, Yan Ma, Jin-min Li, Li Yang, K.L. Paul Sung, Yao-guang Zhang, Silk structure and degradation. Colloids and Surfaces B: Biointerfaces, Volume 131, 2015, Pages 122-128. ISSN 0927-7765. https://doi.org/10.1016/j.colsurfb.2015.04.040.

[5] Aramwit P, Kanokpanont S, De-Eknamkul W, Srichana T. Monitoring of inflammatory mediators induced by silk sericin. J Biosci Bioeng. 2009 May;107(5):556-61. doi: 10.1016/j.jbiosc.2008.12.012. PMID: 19393558.

[6] Vepari C, Kaplan DL. Silk as a Biomaterial. Prog Polym Sci. 2007;32(8-9):991-1007. doi: 10.1016/j.progpolymsci.2007.05.013. PMID: 19543442; PMCID: PMC2699289.

[7] Marsh R, Corey RB, Pauling L. An investigation of the structure of silk fibroin. Biochim Biophys Acta 1955;16:1–34.

[8] Minoura N, Aiba S, Higuchi M, Gotoh Y, Tsukada M, Imai Y. Attachment and growth of fibroblast cells on silk fibroin. Biochem Biophys Res Commun. 1995 Mar 17;208(2):511-6. doi: 10.1006/bbrc.1995.1368. PMID: 7695601.

[9] Guinea GV, Pérez-Rigueiro J, Plaza GR, Elices M. Volume constancy during stretching of spider silk. Biomacromolecules. 2006 Jul;7(7):2173-7. doi: 10.1021/bm060138v. PMID: 16827584.

[10] Pérez-Rigueiro, J.; Madurga, R.; Gañán-Calvo, A.M.; Plaza, G.R.; Elices, M.; López, P.A.; Daza, R.; González-Nieto, D.; Guinea, G.V. Straining Flow Spinning of Artificial Silk Fibers: A Review. *Biomimetics* 2018, *3*, 29. https://doi.org/10.3390/biomimetics3040029

[11] Rockwood, D., Preda, R., Yücel, T. *et al.* Materials fabrication from *Bombyx mori* silk fibroin. *Nat Protoc* **6**, 1612–1631 (2011). https://doi.org/10.1038/nprot.2011.379

[12] Madurga, R., Gañán-Calvo, A.M., Mariscal, T., Plaza Gustavo, R., Guinea Tortuero, G.V., Elices, M. y Pérez-Rigueiro, J. (2019). Production of regenerated silkworm silk fibers from aqueous dopes through straining flow spinning. Textile Research Journal, 89 (21-22), 4554-4567

[13] Hoffmann, Bradley & Gruat-Henry, Catherine & Mulinti, Pranothi & Jiang, Long & Brooks, Benjamin & Brooks, Amanda. (2018). Using hydrodynamic focusing to predictably alter the diameter of synthetic silk fibers. PLOS ONE. 13. e0195522. 10.1371/journal.pone.0195522

[14] Jingxin Zhu, Yaopeng Zhang, Huili Shao, Xuechao Hu, Electrospinning and rheology of regenerated Bombyx mori silk fibroin aqueous solutions: The effects of pH and concentration, Polymer, Volume 49, Issue 12, 2008, Pages 2880-2885, ISSN 0032-3861, https://doi.org/10.1016/j.polymer.2008.04.049

[15] Luo J, Zhang L, Peng Q, Sun M, Zhang Y, Shao H, et al. Tough silk fibers prepared in air using a biomimetic microfluidic chip. Int J Biol Macromol. 2014; 66: 319±324. https://doi.org/10.1016/j.ijbiomac.2014. 02.049 PMID: 24613677

[16] Jin, Y.; Zhang, Y.; Hang, Y.; Shao, H.; Hu, X. A simple process for dry spinning of regenerated silk fibroin aqueous solution. J. Mater. Res. 2013, 28, 2897–2902.

[17] Madurga, R.; Ganan-Calvo, A.M.; Plaza, G.R.; Guinea, G.V.; Elices, M.; Perez-Rigueiro, J. Straining Flow spinning: Production of regenerated silk fibers under a wide range of mild coagulating chemistries. Green Chem. 2017, 19, 3380–3389.

[18] Rodrigo Madurga, Gustavo V. Guinea, Manuel Elices, José Pérez-Rigueiro, Alfonso M. Gañán-Calvo, Straining flow spinning: Simplified model of a bioinspired process to mass produce regenerated silk fibers controllably, European Polymer Journal, Volume 97, 2017, Pages 26-39, ISSN 0014-3057, https://doi.org/10.1016/j.eurpolymj.2017.09.037.

[19] Rodrigo Madurga, Alfonso M. Gañán-Calvo, Gustavo R. Plaza, José Miguel Atienza, Gustavo V. Guinea, Manuel Elices, Patricia A. López, Rafael Daza, Daniel González-Nieto, José Pérez-Rigueiro, Comparison of the effects of post-spinning drawing and wet stretching on regenerated silk fibers produced through straining flow spinning, Polymer, Volume 150, 2018, Pages 311-317, ISSN 0032-3861, https://doi.org/10.1016/j.polymer.2018.07.042

[20] Plaza, G.R., Corsini, P., Pérez-Rigueiro, J., Marsano, E., Guinea, G.V. and Elices, M. (2008), Effect of water on *Bombyx mori* regenerated silk fibers and its application in modifying their mechanical properties. J. Appl. Polym. Sci., 109: 1793-1801. https://doi.org/10.1002/app.28288.

[21] Pérez-Rigueiro J, Biancotto L, Corsini P, Marsano E, Elices M, Plaza GR, Guinea GV. Supramolecular organization of regenerated silkworm silk fibers. Int J Biol Macromol. 2009 Mar 1;44(2):195-202. doi: 10.1016/j.ijbiomac.2008.12.001. Epub 2008 Dec 14. PMID: 19133291.

[22] Cao Y, Wang B. Biodegradation of silk biomaterials. Int J Mol Sci. 2009 Mar 31;10(4):1514-1524. doi: 10.3390/ijms10041514. PMID: 19468322; PMCID: PMC2680630.

[23] Arai, T., Freddi, G., Innocenti, R. and Tsukada, M. (2004), Biodegradation of *Bombyx mori* silk fibroin fibers and films. J. Appl. Polym. Sci., 91: 2383-2390. https://doi.org/10.1002/app.13393

[24] Mingzhong Li, Masayo Ogiso, Norihiko Minoura, Enzymatic degradation behavior of porous silk fibroin sheets, Biomaterials, Volume 24, Issue 2, 2003, Pages 357-365, ISSN 0142-9612, https://doi.org/10.1016/S0142-9612(02)00326-5.

[25] Rebecca L. Horan, Kathryn Antle, Adam L. Collette, Yongzhong Wang, Jia Huang, Jodie E. Moreau, Vladimir Volloch, David L. Kaplan, Gregory H. Altman, In vitro degradation of silk fibroin, Biomaterials, Volume 26, Issue 17, 2005, Pages 3385-3393, ISSN 0142-9612, https://doi.org/10.1016/j.biomaterials.2004.09.020.

[26] Chengchen Guo, Chunmei Li, and David L. Kaplan, Enzymatic Degradation of *Bombyx mori* Silk Materials: A Review, *Biomacromolecules* 2020 *21* (5), 1678-1686, DOI: 10.1021/acs.biomac.0c00090

[27] Srihanam, Prasong & Simchuer, Wilaiwan. (2009). Proteolytic Degradation of Silk Fibroin Scaffold by Protease XXIII. The Open Macromolecules Journal. 3. 10.2174/1874343900903010001.

[28] Jameson Julie F., Pacheco Marisa O., Butler Jason E., Stoppel Whitney L., Estimating Kinetic Rate Parameters for Enzymatic Degradation of Lyophilized Silk Fibroin Sponges, Frontiers in Bioengineering and Biotechnology, 9, 2021, https://www.frontiersin.org/articles/10.3389/fbioe.2021.664306, 10.3389/fbioe.2021.664306

[29] Mouro C, Jung C, Bondon A, Simonneaux G. Comparative Fourier transform infrared studies of the secondary structure and the CO heme ligand environment in cytochrome P-450cam and cytochrome P-420cam. Biochemistry. 1997 Jul 1;36(26):8125-34. doi: 10.1021/bi9700173. PMID: 9201961.

[30] Jung C. Insight into protein structure and protein-ligand recognition by Fourier transform infrared spectroscopy. J Mol Recognit. 2000 Nov-Dec;13(6):325-51. doi: 10.1002/1099-1352(200011/12)13:6<325::AID-JMR507>3.0.CO;2-C. PMID: 11114067.

[31] Goormaghtigh E, Cabiaux V, Ruysschaert JM. Secondary structure and dosage of soluble and membrane proteins by attenuated total reflection Fourier-transform infrared spectroscopy on hydrated films. Eur J Biochem. 1990 Oct 24;193(2):409-20. doi: 10.1111/j.1432-1033.1990.tb19354.x. PMID: 2226461.

[32] Tretinnikov, O. N.; Tamada, Y., Influence of casting temperature on the near surface structure and wettability of cast silk fibroin films. *Langmuir* **2001,** 17, (23), 7406-7413.